Vertical Tail Design

Development of a rapid aerodynamic analysis method

A.P. Hettema

Technische Universiteit Delft

TU Delft Delft University of Technology

Challenge the future

VERTICAL TAIL DESIGN

DEVELOPMENT OF A RAPID AERODYNAMIC ANALYSIS METHOD

by

A.P. Hettema

in partial fulfillment of the requirements for the degree of

Master of Science
in Aerospace Engineering

at the Delft University of Technology,
to be defended publicly on Friday May 1, 2015 at 9:30 AM.

Thesis registration number:	251#15#MT#DAR_FPP	
Equivalent number of words:	24,013	
Supervisors:	dr. ir. R. Vos,	TU Delft
	ir. D. Steenhuizen,	TU Delft
Thesis committee:	dr. A. Gangoli Rao,	TU Delft
	dr. ir. A. C. in 't Veld,	TU Delft

TU Delft Delft University of Technology

PREFACE

This report is the thesis of my graduation project for obtaining the degree of Master of Science in Aerospace Engineering at Delft University of Technology. I could not have completed this thesis or my studies as a whole without the support I received from many people.

I want first of all to thank my advisors Durk Steenhuizen and Roelof Vos for their feedback and advice throughout the project. Crispijn Huijts and Stefan Bernardi were a great help in setting up the windtunnel tests. Furthermore, I want to thank everyone who shared the project rooms with me for turning my thesis project into an enjoyable time socially as well, and for the occasional advice when I was stuck. Special thanks to Marc for his feedback, help, and general willingness to act as a sounding board for both frustrations and possible solutions.

Finally I would like to thank my parents for their years of support and patience during my years of studying at TU Delft, and of course Katharine for her love, support, patience, pep talks, listening ear, and invaluable help.

A.P. Hettema
Delft, April 2015

SUMMARY

The development of unconventional aircraft designs complicates the conceptual design process of aircraft. To manage this increased complexity, it can be helpful to automatize part of this process. The further development of a tool for this automation, called the Initiator, is central to this thesis. The Initiator is a modular tool for preliminary sizing and design analysis. The currently implemented design of the vertical tail in the Initiator is very basic.

The goal of this thesis is to extend the design methodology for vertical tails in the Initiator and thus to develop a rapid aerodynamic analysis method for initial vertical tail design. To achieve this goal, vertical tail design methodology for both conventional and unconventional aircraft configurations was explored. Existing methods for the initial design of vertical tails for conventional aircraft were investigated and a rapid aerodynamic analysis method for vertical tail design for lateral-directional stability and control of conventional aircraft was developed and successfully implemented. This method was validated with existing windtunnel data, and four case studies were performed to analyze the design optimization.

The method is shown in these case studies to match up with the data for comparable reference aircraft. The method does have a trend towards an over-prediction for larger aircraft and an under-prediction for smaller aircraft. The validation of the implemented analysis method shows generally accurate results for most parameters. The main exception to this is the estimation of the tail-off rolling moment due to sideslip.

Windtunnel tests were performed to acquire validation data for blended wing bodies. No suitable rapid analysis method was found for blended wing body aircraft configurations. The empirical method for vertical tail design in conventional aircraft does not work well on a blended wing body; the prediction of tail-off performance was especially inaccurate. A vortex lattice method comes up short when the angles of attack and sideslip become larger than 5°-10°. These are present in some critical cases for vertical tail design, such as crosswind during landing and one engine out at take-off. The estimation of the tail-off yawing moment due to sideslip is inaccurate for the vortex-lattice method as well.

Recommendations for improvement in performance of the module include introducing dynamic stability analysis, of which especially the Dutch roll phenomenon is important in vertical tail design. The module can further be expanded with the inclusion of calculations for propeller aircraft and rudder design. Extra windtunnel tests on blended wing bodies could help in developing a design methodology for these aircraft.

CONTENTS

LIST OF FIGURES

List of Tables

NOMENCLATURE

LATIN SYMBOLS

A	aspect ratio	[-]
b	span	[m]
c	chord	[m]
$\bar{c}$	mean aerodynamic chord	[m]
c_l	two-dimensional lift coefficient	[-]
$\bar{C}$	volume coefficient	[-]
C_l	rolling moment coefficient	[-]
C_{l_β}	rolling moment coefficient due to sideslip	[-]
C_{l_δ}	rolling moment coefficient due to surface deflection	[-]
C_L	lift coefficient	[-]
C_{L_α}	lift curve slope	[-]
C_n	yawing moment coefficient	[-]
C_{n_β}	yawing moment coefficient due to sideslip	[-]
C_{n_δ}	yawing moment coefficient due to surface deflection	[-]
C_Y	side force coefficient	[-]
C_{Y_β}	yawing moment coefficient due to sideslip	[-]
C_{Y_δ}	yawing moment coefficient due to surface deflection	[-]
D	diameter	[m]
D	drag	[-]
F	force	[N]
g	acceleration due to gravity	$[m/s]^2$
h	height	[m]
i	angle of incidence	[deg]
K_f	empirical correction for plain lift increment by flap deflection	[deg]
K_{FV}	fuselage-vertical tailplane lift carry-over effect	[-]
K_i	empirical factor for wing-body interference for C_{y_β}	[-]
K_N	empirical factor for body + wing-body interference for C_{n_β}	[-]
K_{R_l}	empirical factor for the effect of fuselage Reynolds number on wing-body C_{n_β}	[-]
K_{VH}	horizontal-to-vertical tailplane endplate effect	[-]
l	length or moment arm	[m]
L	lift	[N]
L	rolling moment	[Nm]
m	mass	[kg]
M	Mach number	[-]
n	number of	[-]
N	yawing moment	[Nm]
q	dynamic pressure	[Pa]
S	surface area	$[m]^2$
V	velocity	[m/s]
Δy	sharpness factor	[-]
$\bar{Y}$	distance between wing root and mean aerodynamic chord	[m]
$\bar{Z}_V$	distance between vertical tail root and mean aerodynamic chord	[m]

GREEK SYMBOLS

α	angle of attack	[deg]
β	sideslip angle	[deg]
γ	flight path angle	[deg]
Γ	dihedral angle	[deg]
δ	deflection angle	[deg]
Δ	difference	[-]
ϵ	downwash angle	[deg]
λ	taper ratio	[-]
Λ	sweep angle	[deg]
σ	sidewash angle	[deg]
ϕ	bank angle	[deg]

SUBSCRIPTS

a	aileron
A	aircraft
base	base value
clean	configuration without winglets
cross	cross-section
cw	crosswind
C_L	lift coefficient
D	drag
E	engine
f	wing flaps
F	fuselage
h	height
H	horizontal tail
L	lift
LE	leading edge
max	maximum
N	engine nacelles
OEI	one engine inoperative
p	propeller
r	rudder
S	side
T	thrust
V	vertical tail
winglets	configuration with winglets
W	wing
α	angle of attack
β	sideslip
δ	surface deflection
Γ	wing dihedral

1

INTRODUCTION

The development of unconventional aircraft designs complicates the conceptual design process of aircraft. To manage this increased complexity, it can be helpful to automatize part of this process. Tools for this automation are in development within the conceptual design framework of the master track Flight Performance and Propulsion (FPP) at Delft University of Technology. The further development of one of these tools is central to this thesis. The tool in question has been developed in Matlab and is called the Initiator. It is a modular tool for preliminary sizing and design analysis. This modularity means that it can be easily extended with new functionality, and individual parts can be developed further separately. It makes an initial aircraft design based on either a set of top-level requirements and a chosen aircraft configuration, or based on a fully defined aircraft geometry. The Initiator contains a range of analysis modules that can then be used to analyze this design in multiple disciplines, such as weight estimation, mission analysis and cost estimation [1].

1.1. THESIS GOAL AND APPROACH

The currently implemented design of the vertical tail in the Initiator is very basic, and in this thesis the design methodology for vertical tail design is extended. The goal of this thesis can be summed up as follows:

> *The development of a rapid aerodynamic analysis method for initial vertical tail design*

The steps that were taken to achieve this goal are summarized below:

- investigation of rapid aerodynamic analysis methods for initial vertical tail design
- implementation of a vertical tail analysis method for conventional aircraft configurations in the Initiator
- investigation of the applicability of the method to non-conventional aircraft configurations, notably blended wing bodies
- investigation of possible alternative analysis methods for non-conventional aircraft configurations
- validation of the implemented methods using higher fidelity tools, data from literature, or experimental data
- case studies in which the results from the implemented method are compared with the existing implementation in the Initiator and historical aircraft data

1.2. REPORT STRUCTURE

This report starts with the function of the vertical tail and its requirements. This is followed by a description of the basic sizing methodology for the vertical tail. The analysis of lateral-directional static stability and control is discussed next in Chapter 3. The design requirements are then treated again, but this time with a more in-depth analysis of those requirements that tend to drive the design. The module that was developed

[1] http://aircraftinitiator.lr.tudelft.nl/index.php/Synthesis/Initiator, accessed on 6-3-2015

in the Initiator for vertical tail design is then covered. Next is a chapter about windtunnel tests that were performed on a blended wing body for validation of the design method for blended wing body configurations. Penultimately the validations and case studies will be discussed, before finishing with the conclusion and recommendations.

1.3. VERTICAL TAIL FUNCTION AND REQUIREMENTS

The function of the vertical tail is to provide lateral-directional static and dynamic stability, control, and trim, providing equilibrium around the Z-axis in each flight condition. Unlike the wing, it normally operates at only a fraction of its lift potential. In normal flight there is symmetry and so there are no unbalanced aerodynamic yawing moments and no need for trim. Trim is needed in the case of a multi-engined aircraft with one engine out. The lack of thrust on one side and the added drag of the stopped or windmilling engine creates a yawing effect. The vertical tail also provides stability in yaw direction. It is possible to design a stable aircraft without a vertical tail, but this often comes at a cost to another part of the design. The vertical tail design is linked to the design of the rudder. For the rudder sufficient control power is needed in all critical conditions, such as one engine out flight at low speeds, crosswind landing, maximum roll rate, and spin recovery. Control power or control capability is the increase in lift by the vertical tail as a result of rudder deflection. It depends on both the size and type of the rudder, as well as the overall size of the vertical tail. [1, 5] The requirements and design criteria for the vertical tail can be summed up as follows [1, 8, 9]:

- to provide sufficient directional static stability, which is to provide a large enough force to balance the total tail-off forces and moments in the directional plane of motion;
- to provide sufficient dynamic stability;
- to cope with high tailplane angles of attack: the vertical tail should not stall due to high angles of attack that result from oscillation caused by rudder deflection or sudden engine failure.

The requirements for the rudder are [1]:

- to provide a means for achieving a steady state of equilibrium (trim);
- to provide a means to counteract disturbances, such as gusts;
- to provide sufficient directional control capability, up to high sideslip and rudder deflection angles:
  - for maneuvering up to maximum yaw rates;
  - to maintain heading and maneuver during the most critical engine-out situation;
  - for landing in crosswinds of up to 30 kn / 55 km/h;
- to have low control forces.

The three requirements that turn out to be the most critical are landings with maximum crosswind, directional control with one engine out at low airspeeds, and coping with high tailplane angles of attack. The analysis module will design the vertical tail based on these three requirements, and an additional fourth requirement, which is sufficient directional and lateral static stability. The objective in vertical tail design is to meet these requirements with a design that has both a drag and a structural weight that is as low as possible.

These requirements drive the design variables for the vertical tail in different directions. For coping with high angles of attack it is better to have a low aspect ratio and more sweep, while for static stability it is better to have a high aspect ratio and minimum sweep. Coping with high angles of attack is the most stringent requirement. As a result vertical tail surfaces tend to have low aspect ratios and large leading edge sweep or dorsal fins [1].

1.4. GENERAL TAIL GEOMETRY AND ARRANGEMENT

There are many possible configurations for the tail of the aircraft. The most common version is generally called a conventional configuration, used for about 70% of aircraft [5]. It consists of a vertical tail and a horizontal tail that is positioned at the bottom of the vertical tail. This configuration gives adequate stability and control at the lightest weight, combined with structural simplicity. The horizontal surfaces are positioned out of the wing wake and attached at a convenient and strong point at the aft-section of the fuselage [5, 8].

REFERENCE TAIL LAYOUT

The vertical tail shape, like any wing, is defined by the following parameters: span (b), aspect ratio (A), surface area (S), root chord (c_{root}), tip chord (c_{tip}), mean aerodynamic chord ($\bar{c}$), taper ratio (λ), and sweep angle (Λ). The definition of these parameters for a trapezoidal wing are shown in Figure 1.1. The relations between these parameters are defined as follows:

$$b = \sqrt{AS} \tag{1.1}$$

$$c_{\text{root}} = \frac{2S}{b(1+\lambda)} \tag{1.2}$$

$$c_{\text{tip}} = \lambda c_{\text{root}} \tag{1.3}$$

$$\bar{c} = \frac{2}{3} c_{\text{root}} \frac{1+\lambda+\lambda^2}{1+\lambda} \tag{1.4}$$

$$\bar{Y} = \frac{b}{6} \frac{1+2\lambda}{1+\lambda} \tag{1.5}$$

$$\tan \Lambda_{\text{LE}} = \tan \Lambda_{c/4} + \frac{1-\lambda}{A(1+\lambda)} \tag{1.6}$$

The span is defined differently for a vertical tail and wing, as the vertical tail does not extend to both sides of the fuselage. Instead of running from tip to tip as for a wing, the span runs from root to tip. The distance indicated with 'b/2' in Figure 1.1 is thus 'b' for vertical tails. This has some consequences for some of the relations between the parameters. The aspect ratio and span are half of what they are for a similarly shaped wing, and this has to be taken into account when predicting vertical tail behavior using tables and graphs that use wing span and aspect ratio. The equations for the mean aerodynamic chord position $\bar{Y}$ and Λ_{LE} change into the equations that are shown below. $\bar{Y}$ also becomes $\bar{Z}_{\text{V}}$ because of the difference in orientation. Additional definitions for the vertical tail that are used in later calculations are shown in Figure 1.2.

$$\bar{Z}_{\text{V}} = \frac{b_{\text{V}}}{3} \frac{1+2\lambda_{\text{V}}}{1+\lambda_{\text{V}}} \tag{1.7}$$

$$\tan \Lambda_{\text{LE}_{\text{V}}} = \tan \Lambda_{c/4_{\text{V}}} + \frac{1-\lambda_{\text{V}}}{2A_{\text{V}}(1+\lambda_{\text{V}})} \tag{1.8}$$

An alternative for the conventional tail that is also used in the Initiator is the T-tail. It shares the structural

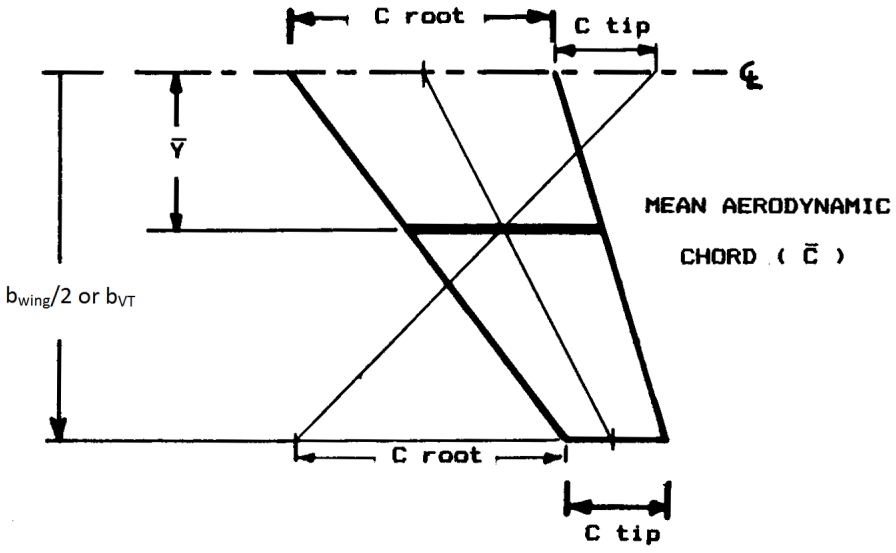

Figure 1.1: Reference (trapezoidal) wing/tail [2]

simplicity with the conventional configuration. The vertical tail needs to support the horizontal tail and this leads to a heavier structure. The horizontal tail creates an endplate effect, which increases the lift-curve slope, and can allow a smaller vertical tail. The horizontal tail is moved out of the wing wake and allows the engines

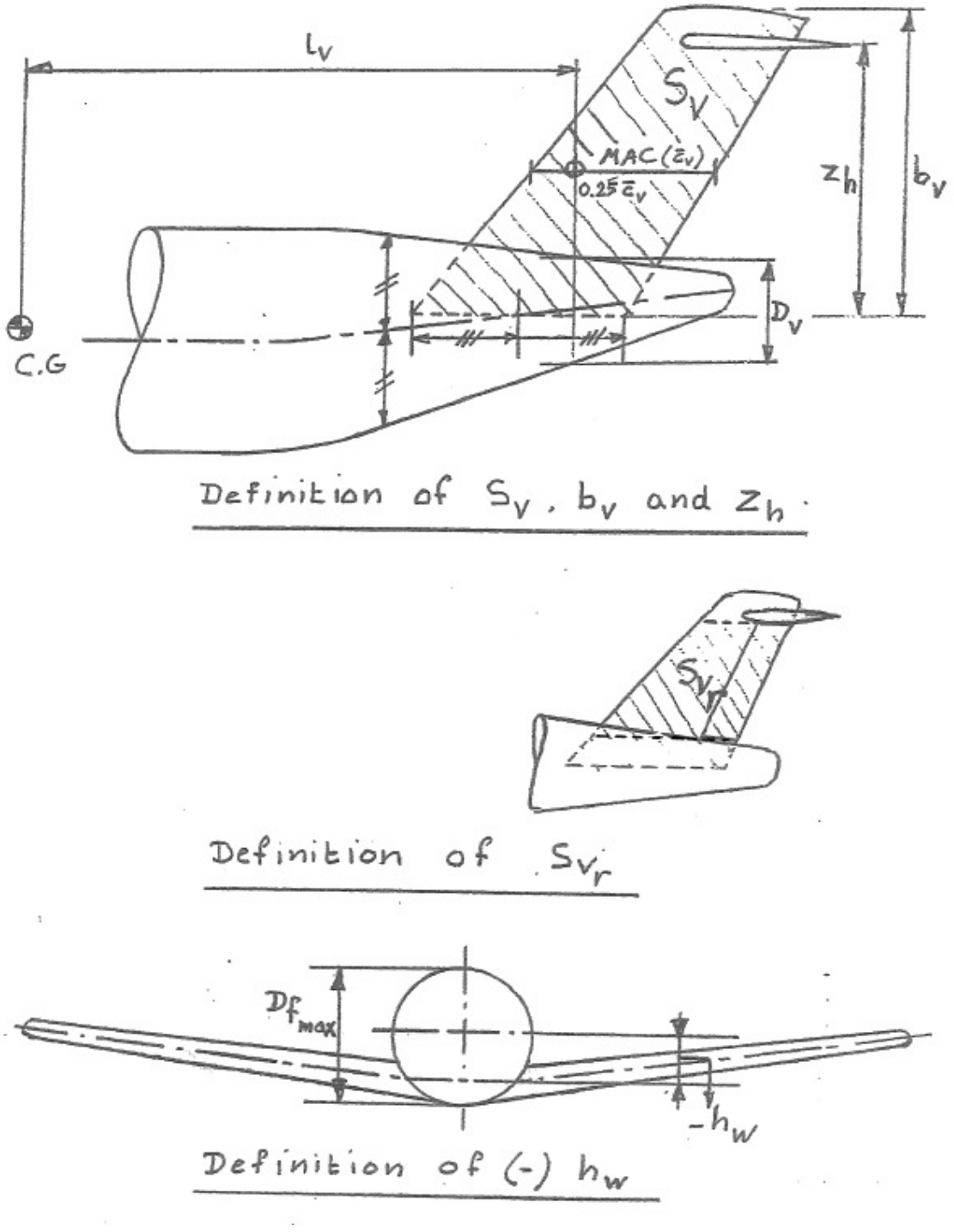

Figure 1.2: Geometrical definitions [1]

to be installed on the aft fuselage. Staying out of the wing wake makes the horizontal tail more efficient and allows it to be smaller. Buffet on the horizontal tail is reduced as well, which reduces fatigue. The last effect that allows for a smaller horizontal tail is achieved with a swept vertical tail, as this increases the moment arm of the horizontal tail. The horizontal tail in the T-tail configuration can become blanketed during deep stall; this is dangerous as it disables the horizontal tail and it necessitates the wing to be designed to not pitch up without a horizontal tail. [5, 8, 9]

2

INITIAL DESIGN OF THE VERTICAL TAIL

Giving general instructions for the preliminary design stage of a tailplane is very difficult. There are many different arrangements possible, and the tailplane arrangement depends more on the general arrangement and layout of the aircraft than any other part. The wing and the engines both have a big effect on the tailplane's effectiveness, especially for propeller aircraft [8]. The location and type of the tail surfaces are chosen first, based on the advantages and disadvantages of different tail types. After that an initial estimation of the size and other parameters is made, based on historical data of other aircraft. This process is elaborated in Section 2.1. Finally calculations are made to check if the vertical tail meets its requirements, such as landing in a crosswind. This process, in which lateral-directional static and dynamic stability and control are taken into account, is addressed in Chapters 3 and 4.

2.1. BASIC SIZING

The general approach in vertical tail design is to start with estimates based on data of comparable existing aircraft. The main design parameters are the tail surface area, aspect ratio, taper ratio, and sweep. The surface area of both the horizontal and the vertical tail is proportional to the wing area, as the wing yawing moments that the vertical tail has to counter are related to wing span [5]. A tail volume coefficient method that utilizes this wing area is used for the initial estimate of the tail surface.

2.1.1. SURFACE AREA SIZING

The tail volume coefficient is defined as follows:

$$\bar{C}_V = \frac{l_V S_V}{S_W b_W} \tag{2.1}$$

In this equation l_V is the moment arm, which is a percentage of the fuselage length. This distance is often approximated as the distance from the wing quarter chord to the vertical tail quarter chord. In early calculations it can be estimated as 50-55% of fuselage length for wing-mounted engines and 45-50% for aft-mounted engines. This leads to the following equation for determining the required surface area of the vertical tail:

$$S_V = \frac{\bar{C}_V S_W b_W}{l_V} \tag{2.2}$$

For a T-tail the area can be reduced by 5% due to the endplate effect that is created by the horizontal tailplane. In case of a computerized active flight control system the area can be reduced by 10%, but only if all requirements for static stability and control are met. The vertical tail area that is determined with this method is the minimum area for the design until the dynamic stability and control analysis is done. The minimum area for the optimization in the Initiator is thus set to the area calculated with the coefficient method, minus 10%. Table 2.1 includes the typical value for the tail volume coefficient for jet transports, as indicated in Reference [5]. Reference [6] uses tables with data of many existing aircraft that can be used to determine the tail volume coefficient with data of the aircraft that are closest to the planned design.

2.1.2. VERTICAL TAIL DESIGN PARAMETERS

Parameters such as the aspect ratio, taper ratio, and sweep can also be selected at the time of the initial estimate. These parameters generally differ little over a large variety of aircraft types. A T-tail often has a lower vertical tail aspect ratio, in order to reduce the weight penalty that comes from having the horizontal tail on top of the vertical tail. An untapered vertical tail is sometimes used in this case, as the effect of taper is small and mainly used to reduce weight or to increase fin rigidity. Tables 2.1 and 2.2 give typical values for these and other parameters, as presented in Reference [5] (Table 2.1) and Reference [6] (Table 2.2). The airfoil sections for vertical tails are symmetrical and use thickness ratios of about 12%. They generally have a relatively large nose radius to permit a large range of angles of attack. [8] The standard airfoil for the vertical tail in the Initiator is the NACA 0012 airfoil. Rudders typically begin at the top of the fuselage and extend to the tip of the tail or to about 90% tail span. [5] A typical value for the relation between vertical tail chord and rudder chord can be found in Table 2.1.

Parameter	Symbol	Value
Aspect ratio (conventional)	A_V	1.3-2.0
Aspect ratio (T-tail)	A_V	0.7-1.2
Taper ratio (conventional)	λ_V	0.3-0.6
Taper ratio (T-tail)	λ_V	0.6-1.0
Tail volume coefficient	$\bar{C}_V$	0.09
Rudder chord ratio	$\frac{c_r}{c_V}$	0.32

Table 2.1: Vertical tail design parameters for jet transports [5]

Parameter	Symbol	Unit	Value
Aspect ratio	A_V	-	0.7 - 2.0
Taper ratio	λ_V	-	0.26 - 0.73
Dihedral angle	Γ_V	°	90
Incidence angle	i_V	°	0
Sweep angle	$\Lambda_{\frac{1}{4}c_V}$	°	33 - 53

Table 2.2: Vertical tail design parameters for jet transports [6]

3

LATERAL-DIRECTIONAL STABILITY AND CONTROL

The static stability is analyzed both laterally and directionally. The main interest for vertical tail design is yaw (directional) control and stability, but yaw (directional) and roll (lateral) are closely coupled and thus analysis of both is necessary. In the analysis the yaw and roll angle are defined as positive to the right. A positive value of a yawing-moment derivative with respect to the sideslip β is stabilizing. A negative value of the rolling-moment derivative with respect to β is stabilizing. The yaw angle drives both the lateral and the directional analysis. Rudder and aileron deflection create moments in both roll and yaw, but the main yawing moment is generally created by the lateral lift of the vertical tail. An additional force is created in the case of interaction between the vertical tail and the propwash from a propeller. The analysis in this thesis is of aircraft with jet engines, so this extra force will not be taken into account.

The moment equations, and the yaw and rolling moment derivatives with respect to sideslip that can be derived from them, are used to analyze if the requirements are met. The steady state airplane aerodynamic side force F_{A_Y}, rolling moment L_A, and yawing moment N_A are first non-dimensionalized as follows:

$$F_{A_Y} = C_Y \bar{q} S \tag{3.1}$$

$$L_A = C_l \bar{q} S b \tag{3.2}$$

$$N_A = C_n \bar{q} S b \tag{3.3}$$

These three coefficients can be expressed as a first order Taylor series, containing the magnitude of the variable in steady flight (0), and the derivatives due to sideslip (β), aileron deflection (δ_a), and rudder deflection (δ_r).

$$C_Y = C_{Y_0} + C_{Y_\beta}\beta + C_{Y_{\delta_a}}\delta_a + C_{Y_{\delta_r}}\delta_r \tag{3.4}$$

$$C_l = C_{l_0} + C_{l_\beta}\beta + C_{l_{\delta_a}}\delta_a + C_{l_{\delta_r}}\delta_r \tag{3.5}$$

$$C_n = C_{n_0} + C_{n_\beta}\beta + C_{n_{\delta_a}}\delta_a + C_{n_{\delta_r}}\delta_r \tag{3.6}$$

For symmetrical airplanes, C_{l_0}, C_{Y_0}, and C_{n_0} are generally equal to zero. The calculation of the other derivatives will be discussed in the sections below. The equations can be summed up in matrix format as follows:

$$\begin{Bmatrix} C_Y \\ C_l \\ C_n \end{Bmatrix} = \begin{bmatrix} C_{Y_\beta} & C_{Y_{\delta_a}} & C_{Y_{\delta_r}} \\ C_{l_\beta} & C_{l_{\delta_a}} & C_{l_{\delta_r}} \\ C_{n_\beta} & C_{n_{\delta_a}} & C_{n_{\delta_r}} \end{bmatrix} \begin{Bmatrix} \beta \\ \delta_a \\ \delta_r \end{Bmatrix} = \begin{Bmatrix} \frac{F_{A_Y}}{\bar{q}S} \\ \frac{L_A}{\bar{q}Sb} \\ \frac{N_A}{\bar{q}Sb} \end{Bmatrix} \tag{3.7}$$

3.1. CALCULATION OF THE TAIL-OFF SIDESLIP DERIVATIVES

In all three equations, the derivative with respect to sideslip can be split up further into components for the effects of different aircraft parts, such as the fuselage, wing, engine nacelles, horizontal tail, and vertical tail. The derivatives for the wing, fuselage, and engine nacelles are calculated as a single assembly in this method, but separately from the horizontal and vertical tail, and are called the tail-off derivatives. The interference

effects of the fuselage, wing, engine nacelles, and horizontal tail on the vertical tail are taken into account in the calculation of the component for the vertical tail.

$$C_{Y_\beta} = C_{Y_{\beta_{\text{WFN}}}} + C_{Y_{\beta_{\text{V}}}} \tag{3.8}$$

$$C_{l_\beta} = C_{l_{\beta_{\text{WFN}}}} + C_{l_{\beta_{\text{H}}}} + C_{l_{\beta_{\text{V}}}} \tag{3.9}$$

$$C_{n_\beta} = C_{n_{\beta_{\text{WFN}}}} + C_{n_{\beta_{\text{V}}}} \tag{3.10}$$

The following three empirical equations are used to calculate these tail-off derivatives; they are only applicable to the linear angle of attack range. The factors K_i, K_N, and K_{R_l} are taken from graphs in [1] and [4] that are shown in Figures A.1, A.2, and A.3. The graph on page I-16 of [1], and the derived factor K_N, combines two graphs from [4], but covers a smaller range of Reynolds numbers than the originals. For this reason the original USAF Datcom graphs were used for the calculations, and the factor K_N was split into two factors: K_N and K_{R_l}. Equation 3.11 considers the tail-off side force as the sum of the side forces due to sideslip of the body, the wing, the wing-body interference, and the wing dihedral effect, but the side force of the wing is neglected as it is small compared to the side force of the body due to sideslip. The wing-body interference is a function of the vertical position of the wing with respect to the body. The side force of the body due to sideslip has been shown in experiments to be mostly independent of wing sweep, wing planform, wing taper ratio, and Mach number. The equation for the yawing moment coefficient does not take the small stabilizing effect of the wings into account, as this is generally negligible compared to the destabilizing effect of the fuselage.

$$(C_{Y_\beta})_{\text{WFN}} = -\frac{S_{\text{F.cross}}}{S_{\text{W}}} K_i \frac{2\pi}{180} - 0.0001\Gamma + (\Delta C_{Y_\beta})_{\text{f}} - 0.00175 n_{\text{N}_\text{W}} - 0.00025 n_{\text{N}_\text{F}} \tag{3.11}$$

$$(C_{l_\beta})_{\text{WFN}} = \left(\frac{C_{l_\beta}}{C_{L_\text{W}}}\right)\frac{C_{L_\text{W}}\pi}{180} + \left(\frac{C_{l_\beta}}{\Gamma}\right)\Gamma - (0.042\frac{z_\text{W}}{D_{\text{F}_\text{max}}} + 0.0005\Gamma)\sqrt{A_\text{W}}\left(\frac{D_{\text{F}_\text{max}}}{b_\text{W}}\right)^2 + (\Delta C_{l_\beta})_{\text{f}} \tag{3.12}$$

$$(C_{n_\beta})_{\text{WFN}} = -K_N K_{R_l} \frac{S_{\text{F}_S}}{S_\text{W}} \frac{l_\text{F}}{b_\text{W}} + (\Delta C_{n_\beta})_{\text{f}} \tag{3.13}$$

The influence of the flaps on the tail-off side force and yawing moment is computed from the graphs in Figure A.4. This figure shows averages for the effect of flap deflection for a collection of windtunnel data in Appendix I of Reference [1]. The influence of the flaps on the tail-off side force and yawing moment is taken from graphs in Reference [1]. No approximation for the effect of flap deflection on the tail-off rolling moment due to sideslip was found in literature. All windtunnel measurements from Appendix I of Reference [1] were collected in a spreadsheet. To improve readability the data were then split over graphs for flap deflections of 15°– 22° and 33°– 42°. Differences were observed between the data for aircraft with fuselage engine nacelles and those with wing engine nacelles. So the data was split again over the two engine nacelle position cases, as can be seen in Figures 3.1a, 3.1b, 3.1c, and 3.1d. The black lines are average trend lines and are used to determine the factor $(\Delta C_{l_\beta})_\text{f}$ in equation 3.12.

The ratios $C_{l_\beta}/C_{L_\text{W}}$ for the lift dependent rolling moment due to sideslip and C_{l_β}/Γ for the effect of uniform geometric dihedral on the rolling moment due to sideslip are deduced from Figures A.5 and A.6. $C_{l_\beta}/C_{L_\text{W}}$ can also be calculated with Equation 3.14; this is the method that is currently used in the module. These graphs cover a range of aspect ratios from 1 to 7 in Figure A.5 and 0 to 8 in Figure A.6. In the initiator a wider range of aspect ratios is encountered and therefore the lines in the graphs were extrapolated to accommodate those higher aspect ratio values. The graphs all determine the derivative with respect to sideslip in radians, except for Figure A.6. In the equations all angles are in degrees and this difference is accounted for where necessary.

$$\left(\frac{C_{l_\beta}}{C_{L_\text{W}}}\right) = -\frac{1}{2}\left[\frac{3}{A_\text{W}(1+\lambda)} + y^\star\left(tan\Lambda_{c/4} - \frac{6}{A_\text{W}}\frac{1-\lambda}{1+\lambda}\right)\right] + 0.05 \tag{3.14}$$

3.2. TAIL CONTRIBUTION TO SIDESLIP DERIVATIVES

The contribution of the vertical tail is influenced by the effect that other aircraft parts have on the flow before it reaches the vertical tail. Some of these flow characteristics are shown in a sketch in Figure 3.2. The main effects of this are changes in effective aspect ratio and angle of attack for the vertical tail. The difference in the angle of sideslip at the vertical tail from the sideslip as experienced by the whole aircraft is called sidewash (σ).

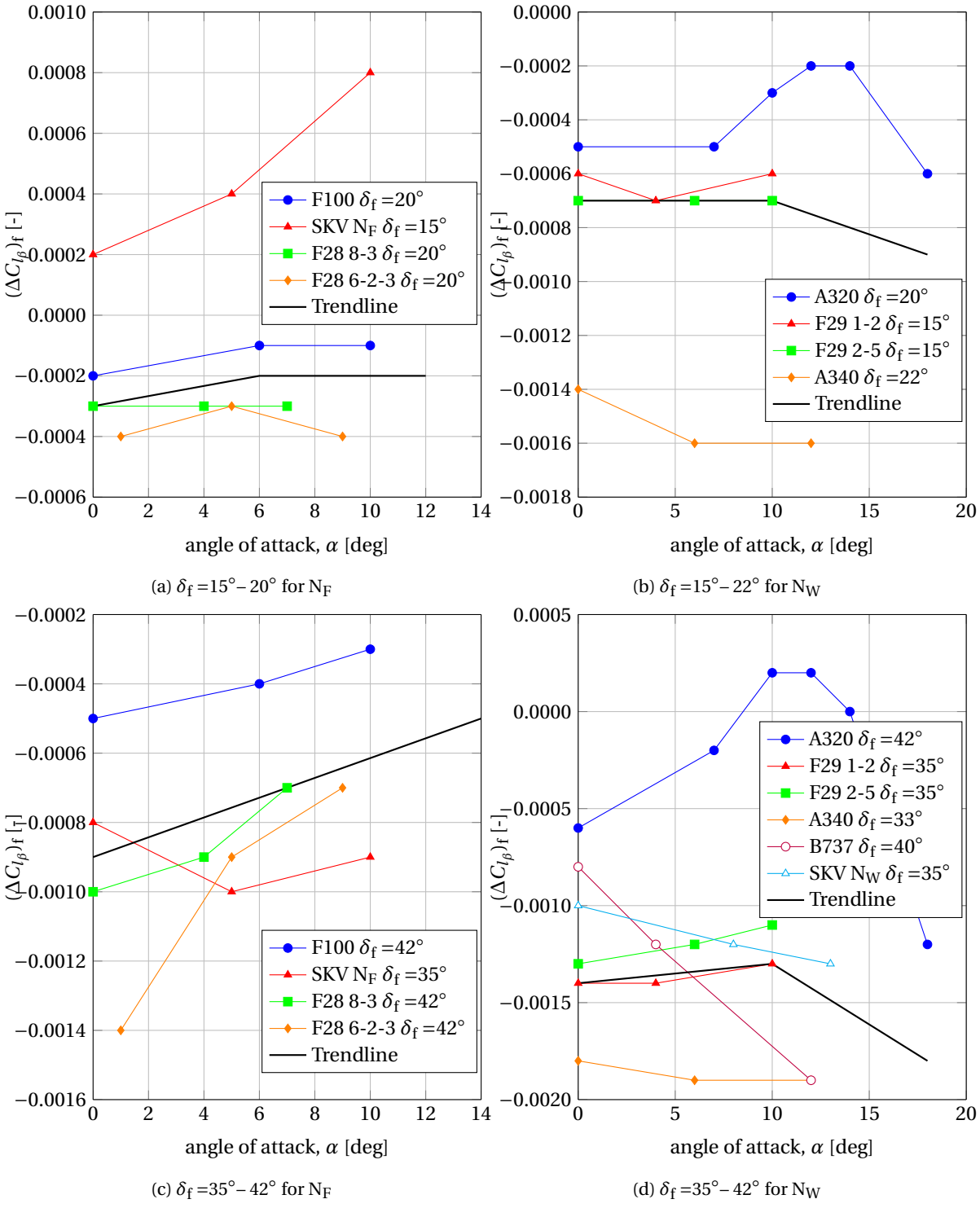

(a) δ_f =15°– 20° for N$_F$

(b) δ_f =15°– 22° for N$_W$

(c) δ_f =35°– 42° for N$_F$

(d) δ_f =35°– 42° for N$_W$

Figure 3.1: Effect of flap deflection on tail-off rolling moment

$$\alpha_V = \beta + \sigma = \left(1 + \frac{\partial \sigma}{\partial \beta}\right)\beta \tag{3.15}$$

As a result of the sidewash the lift coefficient for the vertical tail can be defined as follows:

$$C_{L_V} = C_{L_{\alpha_V}}(\beta + \sigma) = C_{L_{\alpha_V}}\left(1 + \frac{\partial \sigma}{\partial \beta}\right)\beta \tag{3.16}$$

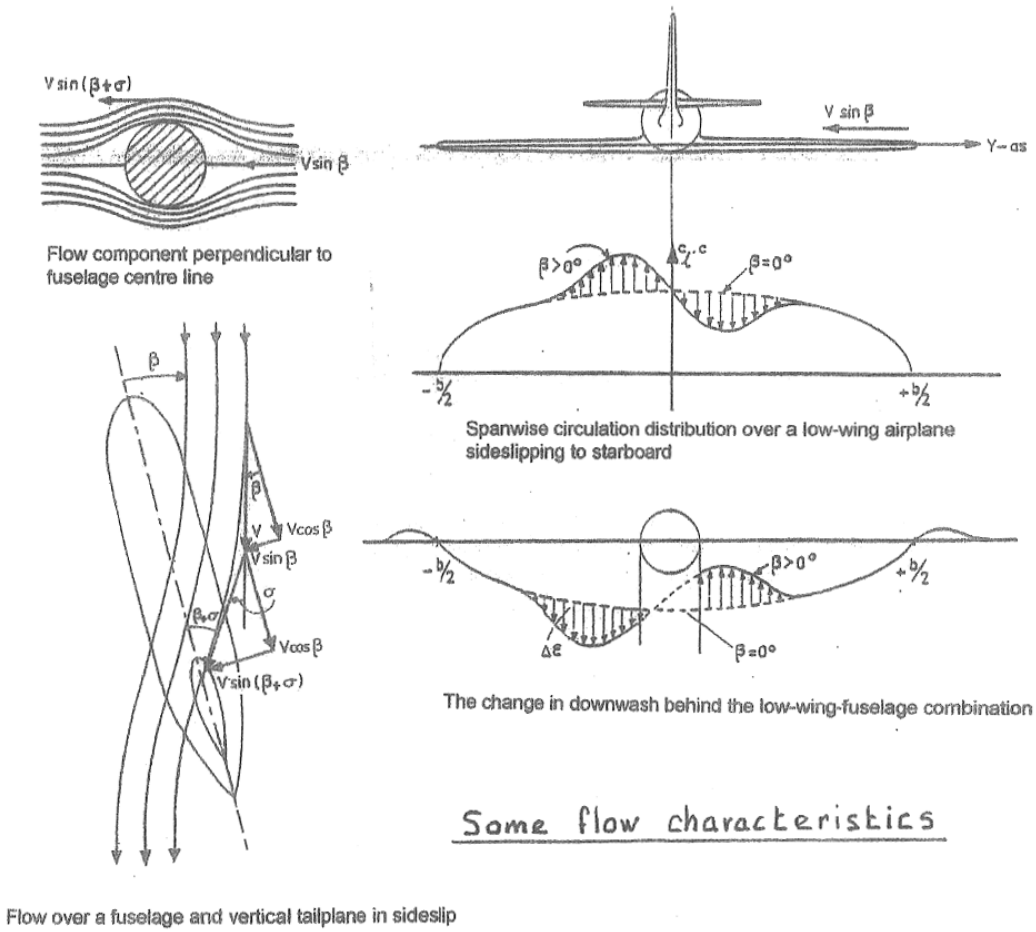

Figure 3.2: Flow characteristics in sideslip [1]

This lift creates a side force:

$$F_{A_{Y_V}} = C_{L_{\alpha_V}}(1+\frac{d\sigma}{d\beta})\beta\bar{q}_V S_V \tag{3.17}$$

$$C_{Y_{\beta_V}}\beta\bar{q}S = C_{L_{\alpha_V}}(1+\frac{d\sigma}{d\beta})\beta\bar{q}_V S_V \tag{3.18}$$

$$C_{Y_{\beta_V}} = C_{L_{\alpha_V V}}(1+\frac{d\sigma}{d\beta})\frac{\bar{q}}{q}\frac{S_V}{S_W} \tag{3.19}$$

The yawing moment due to sideslip due to the vertical tail is the side force due to sideslip due to the vertical tail multiplied by a moment arm along the x-axis from vertical tail aerodynamic center to the airplane center of gravity. The rolling moment is calculated in a similar manner, but with a moment arm along the z-axis. An empirical constant K_{FV} is added to account for the tailplane-fuselage lift carry-over effect, which is detailed in Section 3.2.2.

$$C_{Y_{\beta_V}} = -C_{L_{\alpha_V}}(1+\frac{d\sigma}{d\beta})\frac{\bar{q}}{q}K_{FV}\frac{S_V}{S_W} \tag{3.20}$$

$$C_{l_{\beta_V}} = -C_{L_{\alpha_V}}(1+\frac{d\sigma}{d\beta})\frac{\bar{q}}{q}K_{FV}\frac{S_V l_{Z_V}}{S_W b_W} \tag{3.21}$$

$$C_{n_{\beta_V}} = C_{L_{\alpha_V}}(1+\frac{d\sigma}{d\beta})\frac{\bar{q}}{q}K_{FV}\frac{S_V l_{X_V}}{S_W b_W} \tag{3.22}$$

The horizontal tail influences the rolling moment due to sideslip through the dihedral effect. It is determined similarly to the dihedral effect for the tail-off rolling moment due to sideslip in Section 3.1. The coefficient for

the rolling moment due to sideslip due to the horizontal tail can then be written as follows [7]:

$$C_{l_{\beta_H}} = \left(\frac{C_{l_\beta}}{\Gamma}\right)_H \Gamma_H \left(\frac{\bar{q}_H S_H b_H}{\bar{q} S_W b_W}\right) \tag{3.23}$$

3.2.1. LIFT CURVE SLOPE

Figure 3.3 is used to determine the lift curve slope of the vertical tail. For low aspect ratio tails, especially when $A_V \leq 1.5$, the lift curve slope is only dependent on the aspect ratio. For higher aspect ratios the lift curve slope is influenced by the taper ratio and sweep angle as well. Vertical tails tend to be designed for aspect ratios in the lower end of this graph, because of the benefits of a low aspect ratio on the maximum angle of attack. It can be seen that increasing the aspect ratio is beneficial though for the lift curve slope.

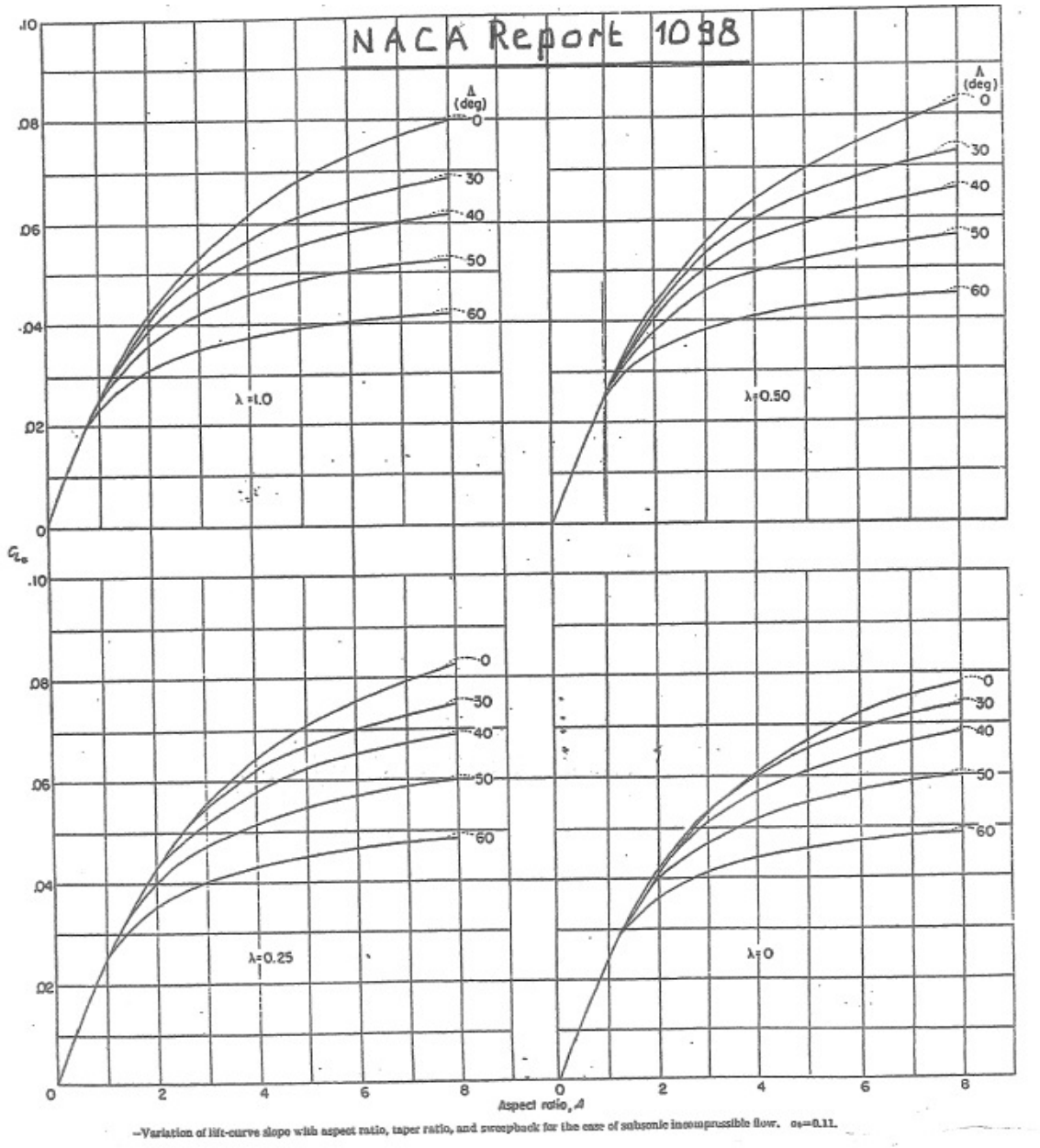

Figure 3.3: Variation of the lift-curve slop with aspect ratio, taper ratio, and sweep for subsonic incompressible flow [10]

3.2.2. DYNAMIC PRESSURE RATIO AND TAILPLANE-FUSELAGE LIFT CARRY-OVER EFFECT

The effective versus free stream dynamic pressure ratio $\frac{q_V}{q}$ takes into account the fuselage boundary layer effect. This ratio is multiplied with the tailplane-fuselage lift carry-over effect K_{FV} to account for the difference in created lift that is due to the presence of the fuselage. The combined effect of $\frac{q_V}{q} K_{FV}$ is calculated using Figure A.7, which is based on wind tunnel measurements of a Fokker F-28.

SIDEWASH OR CROSS-FLOW AT THE VERTICAL TAIL

The sidewash or cross-flow (σ) is the difference in the angle of sideslip at the vertical tail from the angle of sideslip that the whole aircraft experiences. This is detailed in Figure 3.2. The estimation of the sidewash is calculated separately for the different aircraft parts and aerodynamic effects that influence the sidewash. Interference between these effects is assumed to be negligible, based on the set-up and results of the wind-tunnel experiments from Reference [1], on which many of the calculations are based. The separate influences that are taken into account are: the presence of the fuselage $(1+\frac{\partial\sigma}{\partial\beta})_F$, wing-fuselage interference $(\Delta\frac{\partial\sigma}{\partial\beta})_{h_W}$, wing dihedral and wing sweep $(\Delta\frac{\partial\sigma}{\partial\beta})_{\Gamma\Lambda}$, rolling moment due to sideslip $(\Delta\frac{\partial\sigma}{\partial\beta})_{C_{l_\beta}}$, flap deflection $(\Delta\frac{\partial\sigma}{\partial\beta})_{\delta_f}$, and the presence of engine nacelles $(\Delta\frac{\partial\sigma}{\partial\beta})_N$. All sidewash values for the separate influences are added up at the end, after accounting for the fuselage boundary layer and lift carry-over effects when appropriate. This leads to the following calculation for the total sidewash:

$$\left(1+\frac{\partial\sigma}{\partial\beta}\right)_{total} = \left(1+\frac{\partial\sigma}{\partial\beta}\right)_F + \left(\Delta\frac{\partial\sigma}{\partial\beta}\right)_{h_W} + \left(\Delta\frac{\partial\sigma}{\partial\beta}\right)_{\Gamma\Lambda} + \left(\Delta\frac{\partial\sigma}{\partial\beta}\right)_{C_{l_\beta}} + \left(\Delta\frac{\partial\sigma}{\partial\beta}\right)_{\delta_f} + \left(\Delta\frac{\partial\sigma}{\partial\beta}\right)_{N_W} + \left(\Delta\frac{\partial\sigma}{\partial\beta}\right)_{N_F} \tag{3.24}$$

Sidewash due to the presence of the fuselage A cylindrical body in sideslip can be modeled as a cylinder in cross flow, as seen in the upper left of Figure 3.2. The highest flow velocity occurs at the top and bottom of the cylinder. The further the flow is from the body surface, the lower the velocity, until at some point it is again at free-stream velocity. As a result, a large body with a small vertical tail will be more effective per unit area than a large tail on a small body [4]. Figure A.8 shows test data that confirm this theory. The middle curve in the figure is used to estimate the sidewash due to the presence of the fuselage $\left(1+\frac{\partial\sigma}{\partial\beta}\right)_F$, combined with the fuselage boundary layer effect and lift-carry-over effect.

Sidewash due to wing-fuselage interference The wing influences the flow over the fuselage in sideslip. A main parameter for this interference is the relative z-position of the wing compared to the fuselage center line. The results from windtunnel measurements have led to the following linear relation [1]:

$$\left(\Delta\frac{d\sigma}{d\beta}\right)_{h_W}\frac{q_V}{q}K_{FV} = -0.40\frac{h_W}{D_{F_{max}}} \tag{3.25}$$

Sidewash due to wing dihedral and sweep Two other wing parameters that influence the flow are the wing dihedral and sweep. Their effect is combined in one estimation with the equation below, in which $(\Delta C_{l_\beta})_\Gamma$ accounts for the effects of both dihedral and sweep. $(\Delta C_{l_\beta})_\Gamma$ is calculated with Equation 3.27 [1], in which C_{l_β}/Γ is from Section 3.1 and Figure A.6.

$$\left(\Delta\frac{\partial\sigma}{\partial\beta}\right)_{\Gamma\Lambda}\frac{q_V}{q}K_{FV} = \left(110+50\frac{h_W}{D_{F_{max}}}\right)(\Delta C_{l_\beta})_\Gamma \tag{3.26}$$

$$\left(\Delta C_{l_\beta}\right)_\Gamma = \frac{C_{l_\beta}}{\Gamma}\Gamma_W - 0.0005\Gamma_W\sqrt{A_W}\left(\frac{D_{F_{max}}}{b_W}\right)^2 \tag{3.27}$$

Sidewash due to rolling moment due to sideslip The tail-off rolling moment calculated in Section 3.1 creates sidewash as well. This effect is estimated by a linear relation that is shown in the equation below. $(C_{l_\beta})_{WFN}$ is calculated with Equation 3.12 from Section 3.1.

$$\left(\Delta\frac{\partial\sigma}{\partial\beta}\right)_{C_{l_\beta}} = 50\left[(C_{l_\beta})_{WFN} - (C_{l_\beta})_{WFN,C_L=0}\right] \tag{3.28}$$

Sidewash due to flap deflection to the landing position The approximation for the sidewash due to flap deflection to the landing position was derived from the linearized curves for the sidewash versus the tail-off rolling moment.[1]

$$\left(\Delta\frac{\partial\sigma}{\partial\beta}\right)_{\text{f.landing}} = -0.80\left(\frac{b_\text{f}}{b_\text{W}} - 0.67\right) \tag{3.29}$$

For smaller flap deflection angles the sidewash due to flap deflection can be assumed to be proportional to the flap angle, which leads to the more general expression:

$$\left(\Delta\frac{\partial\sigma}{\partial\beta}\right)_{\text{f}} = -0.80\left(\frac{b_\text{f}}{b_\text{W}} - 0.67\right)\frac{\delta_\text{f}}{\delta_{\text{f}_\text{max}}} \tag{3.30}$$

Sidewash due to engine nacelles on the wing The sidewash due to engine nacelles on the wing is estimated by simplifying the data in Figure A.9. The figure shows a slightly higher sidewash with engines mounted. This effect is approximated by:

$$\left(\Delta\frac{\partial\sigma}{\partial\beta}\right)_{\text{N}_\text{W}} = 0.03 \tag{3.31}$$

The effect is shown to be bigger with flaps extended, so for flap deflections of 10 degrees and higher the following crude estimation is used:

$$\left(\Delta\frac{\partial\sigma}{\partial\beta}\right)_{\text{N}_\text{W}} = -0.1 \tag{3.32}$$

Sidewash due to engine nacelles on the fuselage The sidewash due to engine nacelles is estimated with Figure A.10. The estimation is based on the longitudinal and vertical position of the engine nacelles. The definitions of the distances that are used in the figure are based on Figure A.11.

3.2.3. ENDPLATE EFFECT OF THE HORIZONTAL TAILPLANE ON THE VERTICAL TAILPLANE LIFT CURVE SLOPE

The presence of the horizontal tail has an effect on the flow around the vertical tail. When the horizontal tail is present at a relatively high or low position with respect to the vertical tail, then this increases the effectiveness of the vertical tail. This is called the endplate effect of the horizontal tail on the vertical tail lift curve slope and is represented by the constant K_{VH}. This endplate effect is modeled by a change in the effective aspect ratio of the vertical tail (A_V). This effective aspect ratio is then used for determining the lift curve slope of the vertical tail.

Three different effects are taken into account in the determination of K_{VH}. The first is the relative position of the vertical and horizontal tail; this effect is estimated with the help of Figures A.12 and A.13. It is then combined with a factor that models the effect of the relative sizes of the vertical and horizontal tail; this area ratio effect is taken from the top or bottom graph in Figure A.14. The last step is to account for the relative angle of attack of the horizontal tail; this effect is estimated with Equation 3.33. The factor $(K_{\text{VH}})_{\alpha_\text{H}=0}$ in this equation is the combined effect of the horizontal and vertical tail position and area ratio. α^*_H is the horizontal tailplane zero-lift angle of attack, relative to the tailplane reference plane, which is assumed to be 1.5° based on values in Appendix II of Reference [1].

$$K_{\text{VH}} = (K_{\text{VH}})_{\alpha_\text{H}=0}\left[1 - 0.014(\alpha_\text{H} + \alpha^*_\text{H})\right] \tag{3.33}$$

$$\alpha_\text{H} = \alpha - \varepsilon + i_\text{H} \tag{3.34}$$

The effective angle of attack of the horizontal tail is calculated with the aircraft angle of attack, the downwash from the wing and the incidence angle of the horizontal tail. The downwash and incidence angle are taken from the Stabilizing Surface Sizing module for horizontal tail and canard design. When the input from this module is not present the incidence angle is assumed to be zero degrees. The downwash is then calculated with very simple estimations that are taken from Appendix II of Reference [1]. These only take the angle of attack and flap setting into account. The linear estimations from that appendix were collected and arranged by flap setting and an average is used for each of the three flight phases: cruise, take-off, and landing.

$$\varepsilon = 1.7 + 0.28\alpha \quad \text{cruise} \tag{3.35a}$$

$$\varepsilon = 2.9 + 0.35\alpha \quad \text{take-off} \tag{3.35b}$$

$$\varepsilon = 4.7 + 0.37\alpha \quad \text{landing} \tag{3.35c}$$

Some methods for estimating the endplate effect take into account the effect of body cross flow as well. This body cross flow effect can be estimated both as an endplate effect (Figures A.15 and A.16) and as a sidewash effect, with similar results. Both estimations compare the vertical tail span with the fuselage height at the position of the aerodynamic center of the vertical tail. The choice was made to estimate the effect of body cross flow as a sidewash effect (Section 3.2.2) because more data was found for the curve that estimates the effect as sidewash.

3.2.4. EFFECT OF A DORSAL FIN

The sharp leading edge of a dorsal fin creates a vortex over the vertical tail that has several aerodynamic benefits. This vortex increases the maximum angle of attack of the vertical tail. The added lift of the dorsal fin also slightly increases the tailplane lift gradient and shifts the aerodynamic center of the vertical tail forward. It has been shown in windtunnel tests that up to medium yaw angles the yawing moment is not affected by the dorsal fin shape and surface area. The forward shift in the position of the aerodynamic center decreases the moment arm of the vertical tail, and this effect counteracts the increase in side force that is the result of the increased lift gradient [1]. The changes in lift gradient and aerodynamic center position are calculated with two linear relations that are taken from the two graphs in Figure A.17. The increase of the maximum angle of attack as a result of a dorsal fin is hard to estimate. In the graphs with windtunnel results from Appendix I of Reference [1], it can be seen that the difference can be as much as 10 degrees, but also that this difference is not consistent. Most of the graphs from windtunnel tests in Reference [1] do not show the maximum angle of attack for the vertical tail with dorsal fin, but do show where the lift curve for the vertical tail without dorsal fin stops being linear. From the observation of the graphs it was deduced that the difference in maximum angle of attack can safely be assumed to be at least 7 degrees.

3.3. INFLUENCE OF AILERON DEFLECTION ON SIDE FORCE, ROLLING MOMENT AND YAWING MOMENT

The side force coefficient due to aileron deflection $C_{Y_{\delta_a}}$ is negligible, unless the rolling moment controls are close to a vertical surface such as the fuselage or vertical tail. There are no equations for estimating this effect; wind tunnel tests are the only reliable means for obtaining this data. [7] This parameter is thus assumed to be zero in the code. The rolling moment coefficient due to aileron deflection $C_{l_{\delta_a}}$ is estimated with the use of a strip method as seen in Equation 3.36 and Figure A.18 [5]. The part of the wing where the aileron is situated is divided into strips. For every strip the lift increment due to aileron deflection is estimated as a flap effect. This lift increment is multiplied with the strip's moment arm to the aircraft centerline. The factor K_f represents an empirical correction for plain lift increment that depends on flap deflection and relative flap chord and is determined with the help of Figure A.19. The factor $\left(\frac{\partial C_L}{\partial \delta_f}\right)'$ is the theoretical lift increment for plain flaps and is dependent on relative flap chord and thickness to chord ratio; it is determined with the help of Figure A.20.

$$C_{l_{\delta_a}} = \frac{2\sum_{i=1}^{n} K_f \left(\frac{\partial C_L}{\partial \delta_f}\right)' Y_i S_i \cos\Lambda_a}{S_W b_W} \tag{3.36}$$

The yawing moment coefficient due to aileron deflection $C_{n_{\delta_a}}$ is caused by a difference in induced drag that is the result of the difference in lift that is created by the deflection of the ailerons. The coefficient is estimated with the use of the wing lift coefficient and the rolling moment coefficient due to aileron deflection. For most ailerons the coefficient is negative; this adverse aileron-yaw effect is unwanted and can be eliminated with a different aileron design, such as differentially deflected ailerons. The presence of the adverse aileron-yaw effect is assumed in the module.

$$C_{n_{\delta_a}} = -0.2 C_{L_W} C_{l_{\delta_a}} \tag{3.37}$$

3.4. INFLUENCE OF RUDDER DEFLECTION ON SIDE FORCE, ROLLING MOMENT AND YAWING MOMENT

The side force curves in the appendices of Reference [1] generally show linear behavior up to rudder deflections of 25°. The maximum side force is reached at a rudder deflection of 35° for the normal range of rudder-chord-to-tailplane-chord ratios $\frac{c_r}{c_V} = 0.20 - 0.35$. The side force at this maximum rudder deflection is 10–15% smaller than it would have been if the side force curves showed linear behavior up to the maximum

rudder deflection. The following equations are used to estimate the side force due to rudder deflection:

$$(C_Y)_{\delta_r} = C_{Y_{\delta_r}} \delta_r = C_{L_{\alpha_V}} \frac{q_V}{q} K_{FV} K_{VH} \frac{c_{l_\delta}}{c_{l_\alpha}} \frac{S_{V_r}}{S_W} \delta_r \tag{3.38}$$

$$(C_{Y_{max}})_{\delta_r} = 0.9 C_{Y_{\delta_r}} \delta_{r_{max}} \tag{3.39}$$

The ratio $\frac{S_{V_r}}{S_V}$ is introduced to normalize to full-span rudders, so that rudders of different relative span can be compared. The definition of S_{V_r} is shown in Figure 1.2. The ratio $\frac{c_{l_\delta}}{c_{l_\alpha}}$ represents the rudder effectiveness, or the change in vertical tail angle of attack α_{V_0} with rudder deflection. This is related to the rudder-chord ratio as shown in Figure A.21. The rolling moment and yawing moment coefficient due to rudder deflection are calculated by multiplying the rudder side force with the rudder moment arm. For the yawing moment this rudder moment arm is slightly longer than the vertical tail moment arm. The difference in length is about 0.30 $\bar{c}_V$ for the normal range of rudder-chord-to-tailplane-chord ratios. The rolling moment coefficient is a cross-control derivative, and it is preferable for it to be as close to zero as possible.

$$(C_l)_{\delta_r} = C_{l_{\delta_r}} \delta_r = C_{L_{\alpha_V}} \frac{q_V}{q} K_{FV} K_{VH} \frac{c_{l_\delta}}{c_{l_\alpha}} \frac{S_{V_r}}{S_W} \frac{l_{Z_V}}{b_W} \delta_r \tag{3.40}$$

$$(C_n)_{\delta_r} = C_{n_{\delta_r}} \delta_r = C_{L_{\alpha_V}} \frac{q_V}{q} K_{FV} K_{VH} \frac{c_{l_\delta}}{c_{l_\alpha}} \frac{S_{V_r}}{S_W} \frac{l_{X_V} + 0.30\bar{c}_V}{b_W} \delta_r \tag{3.41}$$

$$(C_{l_{max}})_{\delta_r} = 0.9 C_{l_{\delta_r}} \delta_{r_{max}} \tag{3.42}$$

$$(C_{n_{max}})_{\delta_r} = 0.9 C_{n_{\delta_r}} \delta_{r_{max}} \tag{3.43}$$

4

DRIVING REQUIREMENTS

The requirements that drive the vertical tail design can be subdivided into four requirements in three flight conditions. The first is a positive value for the yawing moment coefficient due to sideslip in all conditions. For the cruise condition this is expanded to a goal value that should be met, which helps guide design until a full static and dynamic analysis has been performed. The second requirement is the case of one engine inoperative (OEI) at take-off, and the third is landing with maximum crosswind. The fourth requirement is for the vertical tail not to stall at the maximum sideslip angle. Additionally dynamic stability and control should be checked as well.

The simplest method to correct a vertical tail that does not produce enough lift to meet these requirements is to increase the vertical tail size, but this increases weight and drag. Increasing rudder chord and/or rudder span or using a double-hinged rudder increases rudder effectiveness. An all-moving vertical tail gives even more rudder control power, but is heavy. The response to one engine inoperative can be improved by moving the engines inward, but this does increase the wing structural weight. In the code the size of the vertical tail is adjusted, and the rudder span and rudder chord are kept constant.

4.1. GOAL VALUES FOR YAWING MOMENT COEFFICIENT DUE TO SIDESLIP

A positive static directional stability is required in CS 25.177 for any landing gear and flap position and symmetrical power condition [11]. This requires a positive value for the yawing moment coefficient due to sideslip (C_{n_β}). Figure 4.1 is adopted from Reference [5] and extra reference aircraft from Reference [12] were added to it. The figure provides Mach number-dependent goal values for C_{n_β} that can be used for the initial design of the vertical tail, until a full analysis of both static and dynamic directional stability has been performed. These goal values are incorporated into the code and are used as a requirement for the C_{n_β} value in cruise conditions. Reference [5] also suggests a goal value for the rolling moment coefficient due to sideslip (C_{l_β}). C_{l_β} needs to be negative for positive lateral static stability. The suggested goal value is equal to $-0.5C_{n_\beta}$ at subsonic speeds. For transonic speeds the goal value is equal to -C_{n_β}. This goal value for C_{l_β} is calculated and checked in the module, but is not used as an active requirement. The wing and not the vertical tail is the dominant part in the C_{l_β} calculation. The vertical tail is thus not necessarily the first part that should be changed when the requirement for C_{l_β} is not met.

4.2. ONE ENGINE INOPERATIVE AT TAKE-OFF

The loss of engine thrust in a multi-engined aircraft where the engine that loses thrust is not in the plane of symmetry leads to an asymmetric thrust distribution and thus a yawing moment. This is visible in Figure 4.2, which shows the geometry and the forces and moments for a twin engine aircraft in the case of one engine inoperative. This figure includes the factor F_p that is only applicable to propeller aircraft. The yawing moment that is created is detailed in Equation 4.1 and consists of the thrust of the operative engine (T_E), the drag of the inoperative engine ($D_{\text{engine out}}$), and a moment arm (l_{Y_E}). The factor K_{OEI} is used to estimate the extra drag created by the inoperative engine and is determined with the help of Table 4.1.

$$T_E l_{Y_E} + D_{\text{engine out}} l_{Y_E} = N_{T_E} + N_{D_{\text{engine out}}} = K_{OEI} N_{T_E} \tag{4.1}$$

As a result of the yawing moment the aircraft will yaw in the direction of the inoperative engine. This motion

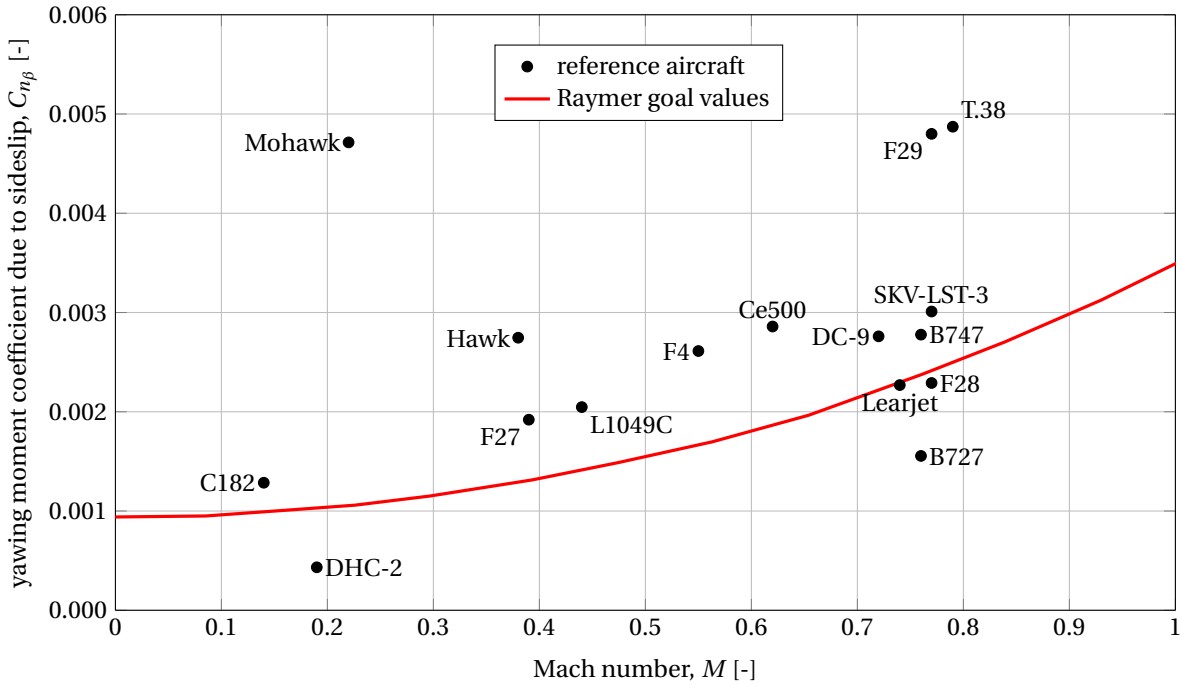

Figure 4.1: Typical yaw moment derivative values

Type of powerplant	Propeller		Turbofan	
	Fixed pitch	Variable pitch	Low BPR	High BPR
K_{OEI}	1.25	1.10	1.15	1.25

Table 4.1: Effect of propulsive installation on K_{OEI} [7]

is counteracted by the yawing moments due to sideslip, yaw, and roll, as well as by the application of rudder and aileron deflection. This leads to steady, straight flight that can be represented by a modified version of Equation 3.7 from Chapter 3. The coefficients $C_{Y_{\delta_a}}$, $C_{l_{\delta_r}}$, and $C_{n_{\delta_a}}$ are negligible and thus zero. A component for the weight (C_L) and yawing moment due to the engine (C_{n_E}) are added, as well as the roll or bank angle (ϕ). This leads to the following equation:

$$\begin{bmatrix} C_L & C_{Y_\beta} & 0 & C_{Y_{\delta_r}} \\ 0 & C_{l_\beta} & C_{l_{\delta_a}} & 0 \\ 0 & C_{n_\beta} & 0 & C_{n_{\delta_r}} \end{bmatrix} \begin{bmatrix} \phi \\ \beta \\ \delta_a \\ \delta_r \end{bmatrix} = \begin{bmatrix} 0 \\ 0 \\ -C_{n_E} \end{bmatrix} \tag{4.2}$$

$$C_L = \frac{\pi}{180} \frac{m_A g \cos\gamma}{\bar{q} S_W} \tag{4.3}$$

$$C_{n_E} = \frac{K_{OEI} N_{T_E}}{\bar{q} S_W b_W} \tag{4.4}$$

There is more than one steady flight condition possible, but the two conditions that are especially important to consider are a roll angle (ϕ) of zero and a sideslip angle of zero. The latter gives minimum aircraft drag. A rudder deflection is necessary to balance the moment that is generated by engine. When $\phi = 0$ it then follows that sideslip is needed to balance the lateral force $C_{Y_{\delta_r}} \delta_r$. For $\beta = 0$ a bank angle that raises the inoperative engine is needed to balance this force. This bank angle (ϕ) has the specific requirement in AMC 25.121 to not exceed 3° during climb. A bigger rudder deflection is needed at $\phi = 0$ as at $\beta = 0$, as the rudder deflection needs to balance both C_{n_E} and $C_{n_\beta}\beta$ [12]. $\phi = 0$ is thus taken as the critical case.

The yawing moment due to the engine is inversely proportional to the square of the airspeed. A lower airspeed is thus more critical. One engine inoperative should be evaluated at either take-off speed (1.1 times stall speed [5]) or at minimum control speed (1.2 times stall speed [6]) and with the most unfavorable center

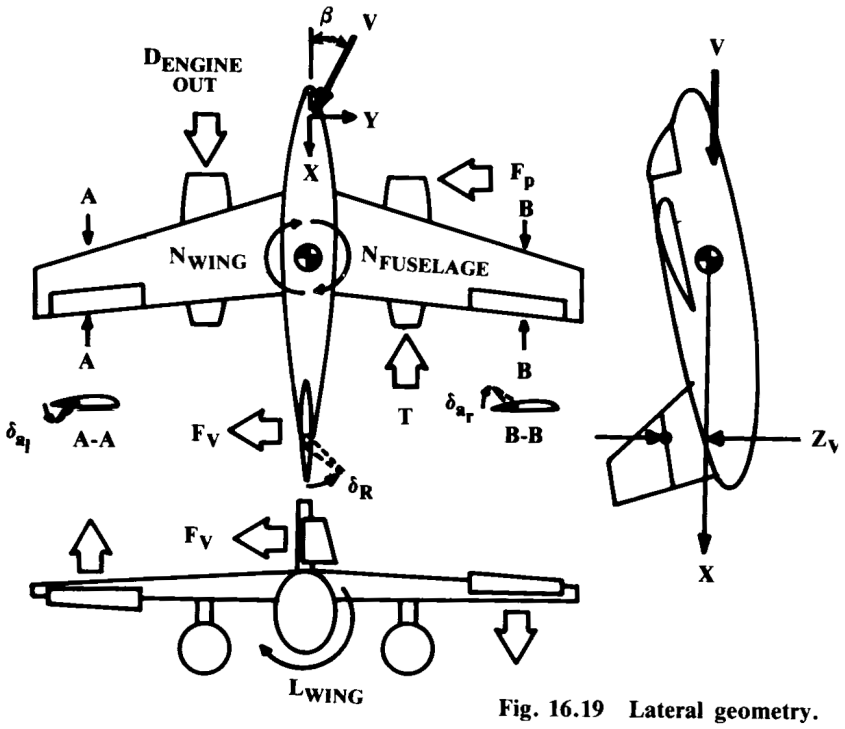

Fig. 16.19 Lateral geometry.

Figure 4.2: Geometry for the lateral-directional analysis with one engine out [2]

of gravity, which is the aft-most position. The necessary rudder deflection should not exceed 20° [5] or 25° [6] so that additional rudder deflection is possible to allow for maneuvering. The more stringent requirements from Reference [5] are used in the module.

In AMC 25.143(b) it is stated that a way of showing compliance is to demonstrate that one can regain full control of the airplane without attaining a dangerous flight condition in the event of a sudden and complete failure of the critical engine. The conditions for this demonstration include the speed (lowest speed for climbing), and for the engines to be at maximum continuous power or thrust, prior to the critical engine becoming inoperative. The demonstration should be made with a delay of two seconds before taking action, to represent the time it may take the pilot to identify the problem and take action [11]. The maximum sideslip angle without pilot action that can be deduced from Equation 4.2 is found with:

$$\beta_{\max} = \frac{-K_{\text{OEI}} N_T}{C_{n_\beta} \bar{q} S_{\text{W}} b_{\text{W}}} \tag{4.5}$$

The equilibrium about the X-axis can then be used to check the amount of aileron deflection that is required to keep the wings level at this maximum sideslip angle.

$$\delta_{\text{a}} = \frac{-C_{l_\beta} \beta_{\max}}{C_{l_{\delta_{\text{a}}}}} \tag{4.6}$$

This aileron deflection is not used in the code as a driving requirement, because wing design and not vertical tail design is the main driver of the rolling moment due to sideslip and the rolling moment due to aileron deflection.

4.3. LANDING WITH MAXIMUM CROSSWIND

The aircraft should be able to land in crosswinds that equal 20% of take-off speed. The equivalent of this is to hold an 11.5° sideslip at take-off speed. The necessary rudder deflection should again not be more than 20°. [5] In CS 25.147(f) [11] it is also stated that there must be enough excess lateral control in sideslip to allow a

limited amount of maneuvering and to correct for gusts. The equilibrium about the Z-axis can be rewritten to solve for the rudder deflection:

$$\delta_r = \frac{C_{n_\beta}\beta + C_{n_{\delta_a}}\delta_a}{-C_{n_{\delta_r}}} \tag{4.7}$$

The sideslip is set to 11.5°, and an aileron deflection of −25° is used as the worst case scenario for the lateral control necessary.

4.4. VERTICAL TAIL STALL

The vertical tail should not stall at high sideslip angles. Two methods are used to ensure that this requirement is met. The first is an approximation for the maximum sideslip angle at which the vertical tail will not stall. The second method uses an empirical boundary to prevent combinations of sweep and aspect ratio that lead to an increased likelihood of tip stall.

4.4.1. MAXIMUM SIDESLIP ANGLE FOR THE VERTICAL TAIL

The vertical tail should not stall at the high sideslip angles that it encounters during high crosswind and right after engine failure, before the pilot has applied corrective rudder action. The sideslip angles that should be managed without vertical tail stall are found in AMC 25.177(c) [11]. The angle is defined as:

$$\beta = \arcsin\left(\frac{V_{cw}}{V}\right) \tag{4.8}$$

The crosswind velocity indicated in AMC 25.177 is 30 knots or 15.5 m/s. It is also indicated that a sideslip angle of 15° is generally appropriate. [11] The angle is calculated in the code for take-off, cruise, and landing. For cruise the value from Equation 4.8 is used for the goal sideslip angle. For landing the angle is set at 15°, unless the value from Equation 4.8 is higher. At take-off the highest value from the three following options is selected: the 15° angle, the angle from Equation 4.8, or the maximum sideslip angle from the OEI calculation. The maximum sideslip angle from the OEI calculation is first multiplied with the sidewash to get the sideslip at the vertical tail.

The maximum sideslip angle for the current vertical tailplane design is predicted using a method for estimating the angle of attack at maximum lift. This method is different for low aspect ratio and high aspect ratio wings. Equation 4.9 is used to determine if a wing qualifies as a low aspect ratio wing. Equation 4.10 shows the area that is the boundary between low and high aspect ratio wings. These can be treated as either in the method. In the code it is chosen to treat them as low aspect ratio wings, as that method is better defined for transonic speeds. The factor C_1 is dependent on the wing taper ratio and is determined with Figure A.22.

$$A \leq \frac{3}{(C_1+1)\cos\Lambda_{LE}} \tag{4.9}$$

$$\frac{3}{(C_1+1)\cos\Lambda_{LE}} \leq A \leq \frac{4}{(C_1+1)\cos\Lambda_{LE}} \tag{4.10}$$

MAXIMUM LIFT CALCULATION FOR LOW ASPECT RATIO WINGS

The maximum lift and its corresponding angle of attack are both subdivided in two separately determined parts, as shown in Equations 4.11 and 4.12. These parts are a base part that represents $C_{L_{max}}$ and $\alpha_{C_{L_{max}}}$ if the lift-curve slope would be linear all the way to stall, and an additional part that represents the nonlinear top part of the curve. The additional part is different for subsonic and transonic speeds. The border between subsonic and transonic is put at Mach 0.6 in this method.

$$C_{L_{max}} = (C_{L_{max}})_{base} + \Delta C_{L_{max}} \tag{4.11}$$

$$\alpha_{C_{L_{max}}} = (\alpha_{C_{L_{max}}})_{base} + \Delta\alpha_{C_{L_{max}}} \tag{4.12}$$

The lift coefficient is determined with the help of Figures A.24, A.25, A.26, A.22, and A.27. The angle of attack at maximum lift is determined with Figures A.28, A.29, A.30. The parameter β in these figures is not the sideslip, but the Prandtl-Glauert factor that accounts for compressibility effects. It is dependent on the Mach number and follows from Equation 4.13. The sharpness parameter (Δy) is the vertical separation between the points on the upper surface of the airfoil at 0.15% and 6% of the airfoil chord (Figure A.23). Values of Δy for common airfoils are given in Table 4.2.

The factors that influence the angle of attack at $C_{L_{max}}$ and thus the maximum sideslip angle for the vertical tail are as follows: aspect ratio, leading edge sweep angle, taper ratio, and Mach number. For a maximum sideslip angle it is beneficial to have a low aspect ratio and a high leading edge sweep angle. The figures are defined for a wing and not for a vertical tail. The vertical tail aspect ratio is thus doubled before it is used as an input for these figures.

$$\beta = \sqrt{1 - M^2} \tag{4.13}$$

Airfoil type	Δy
NACA 4 digit	26 t/c
NACA 5 digit	26 t/c
NACA 64 series	21.3 t/c
NACA 65 series	19.3 t/c
Biconvex	11.8 t/c

Table 4.2: Sharpness parameter Δy for common airfoils [5]

MAXIMUM LIFT CALCULATION FOR HIGH ASPECT RATIO WINGS

The maximum lift for hight aspect ratio wings is calculated with Equation 4.14, where the first term estimates the $C_{L_{max}}$ at Mach 0.2 and the second term corrects for other Mach numbers.

$$C_{L_{max}} = c_{l_{max}} \left(\frac{C_{L_{max}}}{c_{l_{max}}} \right) + \Delta C_{L_{max}} \tag{4.14}$$

$\left(\frac{C_{L_{max}}}{C_{l_{max}}} \right)$ and $\Delta C_{L_{max}}$ follow from Figures A.31 and A.32. The airfoil maximum lift coefficient at Mach 0.2 ($c_{l_{max}}$) is calculated with the ESDU 84026 method [13]. The angle of attack at maximum lift is calculated with Equation 4.15. The first two terms represent the angle of attack if the lift curve would be linear until stall. The zero-lift angle ($\alpha_{L=0}$) is zero for the symmetric airfoils of a vertical tail. The angle of attack increment ($\Delta\alpha_{C_{L_{max}}}$) is determined with Figure A.33. The method does not cover transonic speeds for high aspect ratio wings. In the code the subsonic calculations are used instead and in Figure A.32 the lines are extrapolated to higher Mach numbers.

$$\alpha_{C_{L_{max}}} = \frac{C_{L_{max}}}{C_{L_\alpha}} + \alpha_{L=0} + \Delta\alpha_{C_{L_{max}}} \tag{4.15}$$

4.4.2. VERTICAL TAIL TIP STALL BOUNDARY

Tip stall is a stall in which the tip of the wing or vertical tail stalls first. For vertical tails with high sweep this can result in the center of pressure moving forward, which shortens the moment arm of the vertical tail and reduces its effectiveness. The subsonic boundary in Figure 4.3 is incorporated in the module as a constraint, to avoid the combinations of aspect ratio and sweep at which there is a danger of this effect occurring. The graph is defined for the pitch-up effect in wings, which is due to tip stall as well, and the difference in aspect ratio between normal wings and the vertical tail is taken into account.

4.5. DYNAMIC STABILITY ANALYSIS

The stability analysis so far has only focused on static stability and trim. For a full analysis the dynamic stability has to be analyzed as well. One of the elements of dynamic stability, dutch roll, is an important driver for vertical tail design. Dutch roll is a short period oscillation that is mainly caused by the dihedral effect. It makes the aircraft move from side to side, yawing and rolling. The vertical tail is the main damper of this effect. Until a full six degree-of-freedom (DOF) dynamic stability analysis has been performed, with preferably dynamic derivatives from windtunnel data, it is advised to not reduce the tail area below the statistical estimate that is the result of the coefficient method. One small exception to this is that the initial vertical tail area that is calculated with the coefficient method can be reduced by 10% when the aircraft uses a computerized “active” flight control system. This is only valid if the trim and engine-out requirements are met. [5] As a full six DOF dynamical analysis is not included in the module, a constraint has been added that limits the minimum vertical tail area to 90% of the initial value from the volume coefficient method of Chapter 2.1.

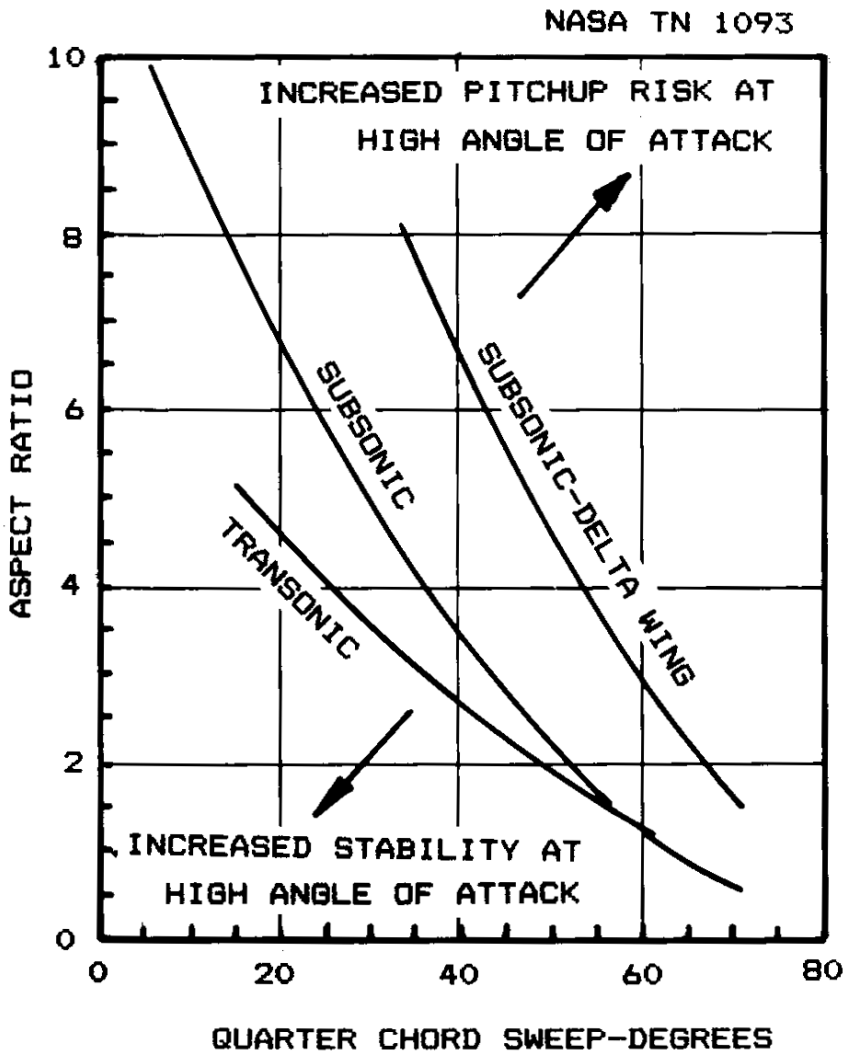

Figure 4.3: Tail-off pitch-up boundaries [2]

4.6. T-TAIL TAPER

For T-tail configurations it is important that the horizontal tail structurally fits on top of the vertical tail. If the taper ratio would be too small, then the top of the vertical tail might not offer enough space and structural rigidity to allow placement of the horizontal tail. For this configuration a constraint is added that ensures that the horizontal tail root chord is not more than 1.1 times larger than the vertical tail tip chord.

5

DIRECTIONAL STABILITY ANALYSIS MODULE

The Directional Stability Estimation (DSE) module is a design module in the Initiator that requires an aircraft's geometry and weight data. It uses these data to create an optimized design for the vertical tail span, aspect ratio, and sweep of a conventional aircraft. Wing, fuselage and horizontal tail geometry; engine thrust, position and nacelle length; and overall aircraft weight all impact the design of the vertical tail, so the module ideally should be placed behind the modules that determine these parameters in the design convergence. The current place of the module in this design convergence can be seen in Figure 5.1. This chart has been adapted from Reference [14]. It shows two black squares: the first indicates the sizing modules that make a first estimation of the aircraft design; the second black square indicates the design and analysis modules for more detailed design and analysis. The 'Other modules'-block includes many modules that are not necessary for the DSE module to run. The red squares indicate loops: an inner loop for the convergence of weight and aerodynamic loads, which excludes wing loading, and an outer loop for the convergence of wing loading and weights [14]. The module consists of four m-files in the module folder itself and many digitized graphs that

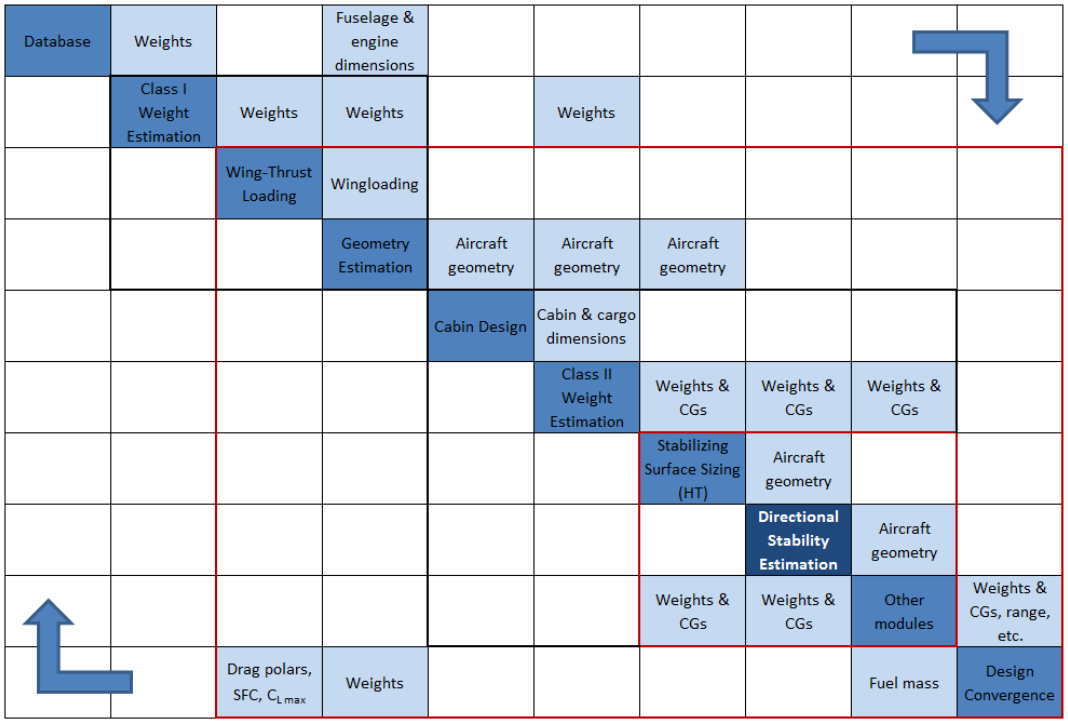

Figure 5.1: N2-chart detailing the position of the module within the design convergence

are found in the *Digitised Figures* folder. *DirectionalStabilityEstimation.m* is the file that contains the class definition. The file *run.m* is the file that is called by the Initiator when the module is run. It checks if the aircraft has a conventional configuration, and if so, it will run *VToptimization.m* and update the vertical tail design after the optimization has finished. If the aircraft does not have a conventional configuration it will show a warning message saying that no optimization has been performed and it will leave the vertical tail parameters unchanged. All the calculations are in the file *VToptimization.m* and this file contains two functions. The first is the optimization function, which optimizes for a minimum vertical tail area with the use of the *fmincon* function with an Sequential Quadratic Programming (SQP) algorithm. The variables in the optimization are the vertical tail span, aspect ratio, and sweep. These variables are normalized by dividing them with their initial values that follow from the volume coefficient method and the initial estimates for the parameters, as described in Chapter 2.1. More details on these variables are given in Table 5.1. The symbols with subscript 0 are the initial estimates. The objective function is defined in Equation 5.1.

Variable	$\bar{x}_0$	Parameter	Unit	Lower bound	Upper bound
x(1)	1.0	span (b_V)	[m]	0.5	3.0
x(2)	1.0	aspect ratio (A_V)	[-]	$0.5/A_{V_0}$	$2.0/A_{V_0}$
x(3)	1.0	sweep (Λ_V)	[deg]	0.0	$55/\Lambda_{V_0}$

Table 5.1: Vertical tail design variables for the optimization

$$\text{objective function} = \frac{\frac{[x(1)b_{V_0}]^2}{x(2)A_{V_0}}}{S_{V_0}} \tag{5.1}$$

The second function in *VToptimization.m* defines the nonlinear constraints that are used in the optimizer, which are described in Chapter 4. The calculation of the parameters that are used in determining these nonlinear constraints is performed with the methods for static stability analysis as described in Chapter 3. In both functions some extra calculations are performed first to make sure that the definition of the vertical tail parameters in the Initiator lines up with the definition in the methods for estimating lateral-directional stability. The main difference in definition is that the Initiator defines the vertical position of the vertical tail root chord as the most aft point where the vertical tail intersects with the fuselage. The stability estimation methods use the intersection of the mid-chord line and the mid-fuselage line, as can be seen in Figure 1.2. The constraints for the optimizer are shown in Figure 5.2. They are discussed in more detail in Chapter 4,

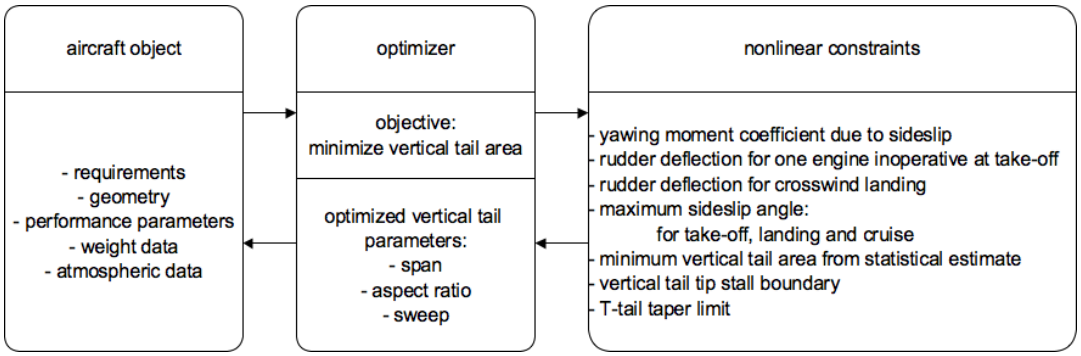

Figure 5.2: Overview chart of *VToptimization.m*

as well as the lateral-directional stability and control calculations that are necessary to evaluate these constraints. The calculations are first performed for cruise, and then in slightly modified form first for take-off and then for landing. Parameters that are not dependent on the flight phase, e.g. those that are independent of flight speed or flap setting, are calculated only once. Figure B.1 and the other figures in Appendix B show the organization of all calculations in increasing detail.

6

WINDTUNNEL TEST

A windtunnel experiment was conducted on a scaled model of a blended wing body (BWB) aircraft. The test was done at different angles of sideslip in order to gain insight into the stabilizing effect of the fuselage-wing combination and of the winglets. This chapter starts with a description of the windtunnel and the model that were used for the test, followed by a description of considerations and corrections for windtunnel testing. Finally the test set-up and test procedure are explained.

6.1. LOW SPEED WINDTUNNEL

The windtunnel tests were performed in the low speed low turbulence windtunnel of Delft University of Technology in Delft, The Netherlands. A schematic of this tunnel is shown in Figure 6.1. The windtunnel is an

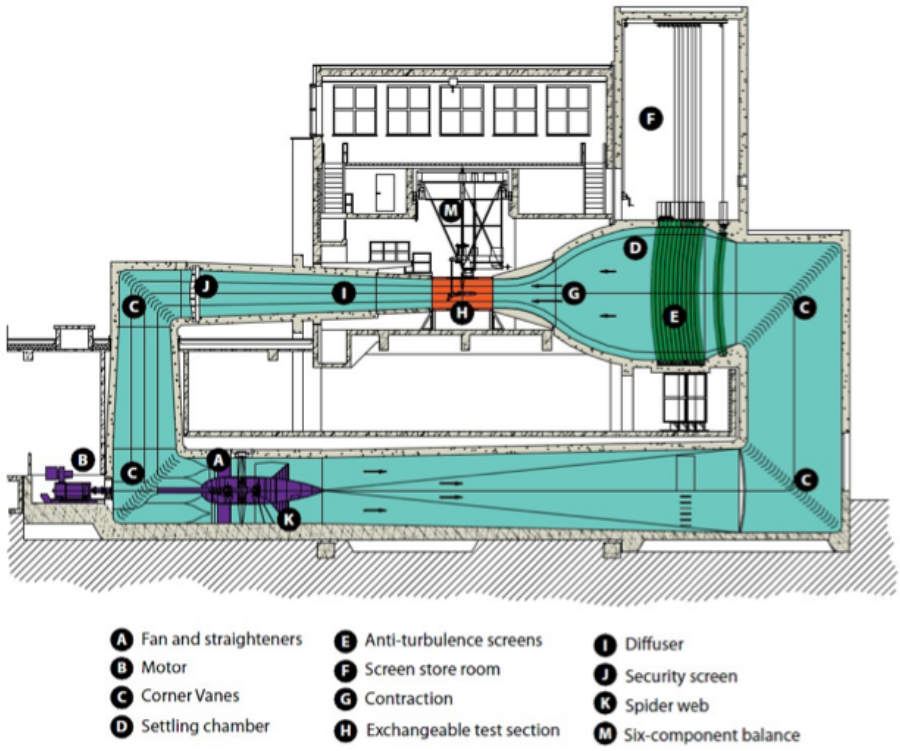

Figure 6.1: Schematic of the windtunnel [3]

atmospheric tunnel of the closed-throat single-return type. The contraction ratio of the windtunnel is 17.8 : 1 and the free-stream turbulence level in the test section varies from 0.015% at 20 m/s to 0.07% at 75 m/s. The

maximum velocity is 120 m/s and the maximum Reynolds number for two-dimensional testing is $3.5 \cdot 10^6$. There are ten interchangeable octagonal test sections, so that new tests can be prepared while another test is being conducted. All test sections have a width of 1.80 m, a height of 1.25 m, and a length of 2.60 m. The forces are measured with a six component balance.[1] The photo in Figure 6.2 shows the windtunnel, the balance, and the computers for the operator. The model is suspended upside down "belly up" in the windtunnel from three suspension arms that are part of the six component balance system that measures the forces. These suspension arms are surrounded by aerodynamically shaped covers that are meant to reduce the influence of the struts on the flow of air through the windtunnel. A system is built into the windtunnel that assures that the angle of incidence of these covers with respect to the flow direction remains the same, regardless of the sideslip angle.

Figure 6.2: Photo of the windtunnel

6.2. ZEFT WINDTUNNEL MODEL

The tests were performed on a model of a blended-wing-body aircraft that was developed at Delft University of Technology in 2010. The aircraft design is called the Zero Emission Flying Testbed (ZEFT) and it was developed as a demonstrator for a zero-emission unmanned aerial vehicle and as a testbed that allowed testing of new technologies for future full-scale BWB aircraft. It was designed for cruise speeds up to 300 km/h and a range of over 800 km. The windtunnel model has a span of 1.45 m and has six manually adjustable plain flaps on each wing and a single adjustable elevator at the rear. The winglets can be removed from the model, as can be seen in Figure 6.4b. The dimensions of the windtunnel model are shown in Figure 6.3 and Table 6.1. The middle suspension arm of the windtunnel is attached to the aft-part of the body of the model. The other two arms are attached to two points on the wing, as can be seen in Figure 6.4b.

6.3. WIND TUNNEL SET-UP AND TEST PROCEDURE

Test section #9 was used for these windtunnel tests. The windtunnel software was calibrated in such a way that it calculates the required data, such as the side force- and yawing moment coefficient. The input for these calculations are the force and moment data from the balance system and an input file that was prepared for previous windtunnel tests on the same model. The coefficients are all calculated with respect to the exact

[1] http://www.lr.tudelft.nl/organisatie/afdelingen/aerodynamics-wind-energy-flight-performance-and-propulsion/facilities/wind-tunnel-lab/low-turbulence-tunnel-lsl/ Accessed on 3-3-2015

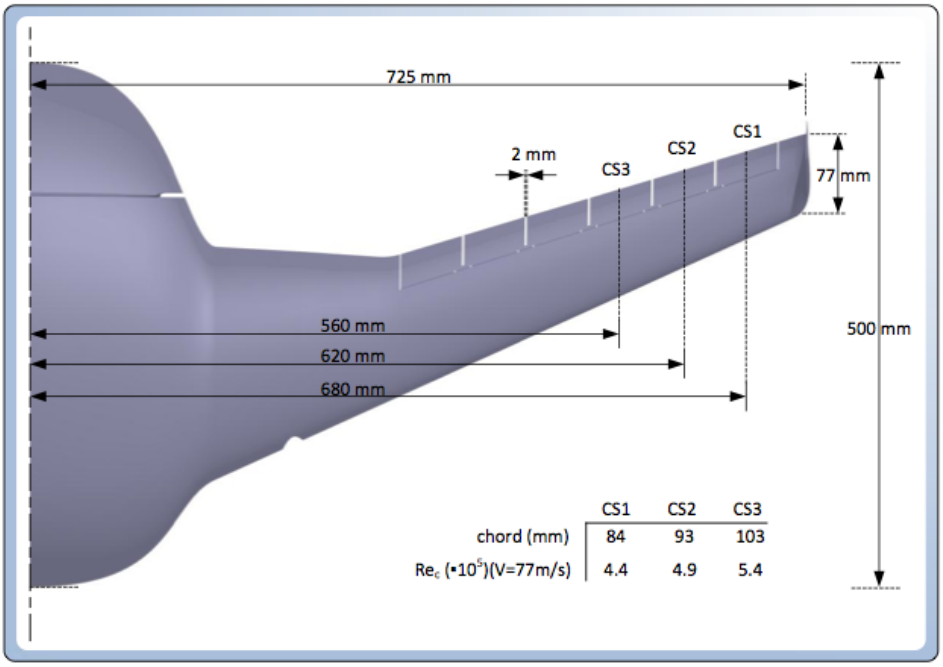

Figure 6.3: Dimensions of the ZEFT model [3]

Span	1.45 m
Wing area	0.2869 m^2
Aspect ratio	8.7
Mid-chord sweep	25 °
Chord (MAC)	0.1585 m
Length	0.5 m
Tip chord	0.077 m

Table 6.1: ZEFT model dimensions

middle of the test section. The suspension arms have been manually measured in the zero sideslip position to check if the model is actually positioned in the exact middle of the test section. This was found to be the case for both the longitudinal and vertical middle of the test section, with a difference of 0 – 0.5 mm and 0 mm respectively. The difference in the lateral positioning is slightly bigger with 1.5 mm. Adjusting this was not really possible. This lateral offset has no influence on the lift-, drag-, or pitch moment coefficient at a zero sideslip angle and thus it had no influence on previous experiments with the same model where a sideslip angle was not used. [15] This lateral difference might have a small influence on the side force coefficient and yawing moment coefficient, and on measurements taken while the model is at a nonzero sideslip angle. This is discussed further in Section 6.5.

Experiences from previous windtunnel tests on the same model [15] led to a selection of an airspeed of about 50 m/s for the tests. There were difficulties with obtaining reliable results at higher airspeeds. The mean aerodynamic chord of 0.1585 m and kinematic viscosity of [0.154]$m/^2s$ meant that a Reynolds number of approximately 515,000 was used. The adjustable flaps and elevator of the ZEFT model were put in neutral position for this test. The test comprised of two sets of ten series of measurements. The first set of measurements was performed with the winglets attached to the model, and the second test was performed with the winglets removed. Every series of measurements that was part of a set was at one of ten different sideslip angles, from zero to −15° with intervals of 2.5°, and at −20° and −25°. There was an additional measurement at 5° to check for symmetry. Within this series measurements were made at eleven different angles of attack, starting at −6° and increasing at 2° intervals to 14°. The angles that were used are also shown in Table 6.2.

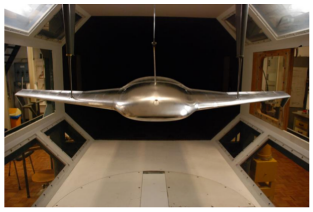

(a) Front view of the ZEFT model [3]

(b) ZEFT model without winglets

(c) ZEFT model at a sideslip angle

Figure 6.4: The ZEFT model suspended in the windtunnel

angle of sideslip, β [°]	angle of attack, α [°]
-25	-6
-20	-4
-15	-2
-12.5	0
-10	2
-7.5	4
-5	6
-2.5	8
0	10
5	12
	14

Table 6.2: Angles used for windtunnel test

6.4. WIND TUNNEL CORRECTIONS

The windtunnel results are corrected for wall effects by the software that is connected to the windtunnel. Five corrections are made: three block effect corrections for the model, the wake, and the slipstream, as well as corrections for wall interference and for buoyancy. The block effect correction is needed because the model, wake, and slipstream all affect the actual area of the cross section of the windtunnel. This difference in cross section needs to be corrected. The walls of the windtunnel are close enough to the model for the lift vortex to be mirrored in the walls. As a result the forces that are generated are different than if the walls were not there. The buoyancy correction deals with the boundary layer that is formed at the walls of the windtunnel.

6.5. WINDTUNNEL TEST RESULTS

The output of the windtunnel software is a collection of digital data files. A printed version of these data files can be found in Appendix D.1 for the test with the winglets attached to the model and in Appendix D.2 for the test with the winglets removed. The data files contain general test data and columns with data such as the angle of attack, lift coefficient, and velocity. The data files were imported into MATLAB and graphs of selected data were made for analysis. These graphs can be found in Appendix D.3; they show coefficients of interest plotted against the sideslip angle. Five graphs were made for every coefficient, showing:

- all measurements with winglets
- all measurements without winglets
- measurements at three selected angles of attack, both with and without winglets
- the difference between the measurements with and without winglets, for all angles of attack
- the difference between the measurements with and without winglets, for three angles of attack

The three selected angles of attack are [0]°, [4]°, and [8]°. These angles were selected because the data for higher angles, including α = [12]° and α = [14]° and sometimes α = [10]°, is often more erratic and sometimes shows different behavior due to flow separation at high angles of attack. Observations on the results and the resulting graphs are discussed in the following section.

6.5.1. OBSERVATIONS ON WINDTUNNEL RESULTS

The values at β = -5 are usually different from those at β = 5. Symmetry would suggest that they should be the same. A possible explanation might be the lateral offset of the model from the center of the test section of 1.5 mm combined with the fact that the coefficients are calculated with respect to the absolute center of the test section. The difference of 1.5 mm is however very small compared to the size of the model. The lines in Figure **??** seem to converge at β = -5, but not at β = 5. Both these discrepancies indicate that something in the set-up of the tests was not entirely correct and this questions the validity of the results. Only one positive sideslip angle was used for testing, so no more data is available for analysis of this difference. This also means that certain curves in the graph that show up at a sideslip angle of $-2.5°$ are not shown at 2.5°. The difference between β = -5 and β = 5 is not present when the difference between a model with and without winglets is plotted.

The graphs show a distinct bump or dip at sideslip angles of $-5°$ and $-2.5°$. A possible explanation for this dip was thought to be the shape of the front of the fuselage. A sudden change of shape in that part of the model could result in an adjustment of the flow. The shape of the model does however not show any clear changes in shape that could explain this dip. The effect of the winglets is clearly visible in Figure **??**; both side force and yawing moment are stronger with winglets, which is their desired effect. The side force and yawing moment both decrease with increasing angle of attack. An explanation for this is that part of the winglets are covered by the wake of the wing. It is noticeable that ZEFT is already stable in the yaw direction without the addition of winglets. Swept back wings tend to have a stabilizing effect and the body being wing-shaped does not have the destabilizing effect that a conventional cylindrical fuselage has. It might therefore also be worthwhile to investigate if estimations for wing-only stability derivatives, such as those given in Reference [16], can give an accurate prediction of the blended wing body stability derivatives.

Approximate values for the derivatives due to sideslip have been calculated. The graphs were assumed to be linear for these approximations. This allows comparison with typical values for the derivatives due to sideslip from conventional aircraft, as given in Reference [7]. Typical values for C_{y_β} range from -0.0017 to -0.0350. The ZEFT measurements are in the lower part of this range. Typical values for C_{n_β} range from 0 to 0.0070. The ZEFT measurements are very low in this range. This is not surprising, as the moment arm is much smaller than it would be for a conventional configuration.

- $(C_{y_\beta})_{\text{winglets}}$ = -0.00333
- $(C_{y_\beta})_{\text{clean}}$ = -0.00197
- ΔC_{y_β} = -0.002
- $(C_{n_\beta})_{\text{winglets}} = 4.67 \cdot 10^{-4}$
- $(C_{n_\beta})_{\text{clean}} = 3.67 \cdot 10^{-4}$
- ΔC_{n_β} = 0.133

7

VALIDATION AND CASE STUDIES

This section describes the procedure and results for the validation of the analysis method in the module for both conventional and unconventional aircraft, the case studies that were performed with the module, and the validation of the use of a vortex-lattice method for the estimation of lateral-directional stability.

7.1. VALIDATION OF THE APPLIED ANALYSIS METHOD FOR CONVENTIONAL AIRCRAFT

The first part of the module that were validated was the analysis method itself. The influences of the optimization in the module and the geometry estimation in the Initiator was negated by making a stand-alone, edited version of the Matlab module. The optimization of the vertical tail shape was omitted from this file and the input was not taken from the Initiator and its geometry files, but instead directly programmed into the file and based on data of existing aircraft. Three versions of this file were created, corresponding with the Fokker F-28 Mark 1000, Boeing 737-100, and Airbus A340-300. The B737 and A340 were chosen because they are the type of aircraft for which the Initiator is being developed, while also having windtunnel data available from the appendices in Reference [1]. The resulting data from both the Matlab-file and from the appendices of Reference [1] is shown in Tables 7.1, 7.2, and 7.3. Only those results for which corresponding reference values could be found are shown in the tables. The coefficients for which the calculated values do not line up with the reference values are discussed below.

7.1.1. VALIDATION RESULTS FOR THE AIRBUS A340-300

Most values for the Airbus A340-300 line up very well with their reference values. The main difference is observed for $C_{l_{\beta_{\mathrm{WFN}}}}$, which is underestimated for take-off and landing. This underestimation was even stronger when the parameter $(\Delta C_{n_\beta})_{\mathrm{f}}$ had not been introduced yet. Without $(\Delta C_{n_\beta})_{\mathrm{f}}$ the value for $C_{l_{\beta_{\mathrm{WFN}}}}$ at take-off and landing is -0.0016 and -0.0015 respectively. The value for $(C_{l_\beta}/C_{L_{\mathrm{W}}})$ is even more incorrect; this coefficient is part of the calculation of $C_{l_{\beta_{\mathrm{WFN}}}}$.

7.1.2. VALIDATION RESULTS FOR THE BOEING 737-100

For the Boeing 737-100 the value of $C_{l_{\beta_{\mathrm{WFN}}}}$ is again incorrect, but this time only for cruise. For the other two flight phases the values were -0.0024 and -0.0023 before the correction with $(\Delta C_{n_\beta})_{\mathrm{f}}$ was applied. $C_{n_{\delta_{\mathrm{r}}}}$ was underestimated and $C_{Y_{\delta_{\mathrm{r}}}}$ was overestimated; these coefficients are related, with the main difference in the equation being the moment arm. It is likely that the moment arm was underestimated in the inputs for the Matlab file, due to uncertainty as to the exact position of the center of gravity.

7.1.3. VALIDATION RESULTS FOR THE FOKKER F-28 MK 1000 MODEL 8-3

For the Fokker F-28 $C_{l_{\beta_{\mathrm{WFN}}}}$ is overestimated for both cruise and take-off. $(C_{l_\beta}/C_{L_{\mathrm{W}}})$ is correct for cruise, but Equation 3.14 only takes parameters into account that do not change with flight phase. The estimation is thus off for both take-off and landing. $\mathrm{C}_{\mathrm{n}_{\beta_{\mathrm{WFN}}}}$ is overestimated for all three flight phases, but the differences between cruise, take-off and landing are similar between the calculated and windtunnel values. This overestimation can be completely attributed to a difference in Reynolds number, which is an important factor in

the determination of $C_{n_{\beta_{WFN}}}$. The windtunnel test was performed on a 2 m long model at $Re = 1.4\dot{1}0^6$ and the dimensions of the real aircraft were the input for the Matlab file, with $Re \approx 1.5\dot{1}0^7$ for take-off and landing and $Re \approx 2.3\dot{1}0^7$ for cruise. The same calculation is shown in the table with windtunnel results in Reference [1] and this shows a value for $C_{n_{\beta_{WFN}}}$ of -0.00146. The result of $C_{n_{\beta_{WFN}}}$ being more negative than expected is that C_{n_β} is underestimated, even though there is a bit of an overestimation for $C_{n_{\beta_V}}$ and $C_{Y_{\beta_V}}$. The total sidewash is overestimated, which is due in part to an overestimation of the sidewash due to the fuselage. Not all components of the total sidewash could be checked, so it is hard to pinpoint the other reasons for the difference. The overestimation of the total sidewash does explain why both $C_{n_{\beta_V}}$ and $C_{Y_{\beta_V}}$ are overestimated as well, as they are directly related: see Equation 3.19.

7.1.4. VALIDATION CONCLUSIONS

Overall, the most frequent inaccuracy is in the estimation of $C_{l_{\beta_{WFN}}}$. It is advisable to look into other estimation methods for this coefficient, preferably methods that adapt well to different flap settings and angles of attack. Many of the other differences can be attributed to the estimation being an average over a large sample of aircraft, where the data for the aircraft in question are not in line with this average. This is the case for the sidewash due to the fuselage, or fuselage-fin interference factor, for example.

7.2. CASE STUDIES FOR VERTICAL TAIL OPTIMIZATION FOR CONVENTIONAL AIRCRAFT

The first method of comparison attempted is to write a specific input file for the Initiator that closely resembles the specifics and dimensions of an actual aircraft, of which preferably some windtunnel measurement data are known. The Directional Stability Estimation module is then run in the Initiator using that specific input file. The resulting vertical tail design and the calculated data that the design is based on are then compared to the actual vertical tail design and windtunnel data of the specific aircraft. The problem with this method lies in the design of the aircraft geometry within the Initiator. The geometry in the input file has to be complete in order for the Initiator not to run the Geometry Estimation module. The final aircraft design for these incomplete input files in the Initiator turns out to be too different from the geometry of the aircraft that was used as an input. An input file with just the most critical geometrical characteristics is not sufficient. There are four input files that already have a complete geometry and that have been proven to run reliably in the Initiator; these were used in the case studies. These input files still differ slightly in geometry, mass, and other characteristics from the original aircraft. This is due sometimes to slight differences in geometrical definitions, and other times to the demands of the Initiator; for example, most input files have a lower range requirement than the actual range of their real world counterpart, as selecting a more realistic range often leads to errors. These geometrically fully defined input files have GEOM at the end of their file-names, and from now on will be called GEOM-files.
Next to the GEOM-files, other more basic input files that more closely represent the full working of the Initiator were used in the case studies as well. These will additionally show the difference with the initial estimate from the Geometry Estimation module. Not only the aircraft models that were the basis for the input files were chosen as reference aircraft, but also some other aircraft models with a similar role and configuration. The four different cases and the aircraft used in them are listed below (dse indicates an input file that was adapted from original file in the Initiator to more closely resemble the aircraft in question). Behind every entry it is indicated if data for this aircraft was used as a reference, or if it was used as an input file for an optimization in the Initiator.

- Aircraft that seat around 300 passengers in a 3-class set-up, with wing mounted engines
  - Airbus A340-300 (reference)
  - Airbus A350-900 (reference)
  - Boeing 777-200 (reference)
  - Boeing 787-10 (reference)
  - A340-300dse (input file)
  - B777-300 (input file)
- Aircraft that seat around 150 passengers in a 2-class set-up, with wing mounted engines

  - Airbus A320-200 (reference)
  - Boeing 737-800 (reference)
  - Bombardier CS300 (reference)
  - A320-200-GEOM (input file)
  - B737-800-GEOM (input file)
  - A320-200 (input file)
- Aircraft that seat around 100 to 150 passengers in a 2-class set-up, with fuselage mounted engines
  - Fokker F100 (reference)
  - Boeing 717-200 (reference)
  - McDonnell Douglas DC-9-30 (reference)
  - McDonnell Douglas MD-88 (reference)
  - MD-80-GEOM (input file)
  - F100 (input file)
  - MD-80dse (input file)
- Aircraft that seat around 250 passengers in a 3-class set-up, with two wing and one vertical tail mounted engines
  - McDonnell Douglas DC-10-30 (reference)
  - Lockheed L-1011 TriStar (reference)
  - DC10-30-GEOM (input file)
  - DC10-30 (input file)

The initial optimizations optimized four different variables for the vertical tail: span, aspect ratio, sweep, and taper ratio. It was found that for some aircraft with conventional tail configurations, the end result had taper ratios that were close to one, so much higher than expected. It is thus not sufficiently suited to optimizing the taper ratio and therefore it was decided only to optimize for three variables: span, aspect ratio, and sweep. Results for both three and four variables can still be observed in Figure 7.2a. The resulting vertical tail areas are normalized with the wing area and then plotted against the wing area in Figures 7.1 and 7.2. The initial value from the volume coefficient method in Chapter 2.1 is linked to the optimized result with a dotted line. The figures show that this initial estimation that was present in the Initiator is too low, and that the new estimations based on static stability are much closer to the vertical tail areas observed in actual aircraft. A general trend is visible in that the normalized vertical tail area seems to decrease with increasing wing area for the reference aircraft. This effect is not present in the analysis method and as a result the vertical tail area is slightly underestimated for smaller aircraft and overestimated for larger aircraft. All cases are mainly driven by the suggested goal values for the yaw moment coefficient due to sideslip. This goal coefficient is only dependent on the Mach number during cruise and does not adjust for aircraft size. The end result for aircraft such as the McDonnell Douglas DC-10-30 is reasonably accurate, despite the difference of having an engine in the tail. The calculation of the tail span and area is such that the approximate effective area of the engine is taken into account, but this is the only way in which the tail-engine is accounted for.

7.3. VALIDATION OF THE APPLIED ANALYSIS METHOD FOR BLENDED WING BODIES

The applicability of the analysis method to blended wing body aircraft configurations was tested as well. This was done by creating a special version of the module in which the airplane dimensions of the ZEFT model were a direct input for the file. The file was adapted further by deleting parts of the calculations that are too specific to a conventional aircraft lay-out. Examples of this are the sidewash calculations that are no longer applicable, as the vertical tail at the rear of the aircraft has been replaced by two winglets in a completely different position. The basic approximations for the tail-off side force, yawing, and rolling moment coefficients were maintained, as well as the basic equations for side force, yawing, and rolling moment coefficients for

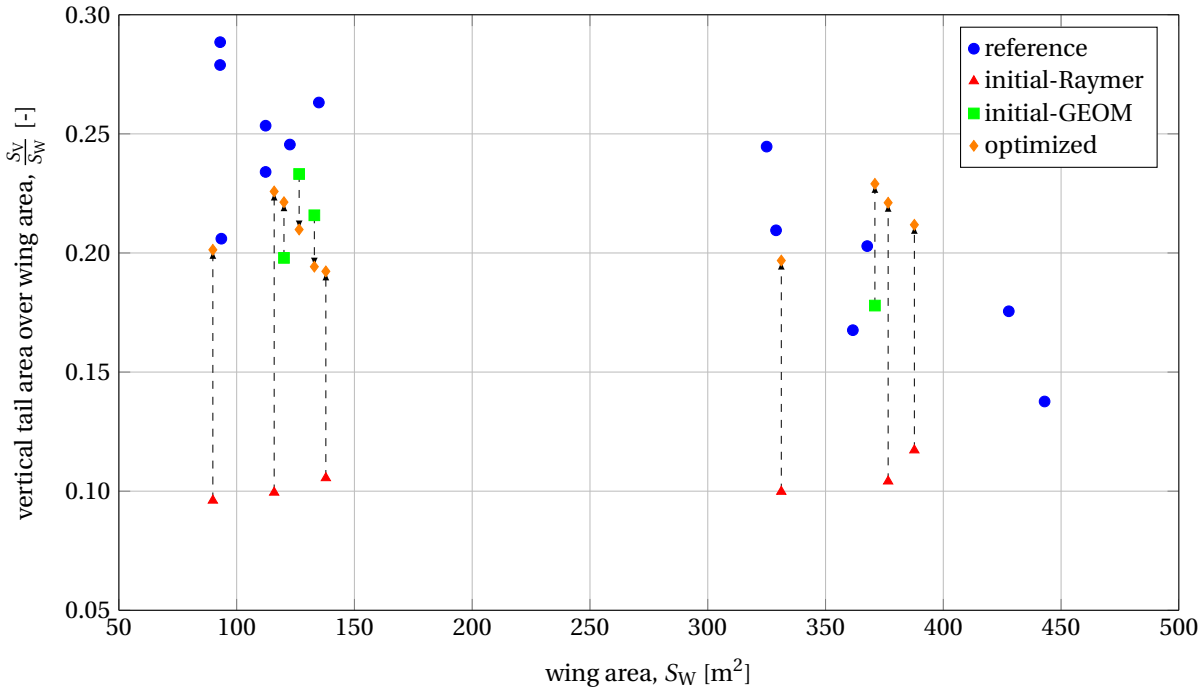

Figure 7.1: Combined case study results

the vertical tail only. The results are plotted in three graphs in Figures 7.5, 7.3 and 7.4 for the three coefficients along with windtunnel results from the tests described in Section 6. The results of the reduced analysis method hardly differ for variances in the angle of attack and are thus represented by a single line in the graph. The figures show that the tail-off or clean coefficients are consistently incorrect. This result was somewhat expected, as the equations used are based on empirical relations for conventional configurations. The values for total side force, yawing moment, and rolling moment are thus incorrect as well. The effect of the winglets is reasonably approximated for the side force and yawing moment; this can be deduced from the difference between the results for clean and winglet configurations.

7.4. AVL AS ANALYSIS METHOD

AVL (Athena Vortex Lattice) is a software tool that uses a vortex-lattice method for aerodynamic analysis. The configurations for which it works best are thin lifting surfaces at small angles of attack and sideslip. The experience with modeling fuselages in AVL is relatively limited, but its results are consistent with slender-body theory [1].

Two aircraft were modeled in AVL: the Fokker F-28 and the ZEFT blended wing body windtunnel model. The models are shown in Figures C.1 and C.2, and the AVL input files can be found in Appendix E. Both models use a vertical plane to model the fuselage. As a method of estimating side force and yawing moment data. This vertical plane is modeled to represent the shape of the fuselage. AVL was run for variations of the angle of attack and sideslip for which windtunnel data is available, with the stability derivatives as the output file.

7.4.1. CONVENTIONAL AIRCRAFT CONFIGURATION IN AVL

The AVL runs for the F-28 model were done at three angles of attack that were also used in the windtunnel tests from Reference [1] that will be used as a reference: 0.1°, 5.3°, and 9.5°. The AVL model from Figure C.1 was used for the test runs on the whole aircraft, which is indicated as WFVH in the graphs. A different input file in which the vertical and horizontal tail were deleted was used for the tail-off test runs, indicated as WF. The results for side force, yawing moment, and rolling moment will be discussed separately.

[1] http://web.mit.edu/drela/Public/web/avl/avl_doc.txt, accessed on 10-3-2015

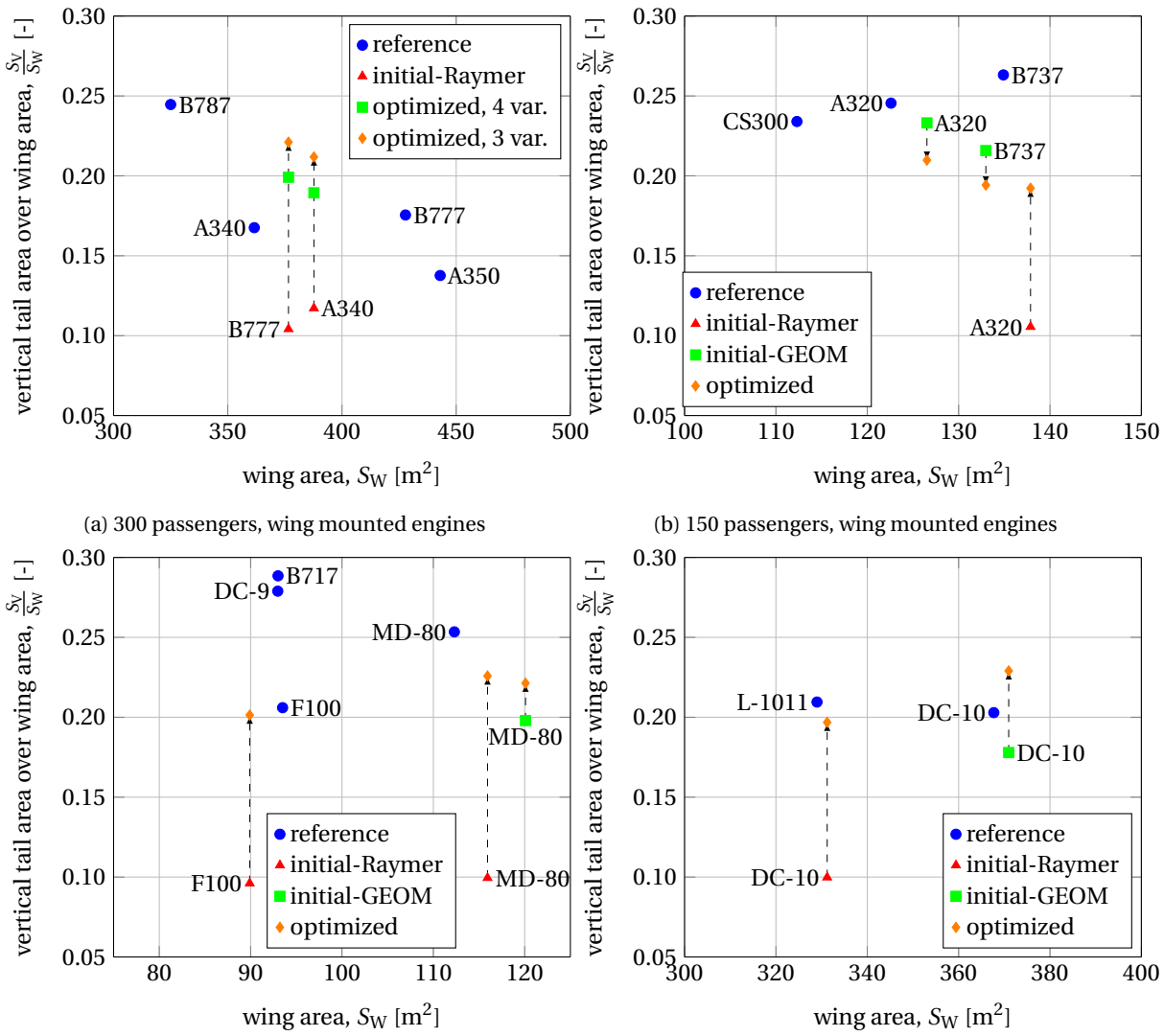

(a) 300 passengers, wing mounted engines

(b) 150 passengers, wing mounted engines

(c) 100–150 passengers, fuselage mounted engines

(d) 250 passengers, 3 engines

Figure 7.2: Case study results for four separate cases

SIDE FORCE

The results for the side force are found in Figures 7.6. It should be noted that the windtunnel test results for angles of attack (α) of 0.1° and 5.3° are the same. The main observation for the tail-off configuration is that AVL predicts a decreasing side force with increasing angle of attack that does not occur in the windtunnel tests. The accuracy at low angles of attack seems good. The effect of the vertical tail is predicted well up to angles of sideslip of −10°; after that the results diverge and AVL under-predicts. This divergence at higher sideslip angles is also seen for the tail-off configuration.

ROLLING MOMENT

For the rolling moment coefficient only reference data for the tail-off configuration was found. AVL overestimates this tail-off rolling moment coefficient at all angles of attack.

YAWING MOMENT

The yawing moment coefficient is shown in Figure 7.8 for the tail-off and total yawing moment coefficient, and in Figure 7.9 for the effect of the vertical tail only. This effect of the vertical tail is estimated correctly, with some divergence at sideslip angles over −15°. The destabilizing effect of the tail-off yawing moment however is underestimated, especially for larger sideslip angles. As a result, the total yawing moment is off as

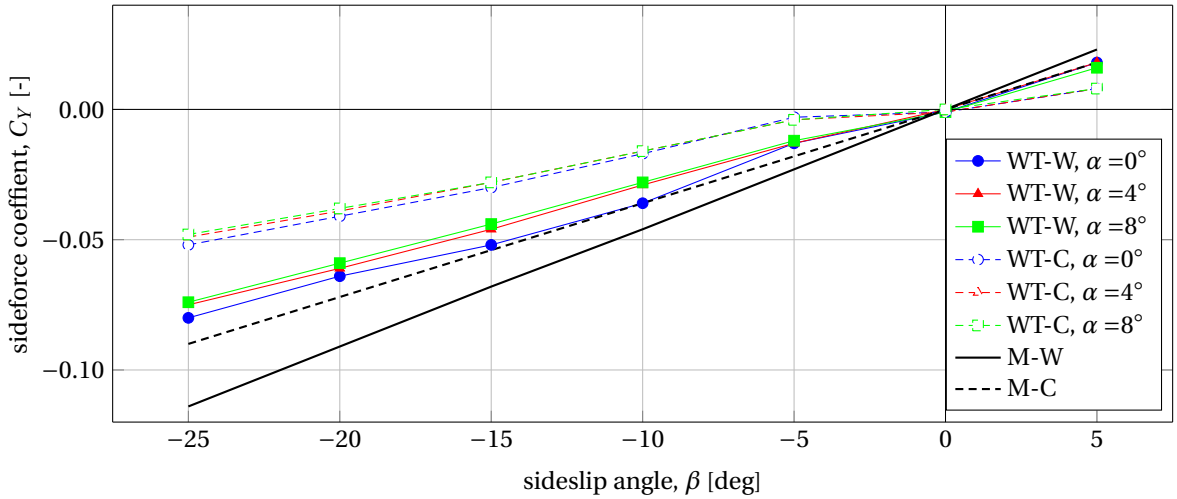

Figure 7.3: Sideforce versus sideslip for ZEFT model

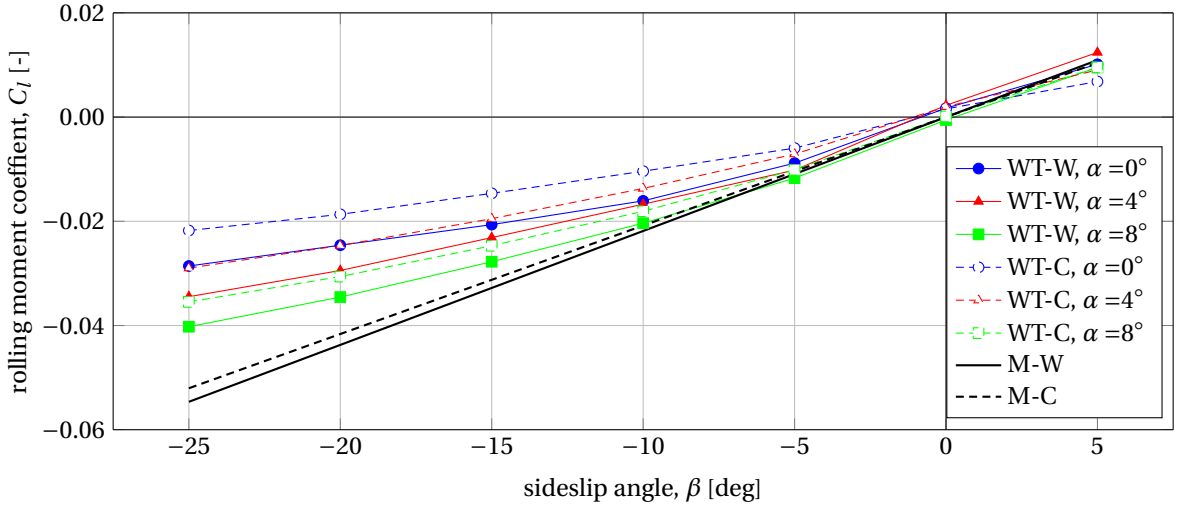

Figure 7.4: Rolling moment versus sideslip for ZEFT model

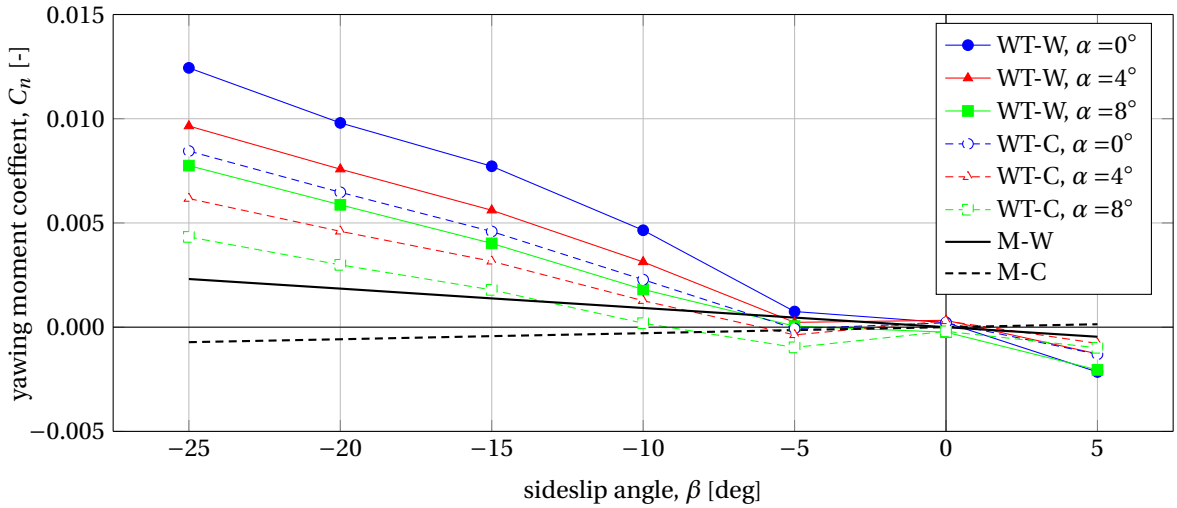

Figure 7.5: Yawing moment versus sideslip for ZEFT model

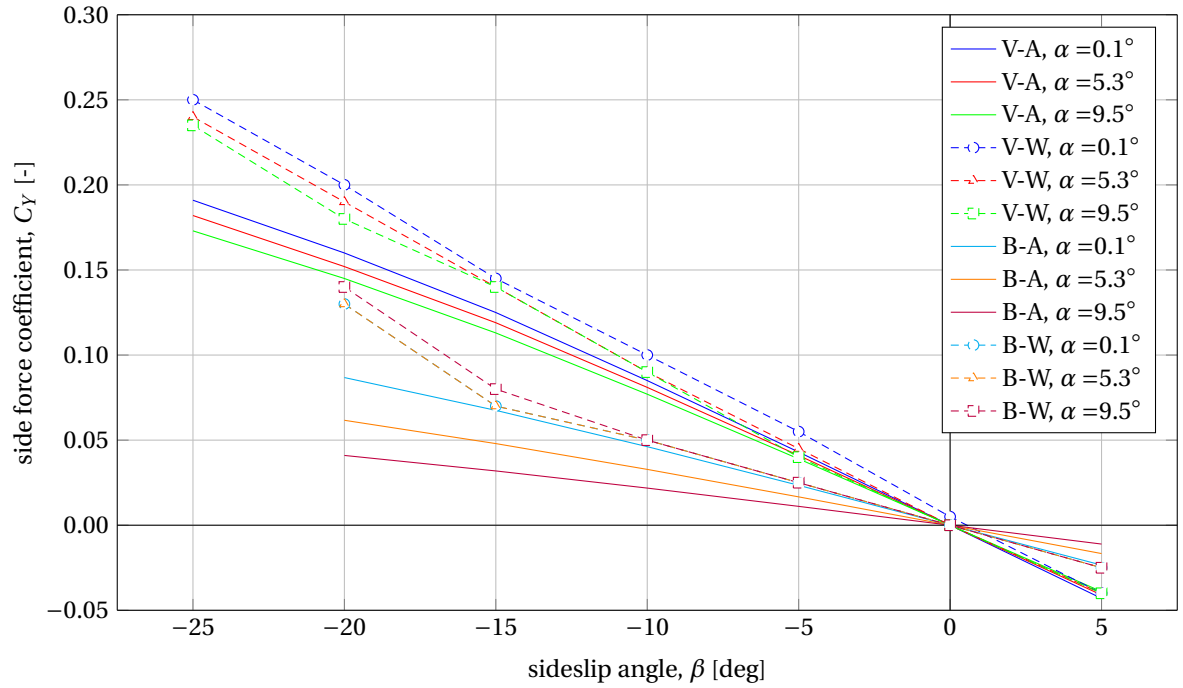

Figure 7.6: Comparison of AVL (A) and windtunnel (W) results for the Fokker F-28, of the side force coefficient (C_Y) versus sideslip angle (β) for the wing-body alone (B) and for the vertical tail (V)

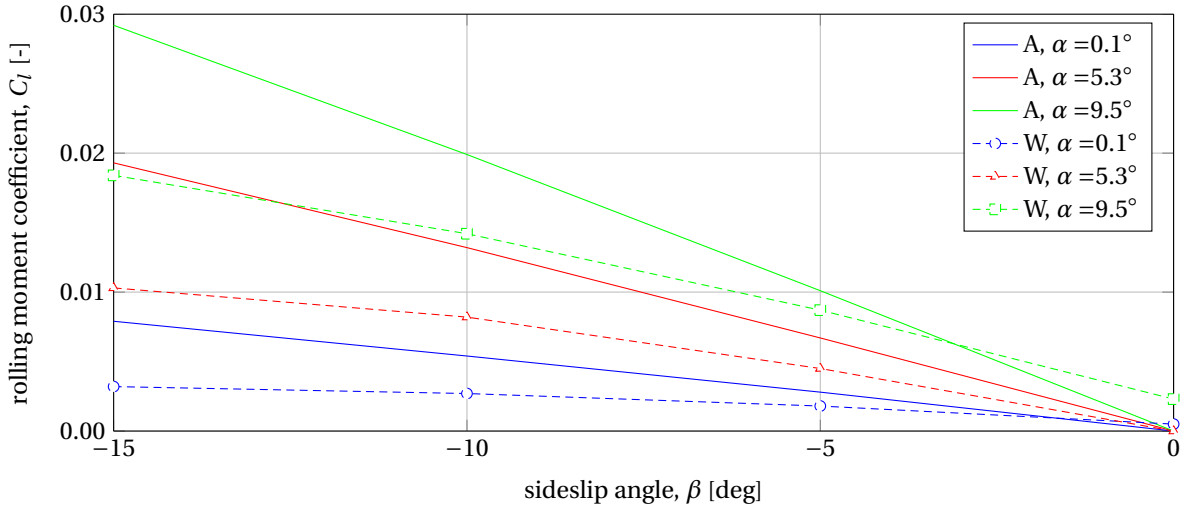

Figure 7.7: Comparison of AVL (A) and windtunnel (W) results for the Fokker F-28, of the rolling moment coefficient (C_l) versus sideslip angle (β) for the body without tail

well. Again, there is a bigger difference between the results at varying angles of attack than in the windtunnel results, with the low angle of attack being the most accurate.

7.4.2. BLENDED WING BODY IN AVL

The AVL runs for the ZEFT model were done at three different angles of attack that were used in the windtunnel tests discussed in Chapter 6: 0°, 4°, and 8°. The AVL model from Figure C.2 was used for the test runs on the whole aircraft, which has no special indication in the graphs. A different input file in which the winglets were deleted was used as well, and these runs are indicated as 'Clean.' A third input file without winglets and the vertical representation of the body was used as well, but only tested at AoA = 0°. This is meant to test if applying the vertical surface has the desired effect.

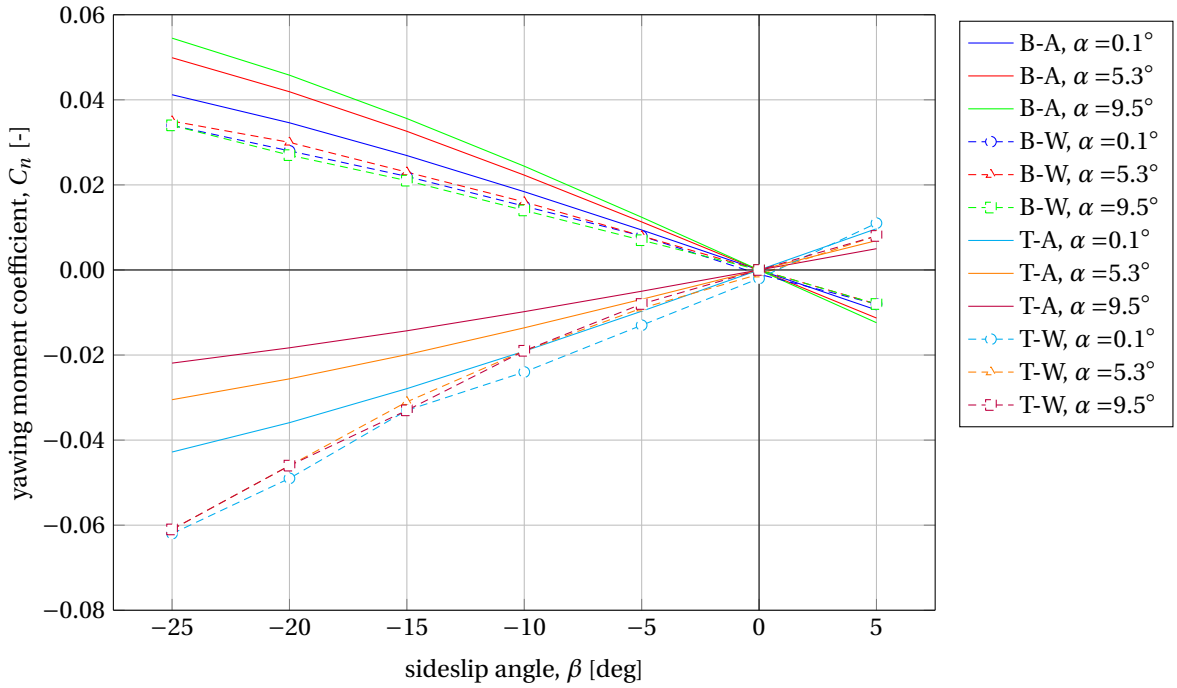

Figure 7.8: Comparison of AVL (A) and windtunnel (W) results for the Fokker F-28, of the yawing moment coefficient (C_n) versus sideslip angle (β) for the body alone (B) and for the whole aircraft (T)

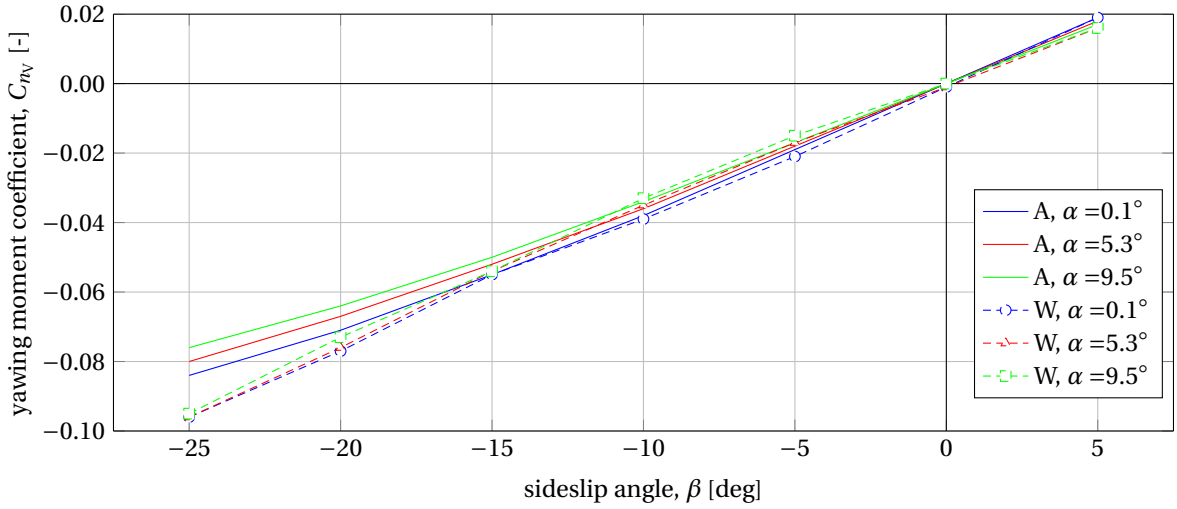

Figure 7.9: Comparison of AVL (A) and windtunnel (W) results for the Fokker F-28, of the yawing moment coefficient (C_n) versus sideslip angle (β) for the vertical tail

SIDE FORCE

The results for the side force are shown in Figures 7.10 and 7.11. AVL does not show the nonlinear behavior around a sideslip angle of −5°, and for the clean configuration the results start to diverge again when the sideslip goes beyond −10°. The results at low angles of attack are better than for higher angles. Not using the vertical surface to represent the body clearly leads to an underestimation. The effect of the winglets is accurately reflected up to a sideslip of −10° for AoA = 0°, but diverges earlier for higher angles of attack.

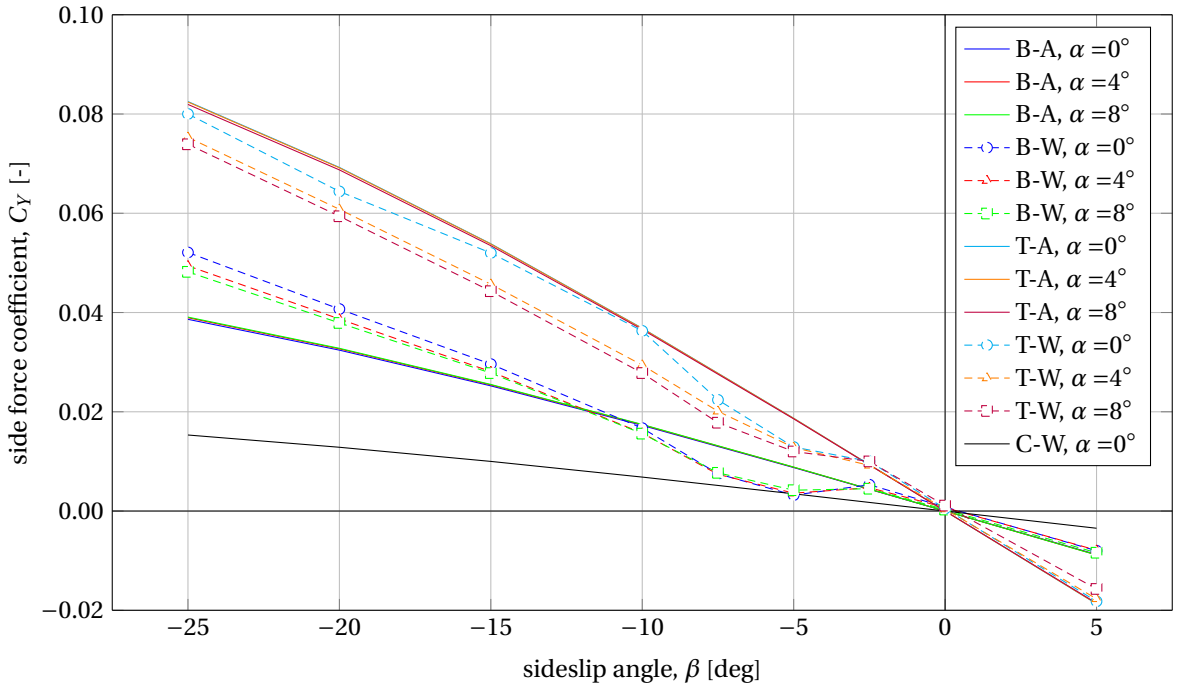

Figure 7.10: Comparison of AVL (A) and windtunnel (W) results for the ZEFT model, of the side force coefficient (C_Y) versus sideslip angle (β) for the clean wing-body alone (B), the whole aircraft (T), and the clean wing (C)

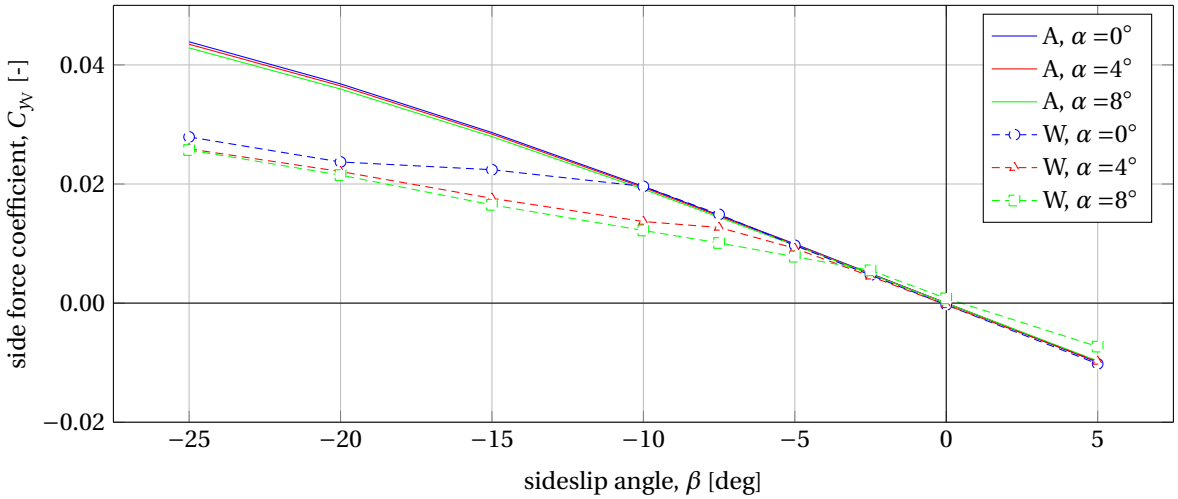

Figure 7.11: Comparison of AVL (A) and windtunnel (W) results for the ZEFT model, of the change in side force coefficient due to winglets (C_{Y_V}) versus sideslip angle (β)

YAWING MOMENT

The results for the yawing moment are shown in Figures 7.12 and 7.13. For the yawing moment the results from AVL for the effect of the winglets are reasonably accurate up to sideslip of −15°, although the windtunnel results are less linear. The yawing moment for the wing-body only, however is not accurate. For this configuration the windtunnel tests show highly nonlinear behavior up to sideslip angles of −10°. The windtunnel tests further show that the wing-body alone is already stable, except for higher angles of attack combined with a sideslip angle around −6°. The AVL results show an unstable wing-body that is made stable by the addition of winglets, which is similar in characteristics to conventional aircraft. Modeling the wing-body without a vertical body surface has as a result that the estimated yawing moment is close to zero.

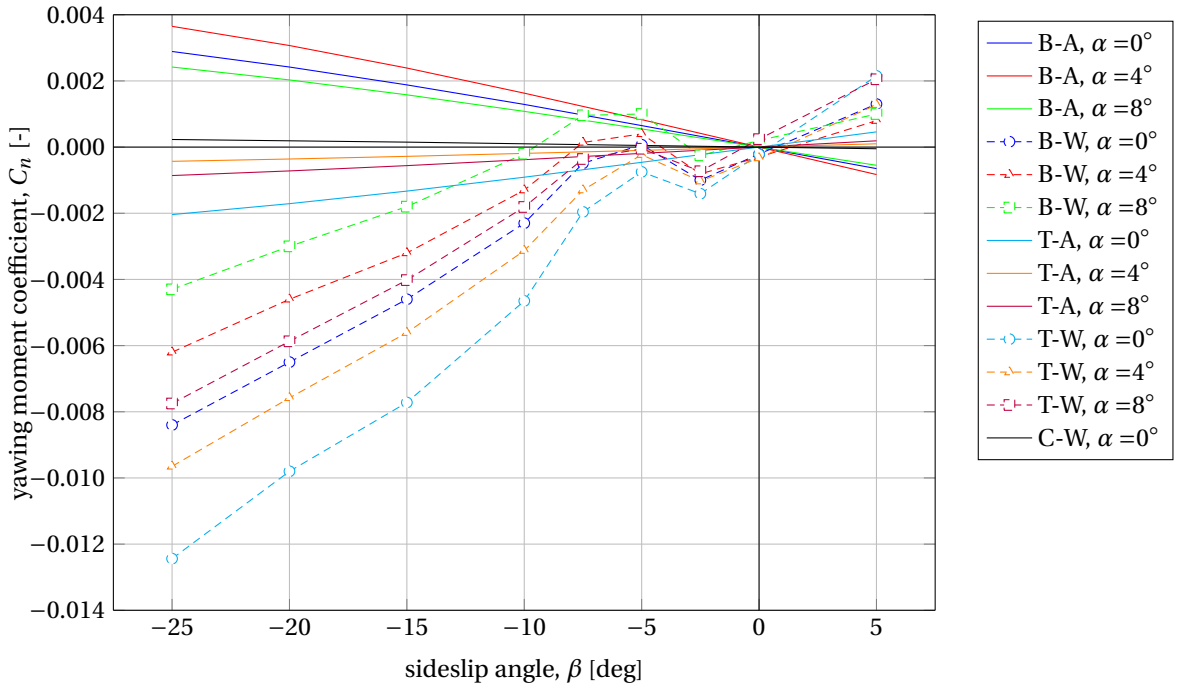

Figure 7.12: Comparison of AVL (A) and windtunnel (W) results for the ZEFT model, of the yawing moment coefficient (C_n) versus sideslip angle (β) for the clean wing-body alone (B), the whole aircraft (T), and the clean wing (C)

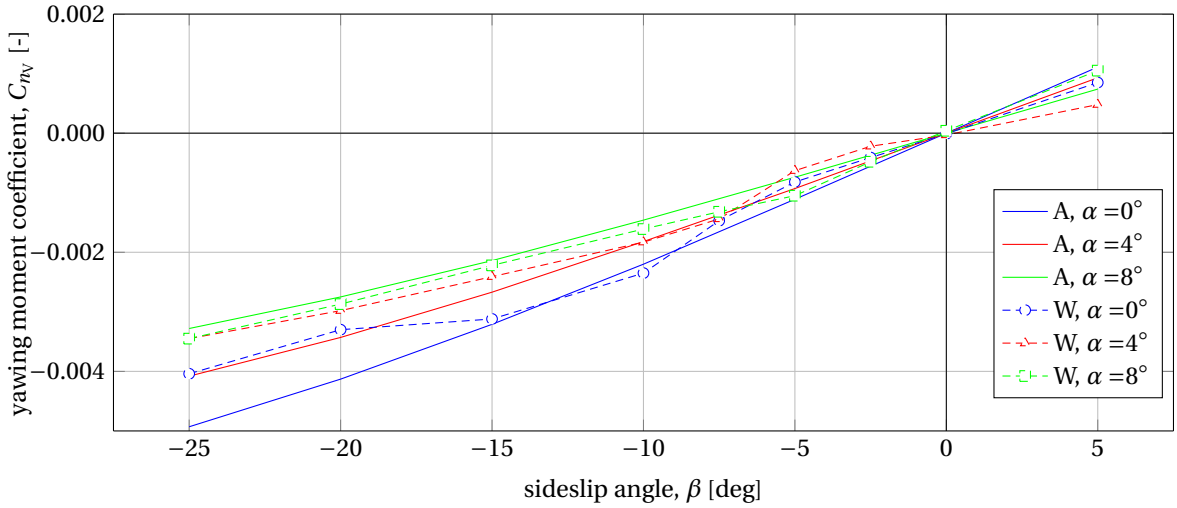

Figure 7.13: Comparison of AVL (A) and windtunnel (W) results for the ZEFT model, of the change in yawing moment coefficient due to winglets (C_{n_V}) versus sideslip angle (β)

ROLLING MOMENT

The results for the rolling moment are shown in Figures 7.14 and 7.15. The clean and total rolling moment results seem relatively reasonable approximations for sideslip angles up to −5°; the results start to diverge at higher sideslip angles. The graph for the effect of the winglets shows however that the results are not as accurate as they appear from the graphs for the clean and total rolling moment. The inclusion of the vertical surface that represents the body has no effect on the rolling moment estimation.

7.4.3. CONCLUSIONS FOR THE USE OF AVL

The first conclusion that can be drawn is that the results at higher angles of attack and sideslip are not accurate enough. The estimation of the tail-off rolling moment for conventional aircraft is inaccurate as well. The biggest issue for the application of AVL for the stability estimation of blended wing bodies is the inac-

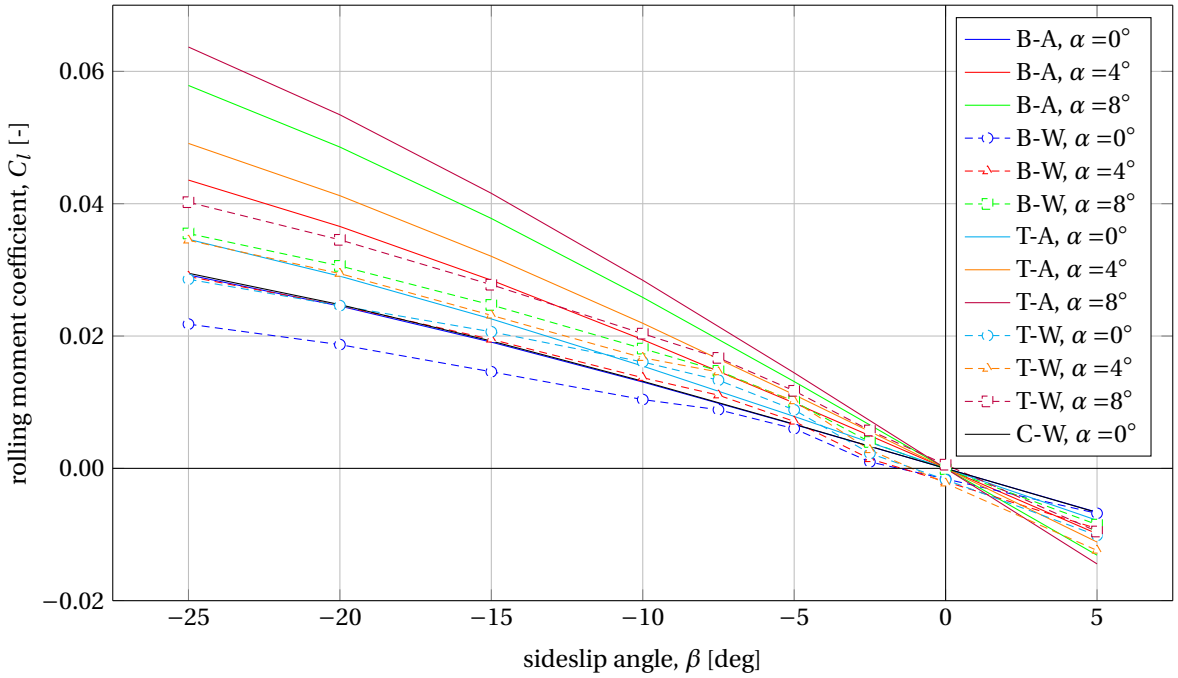

Figure 7.14: Comparison of AVL (A) and windtunnel (W) results for the ZEFT model, of the rolling moment coefficient (C_l) versus sideslip angle (β) for the clean wing-body alone (B), the whole aircraft (T), and the clean wing (C)

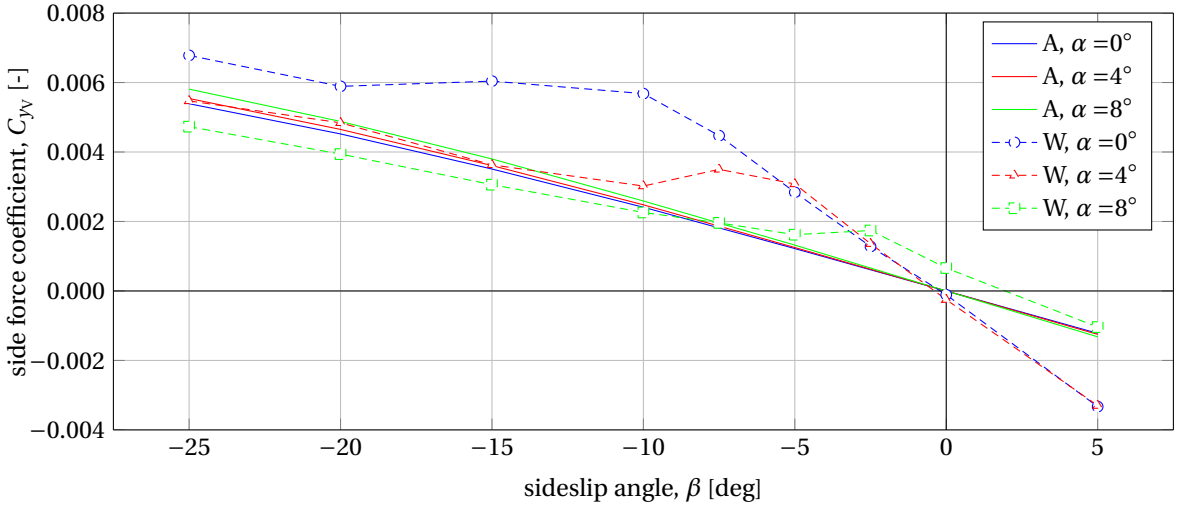

Figure 7.15: Comparison of AVL (A) and windtunnel (W) results for the ZEFT model, of the change in rolling moment coefficient due to winglets (C_{l_V}) versus sideslip angle (β)

curate estimation of the yawing moment for the wing-body combination. The inclusion of a vertical surface to represent the body or fuselage is especially useful for the estimation of the side force. In general it can be concluded that the results from AVL are not accurate enough for both the yawing moment and the required range of angles of attack and sideslip for AVL to be used to estimate lateral-directional stability in the Initiator.

Table 7.1: Validation results for the Airbus A340-300

	Cruise			Take-off			Landing		
	Method	Reference	% Difference	Method	Reference	% Difference	Method	Reference	% Difference
$C_{L_{\alpha_V}}$	0.0368	0.0367	0.3	0.0347			0.0329		
$C_{l_{\beta_{WFN}}}$	-0.0015	-0.0018	-19.3	-0.0023	-0.0040	-59.6	-0.0033	-0.0048	-68.7
$\left(\frac{C_{l_\beta}}{C_{L_W}}\right)$ (deg)	-0.0020	-0.0012	63.0	-0.0020			-0.0020		
$\frac{C_{l_\beta}}{\Gamma}$	-0.00021	-0.00022	-2.6						
$C_{l_{\beta_\Gamma}}$	-0.0010	-0.0011	-3.3						
$C_{n_{\beta_V}}$	0.0037	0.0036	3.6	0.0031	0.0034	-9.1	0.0030	0.0033	-10.1
$C_{n_{\delta_r}}$		-0.0013		-0.0014			-0.0013	-0.0013	0.0
$C_{Y_{\beta_V}}$	-0.0081	-0.0076	6.3	-0.0069	-0.0073	-5.9	-0.0066	-0.0071	-6.6
$C_{Y_{\delta_r}}$				0.0030			0.0027	0.0032	-15.9
K_{VH}	1.103	1.080	2.1	0.983			0.886		
$\frac{q_V}{q} K_{FV}$	0.940	0.940	0.0	0.971	1.010	-3.8	1.005	1.065	-5.6
$\left(1+\frac{\partial\sigma}{\partial\beta}\right)_F \frac{q_V}{q} K_{FV}$	1.2444	1.3300	-6.4	1.2444			1.2444		
$\left(\Delta\frac{\partial\sigma}{\partial\beta}\right)_{h_W} \frac{q_V}{q} K_{FV}$	0.0922	0.0810	13.8	0.0922			0.0922		
$\left(\Delta\frac{\partial\sigma}{\partial\beta}\right)_{\Gamma\Lambda} \frac{q_V}{q} K_{FV}$	-0.1034	-0.1160	-10.9	-0.1034			-0.1034		
$\left(\Delta\frac{\partial\sigma}{\partial\beta}\right)_{\delta_f}$	0			0.012			0.024	0.020	20.0
$\left(1+\frac{\partial\sigma}{\partial\beta}\right)_{total}$	1.3363	1.2930	3.3	1.1329	1.1650	-2.8	1.0516	1.0740	-2.1

Table 7.2: Validation results for the Boeing 737-100

	Cruise			Take-off			Landing		
	Method	Reference	% Difference	Method	Reference	% Difference	Method	Reference	% Difference
$C_{L_{\alpha_V}}$	0.0416	0.0425	-2.0	0.0395			0.0379		
$C_{l_{\beta_{WFN}}}$	-0.0022	-0.0009	145.7	-0.0031	-0.0030	2.5	-0.0039	-0.0045	13.4
$C_{n_{\beta_V}}$	0.0061	0.0059	2.8	0.0057	0.0060	-4.3	0.0048	0.0062	-22.9
$C_{n_{\delta_r}}$				-0.0021	-0.0027	-21.8	-0.0020		
$C_{Y_{\beta_V}}$	-0.0157	-0.0176	-11.0	-0.0148	-0.0165	-10.4	-0.0124	-0.0125	-1.0
$C_{Y_{\delta_r}}$				0.0054	0.0060	-10.4	0.0049		
K_{VH}	1.061	1.060	0.1	0.969			0.899		
$\frac{q_V}{q} K_{FV}$	0.940	0.940	0.0	0.971	0.970	0.1	0.995	1.045	-4.8
$\left(1 + \frac{\partial \sigma}{\partial \beta}\right)_{total}$	1.3251	1.2170	8.9	1.1388	1.1680	-2.5	1.0868	1.126	-3.5

Table 7.3: Validation results for the Fokker F-28 Mk 1000 model 8-3

	Cruise			Take-off			Landing		
	Method	Reference	% Difference	Method	Reference	% Difference	Method	Reference	% Difference
$C_{L_{\alpha_V}}$	0.0326	0.0355	-8.3	0.0334	0.0348	-4.1	0.0328	0.0353	-7.0
$C_{l_{\beta_{WFN}}}$	-0.0013	-0.0003	422.1	-0.0017	-0.0011	65.0	-0.0021	-0.0019	11.8
$\left(\frac{C_{l_\beta}}{C_{L_W}}\right)$ (deg)	-0.0014	-0.0013	8.8	-0.0014	-0.0009	57.2	-0.0014	-0.0005	182.9
C_{n_β}	0.0014	0.0024	-43.5	0.0017	0.0024	-29.2	0.0020	0.0025	-18.8
$C_{n_{\beta_{WFN}}}$	-0.0029	-0.0016	89.8	-0.0026	-0.0012	117.8	-0.0021	-0.0009	135.4
$C_{n_{\beta_V}}$	0.0043	0.0038	11.6	0.0044	0.0036	20.2	0.0041	0.0037	12.1
$C_{n_{\delta_r}}$				-0.0009	-0.0010	-17.6	-0.0010	-0.0010	0
C_{Y_β}	-0.0159	-0.0147	8.3	-0.0170	-0.0156	8.9			
$C_{Y_{\beta_{WFN}}}$	-0.0058	-0.0050	15.4	-0.0068	-0.0061	11.0			
$C_{Y_{\beta_V}}$	-0.0102	-0.0097	4.9	-0.0102	-0.0095	7.5	-0.0098	-0.0094	4.5
$C_{Y_{\delta_r}}$				0.0032	0.0030	5.8	0.0033	0.0030	8.5
K_{VH}	1.177	1.203	-2.2	1.240	1.196	3.7	1.197	1.196	0.1
$\frac{q_V}{q} K_{FV}$	0.954	0.940	1.5	0.953	0.965	-1.2	1.030	1.000	3.0
$\left(1+\frac{\partial\sigma}{\partial\beta}\right)_F \frac{q_V}{q} K_{FV}$	1.2544	1.1500	9.1	1.2544			1.2544		
$\left(\Delta\frac{\partial\sigma}{\partial\beta}\right)_{\Gamma\Lambda} \frac{q_V}{q} K_{FV}$	-0.0564	-0.0610	-7.5	-0.0564			-0.0564		
$\left(\Delta\frac{\partial\sigma}{\partial\beta}\right)_{\delta_f}$	0			0.053			0.112	0.075	49.3
$\left(1+\frac{\partial\sigma}{\partial\beta}\right)_{total}$	1.2740	1.1170	14.1	1.2594	1.0290	22.4	1.1300	1.0100	11.9

8

Conclusion and Recommendations

The rapid analysis method for lateral-directional stability and control was successfully implemented in the Initiator for conventional aircraft configurations. The case studies show results that match up with the data for comparable reference aircraft, and the results are much closer to the vertical tail parameters of the reference aircraft than those that were estimated by the Initiator before the addition of the module. There is however a trend towards an over-prediction for larger aircraft such as the Airbus A340-300 and an under-prediction for smaller aircraft such as the Boeing 737-800. This is tied to the fact that the goal values for the yawing moment coefficient due to sideslip are the driving requirement in all designs.

The validation of the implemented analysis method showed generally accurate results for most parameters. The biggest exception to this is the estimation of the tail-off rolling moment coefficient due to sideslip. Investigating an alternative for the estimation method that is used now should be the first step for improving the current analysis method. The solution is not a vortex lattice method, as this was also found to be inaccurate for the tail-off rolling moment coefficient due to sideslip in conventional aircraft configurations.

The design method can be improved by adding calculations for dynamic stability, especially for Dutch roll. This will require additional estimation methods and data for validation for the parameters that are specific to dynamic stability. Expanding the method to include the design of propeller aircraft would be an improvement that allows a wider range of usage for the Initiator. Additionally, rudder design could be included as well. The relative chord length and span of the rudder are design inputs at this moment. Including them in the optimization is a possibility that could be explored, but that would require the inclusion of extra calculations and requirements, one example being for control forces.

No suitable rapid analysis method was found for unconventional aircraft configurations. As could be expected, the empirical method for conventional aircraft does not work well on a blended wing body; the prediction of tail-off performance was especially inaccurate. The vortex lattice method comes up short when the angles of attack and sideslip become larger, and these larger angles are present in some critical cases for vertical tail design, such as crosswind during landing and one-engine-out at take-off. The estimation of the tail-off yawing moment due to sideslip was inaccurate as well.

An additional consideration is that the accuracy of the windtunnel results for the blended wing body is not entirely certain. This has a big impact on the validations for blended wing bodies, as these completely rely on the windtunnel results. Obtaining more windtunnel data for unconventional aircraft would therefore be very useful. In the case of the ZEFT blended wing body it is especially worth looking at the behavior between 0 and 10 degrees. These windtunnel data could then possibly be used to derive or validate dedicated empirical relations for blended wing bodies. The shape of a blended wing body means that wing-only approximations for the stability derivatives could be suitable for analysis.

A

FIGURES USED IN CALCULATIONS

A.1. FIGURES FOR THE CALCULATION OF TAIL-OFF COEFFICIENTS

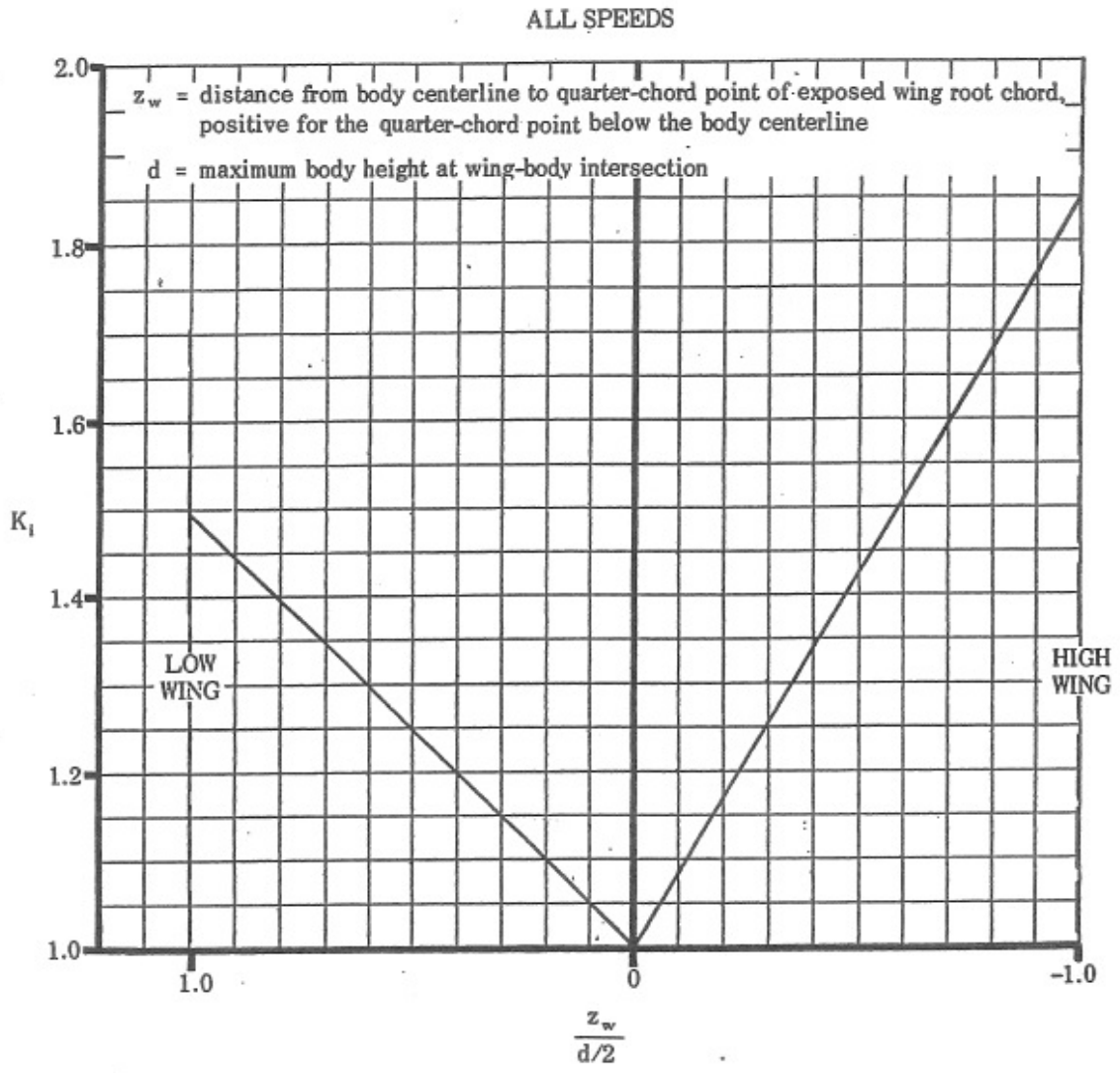

Figure A.1: Wing-body interference factor [1]

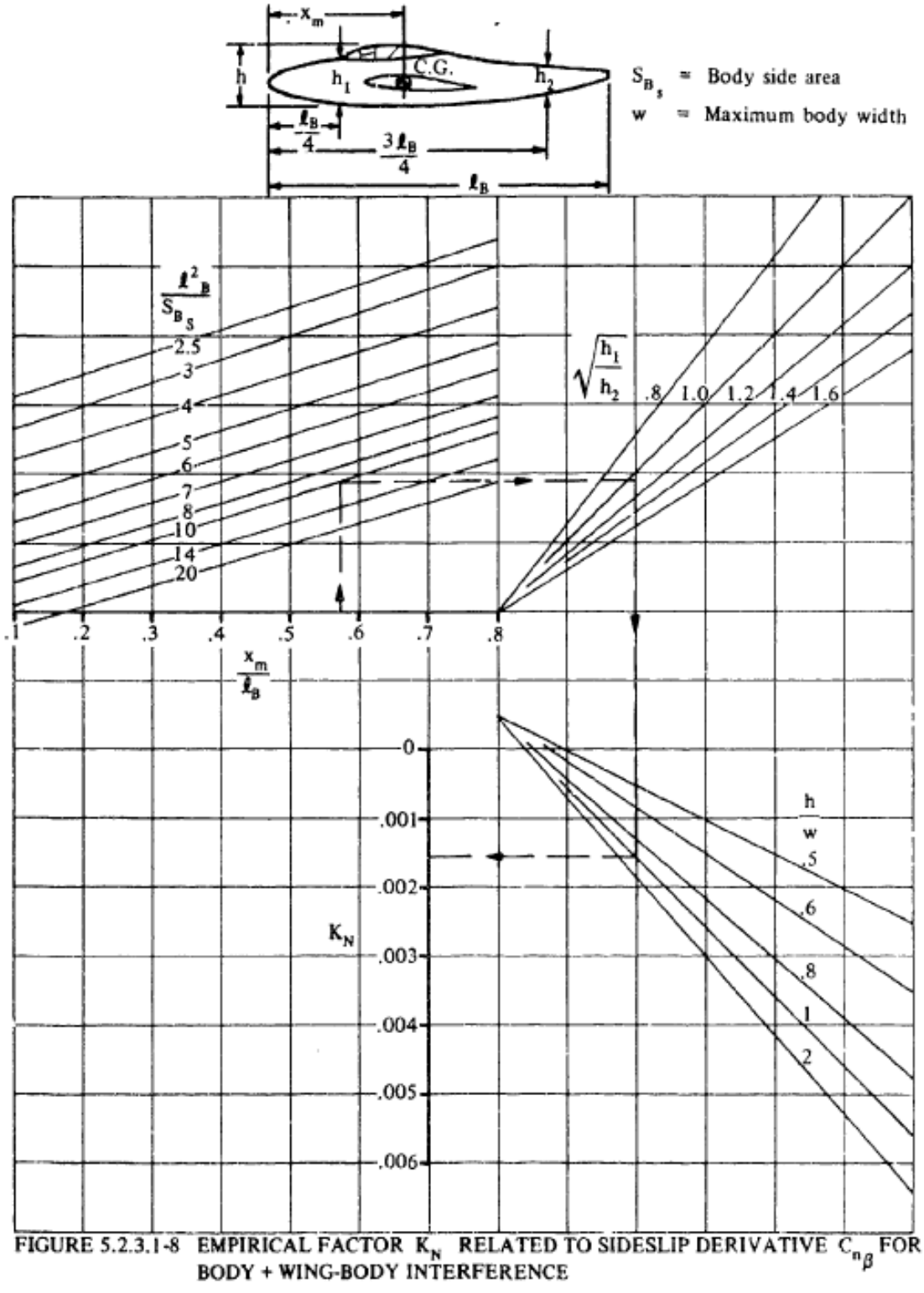

FIGURE 5.2.3.1-8 EMPIRICAL FACTOR K_N RELATED TO SIDESLIP DERIVATIVE C_{n_β} FOR BODY + WING-BODY INTERFERENCE

Figure A.2: Body-wing-body interference factor [4]

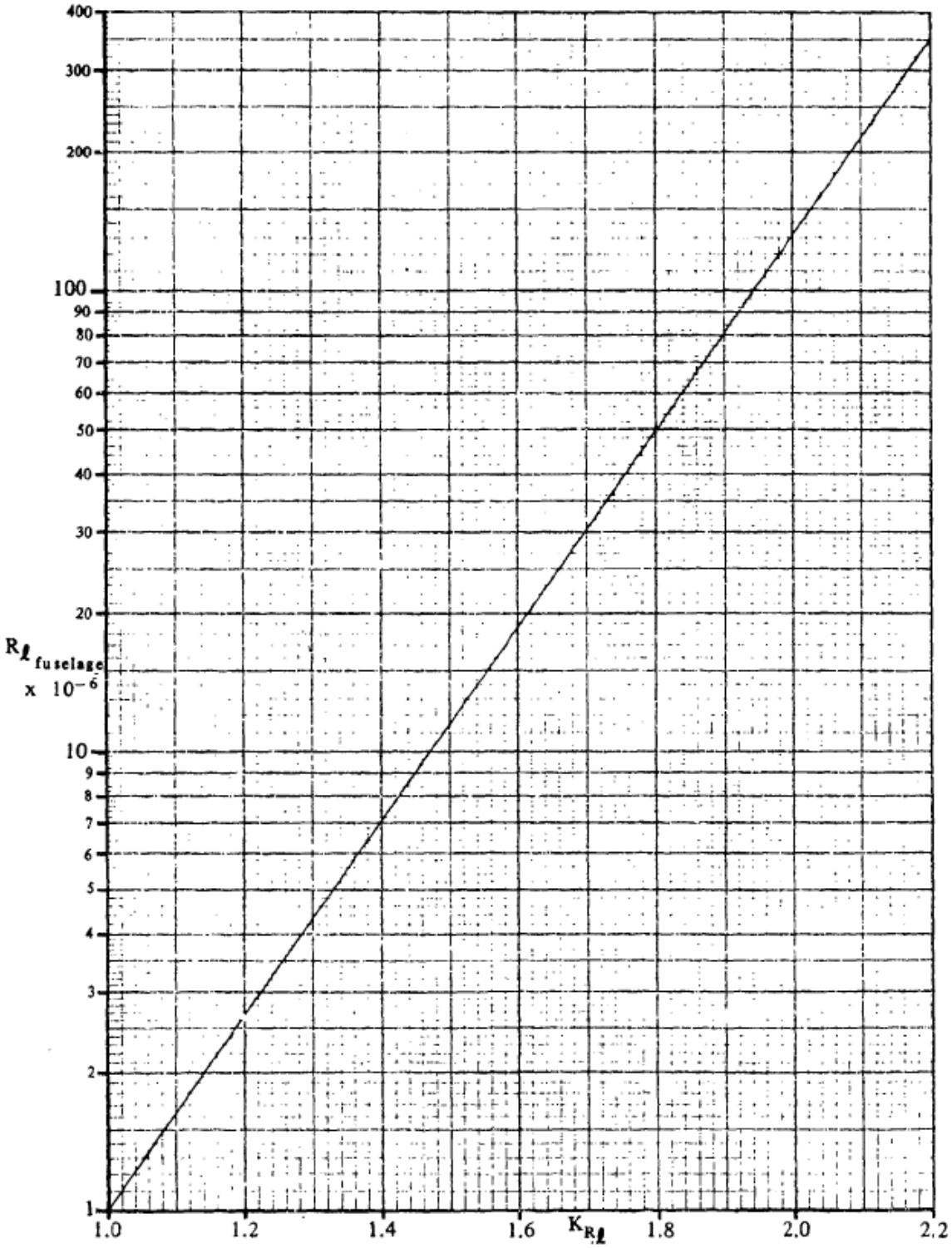

FIGURE 5.2.3.1-9 EFFECT OF FUSELAGE REYNOLDS NUMBER ON WING-BODY C_{n_β}

Figure A.3: Effect of fuselage Reynolds number on $C_{n_{\beta_{WFN}}}$ [4]

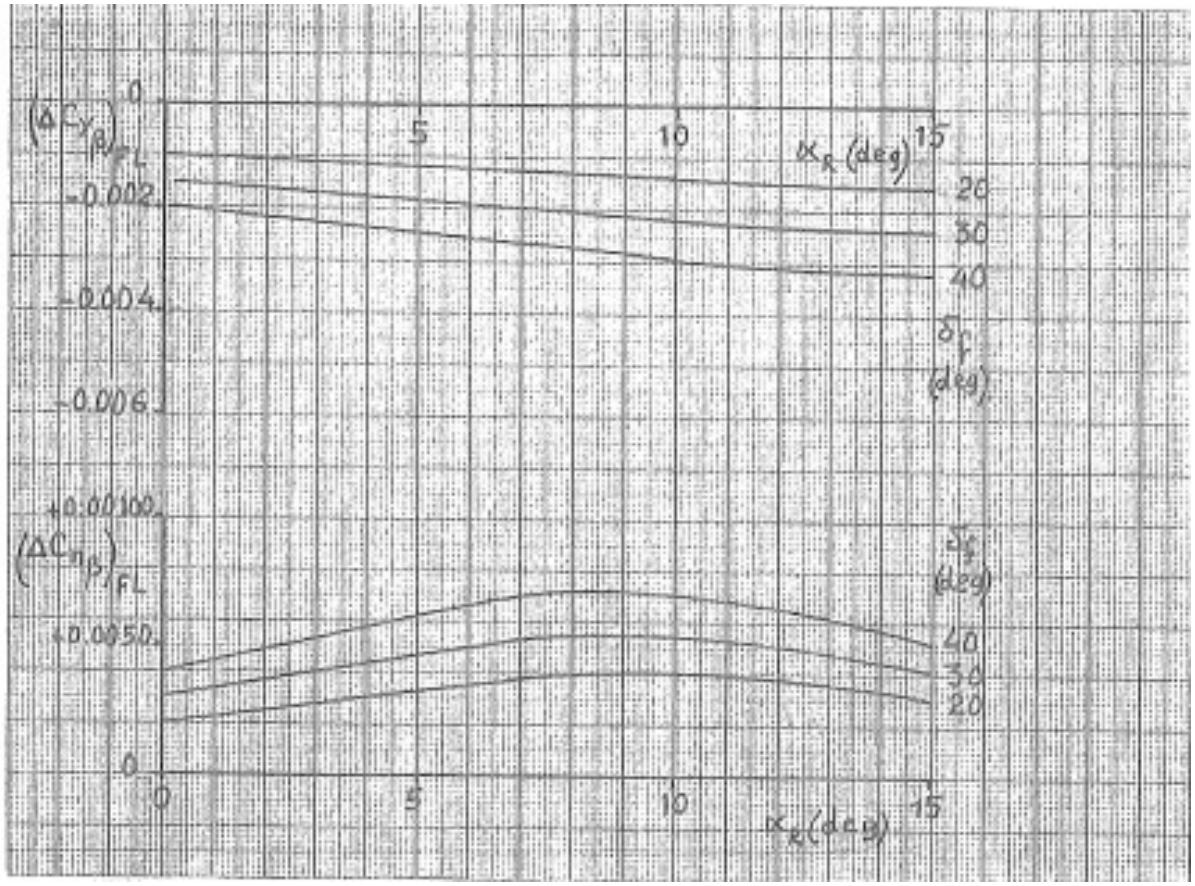

Figure A.4: Effect of flap deflection on tail-off side force and yawing moment [1]

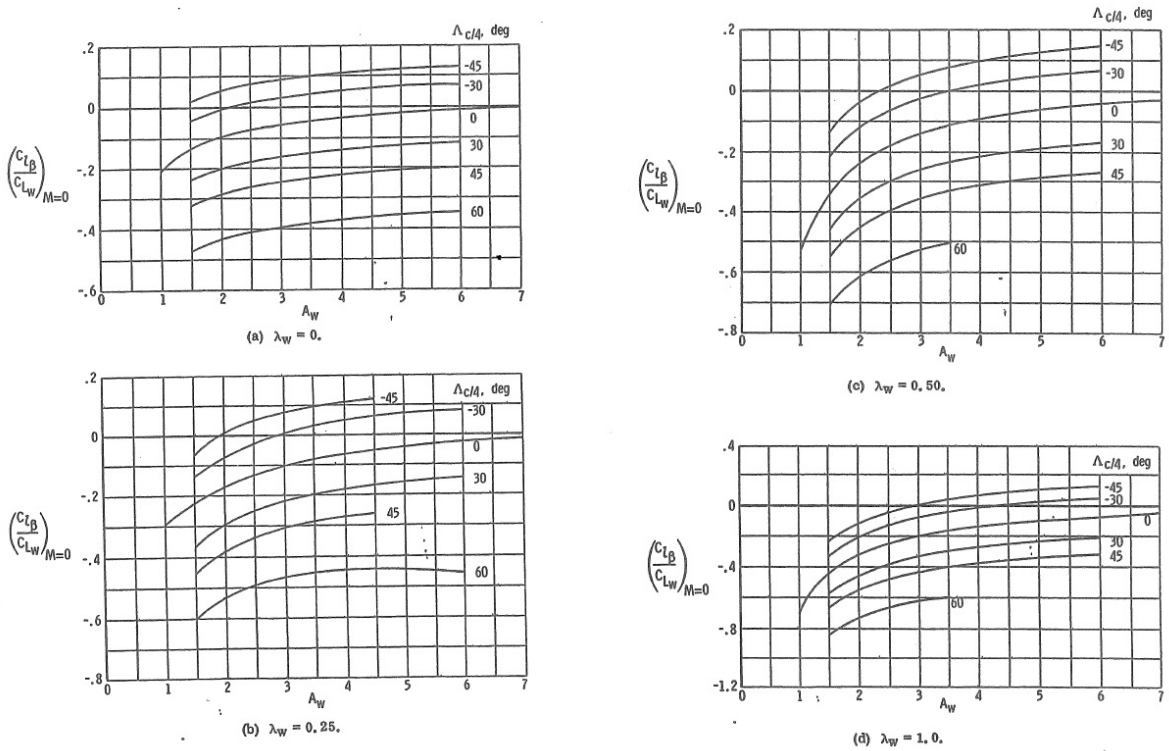

Figure A.5: Lift-dependent rolling moment due to sideslip [1]

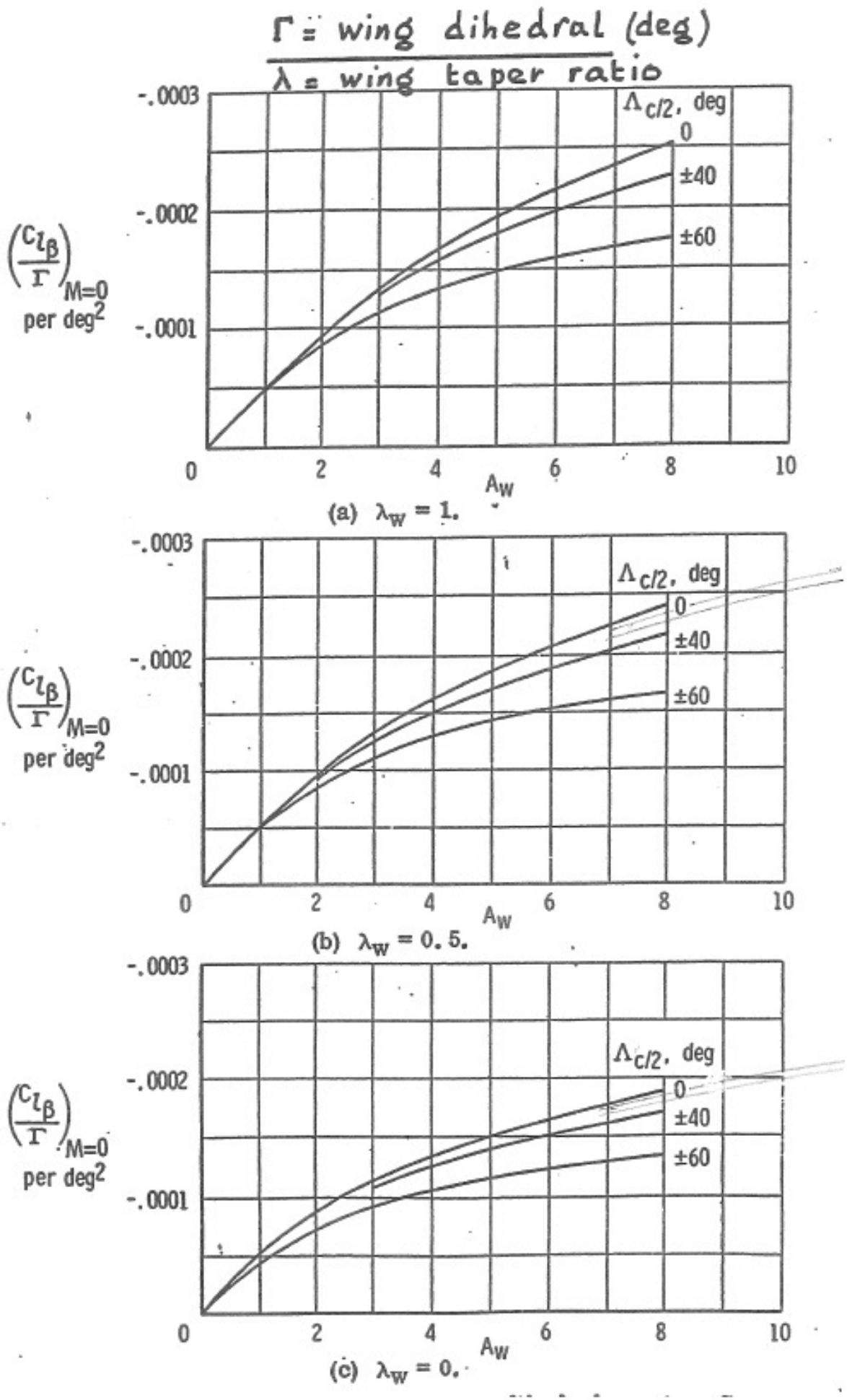

Figure A.6: Effect of uniform geometric dihedral on the rolling moment due to sideslip [1]

A.2. FIGURES FOR THE CALCULATION OF VERTICAL TAIL RELATED COEFFICIENTS

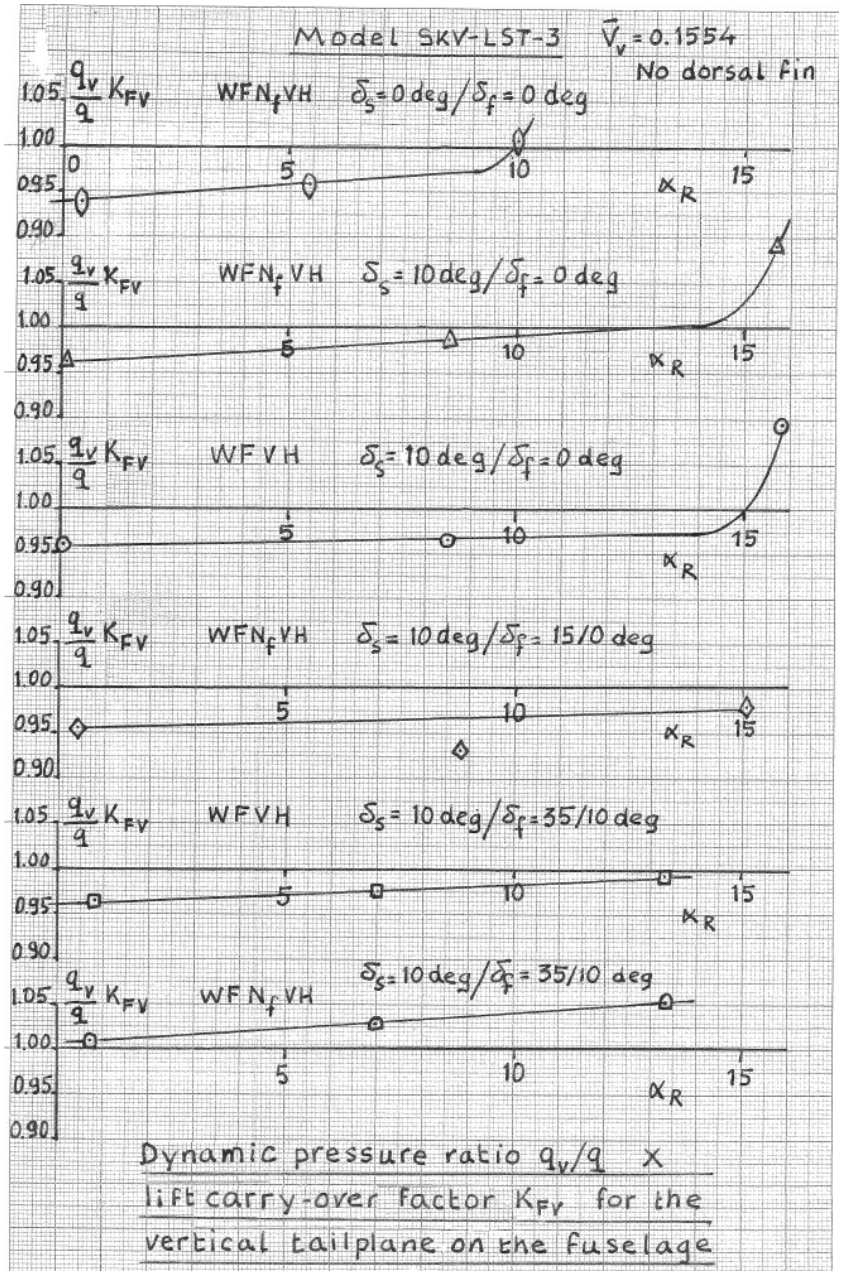

Figure A.7: Dynamic pressure ratio times lift carry-over factor for the vertical tailplane on the fuselage [1]

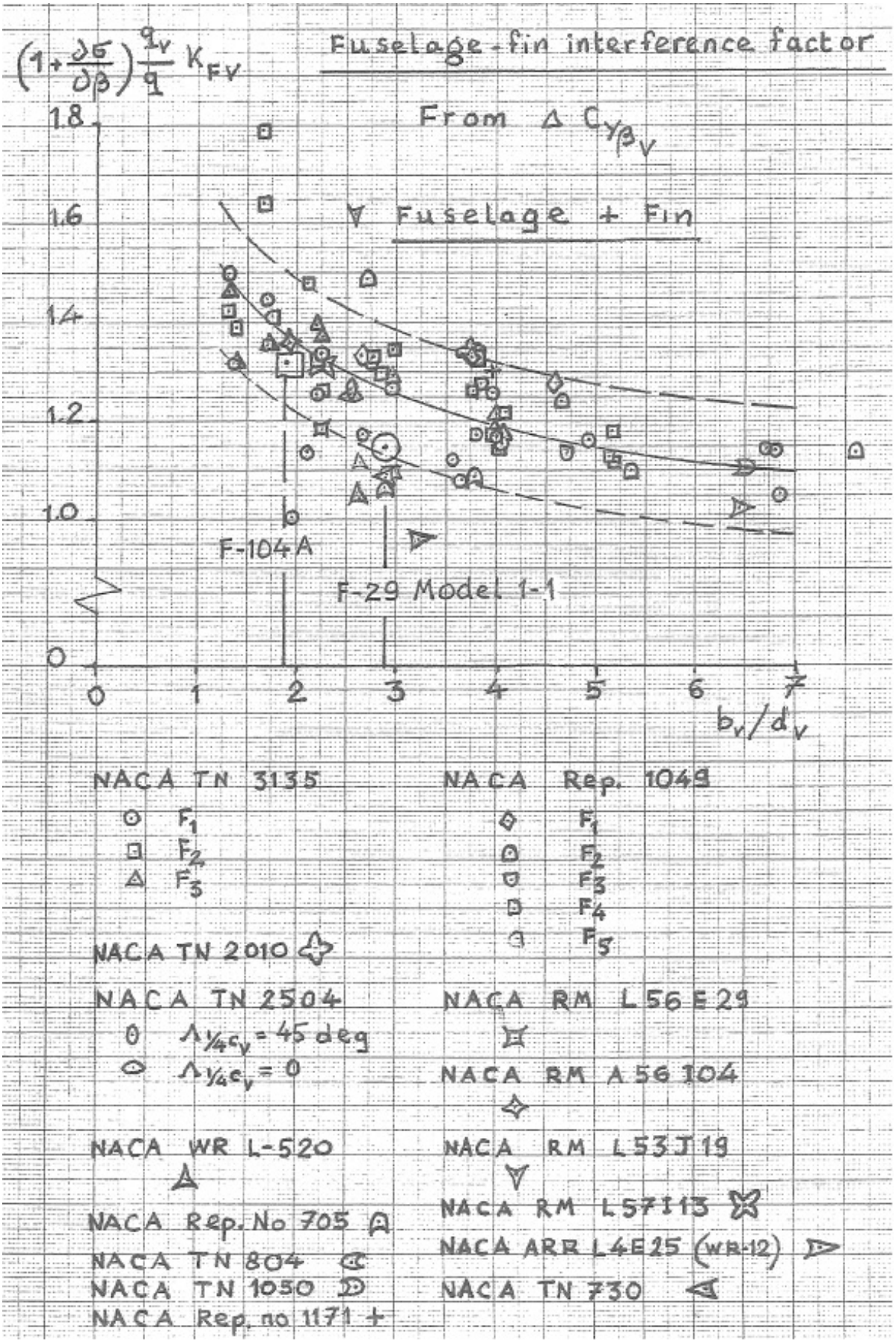

Figure A.8: Fuselage-fin interference factor [1]

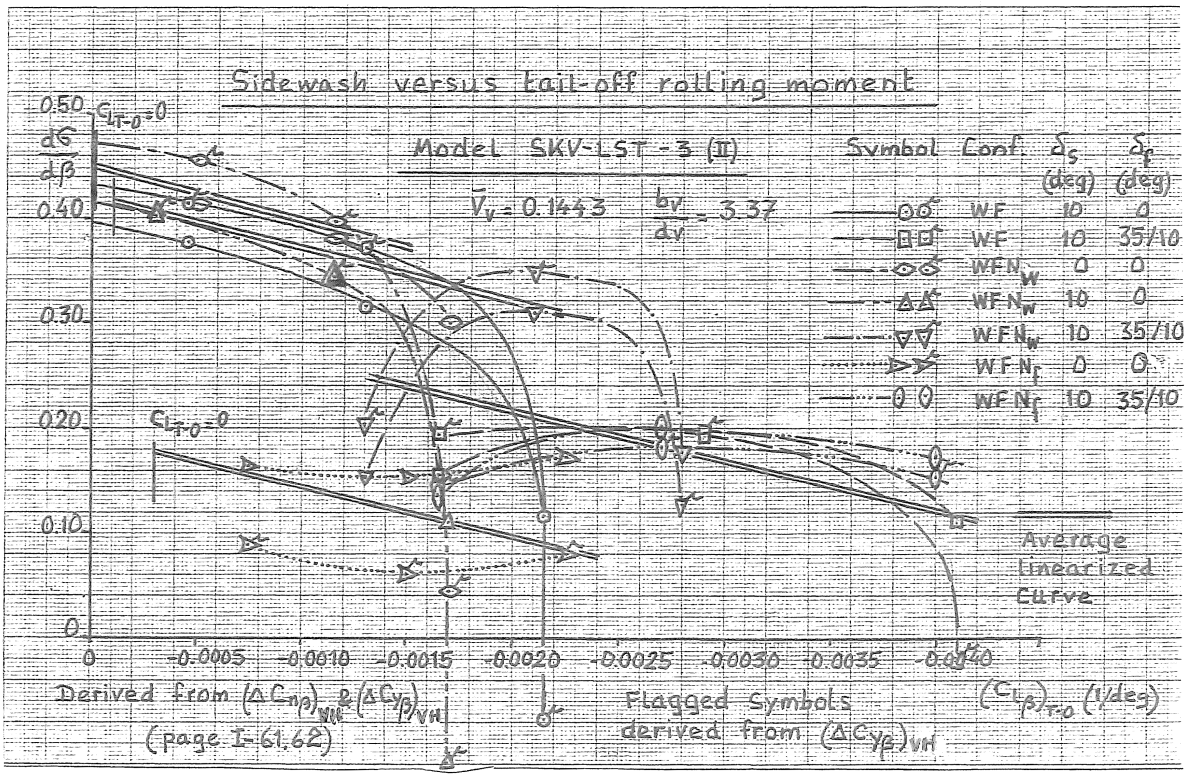

Figure A.9: Sidewash versus tail-off rolling moment [1]

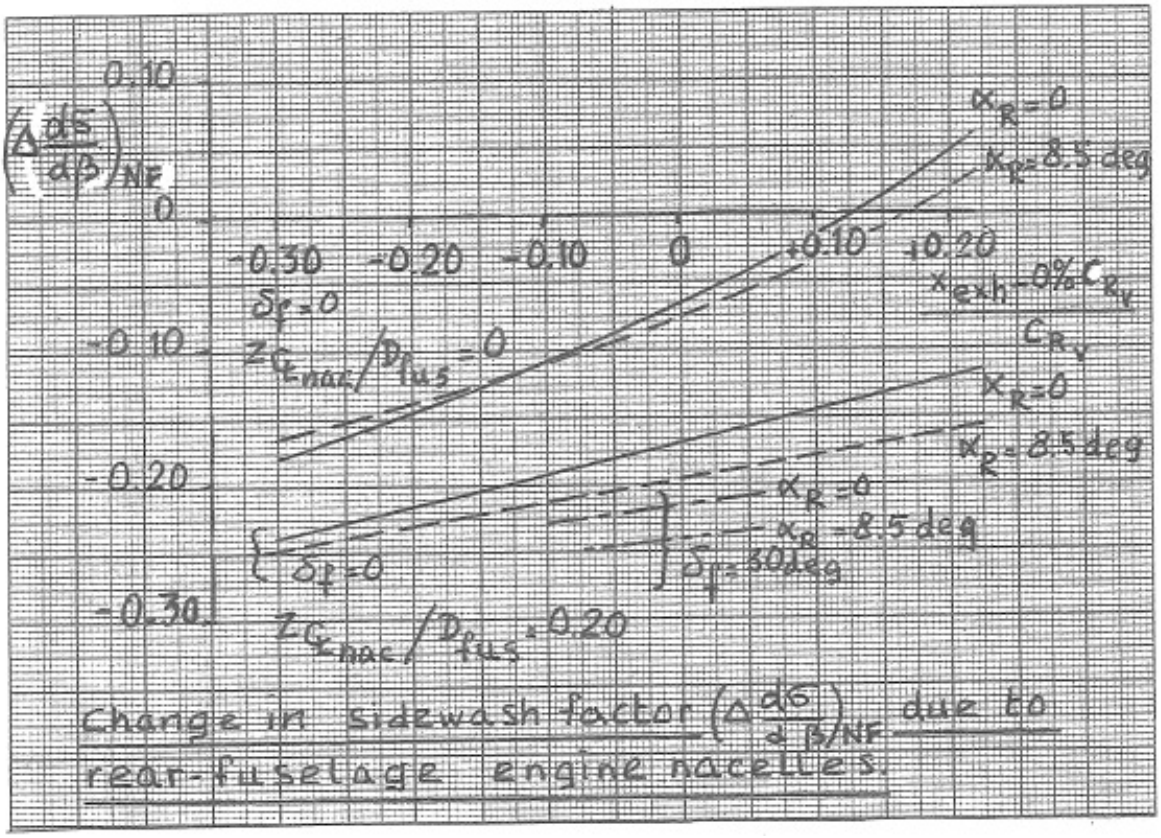

Figure A.10: Change in sidewash factor due to rear-fuselage engine nacelles [1]

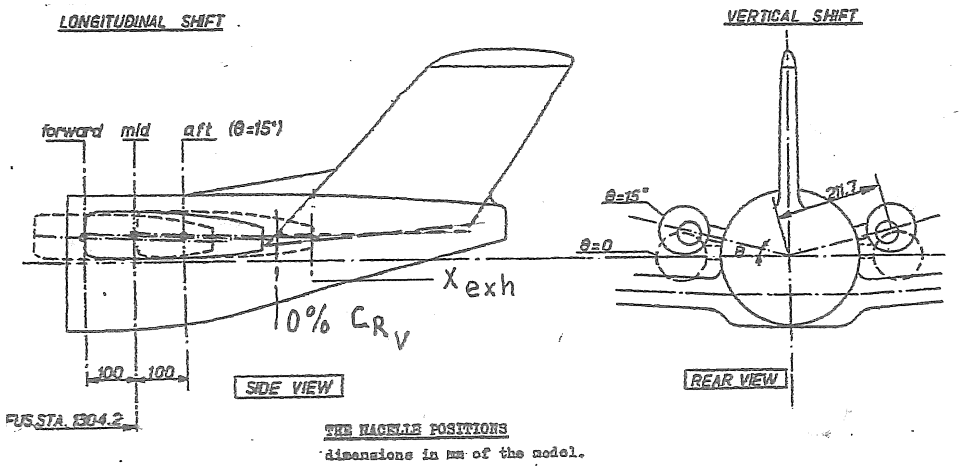

Figure A.11: Definition of dimensions used for rear-fuselage engine nacelles [1]

A.3. FIGURES FOR CALCULATING THE HORIZONTAL TAIL ENDPLATE EFFECT

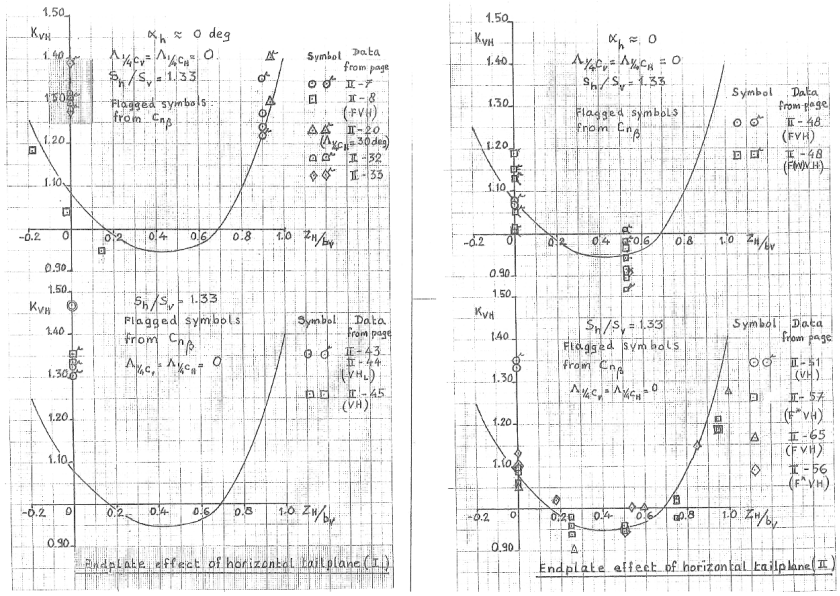

Figure A.12: Positional endplate effect of horizontal tail on vertical tail [1]

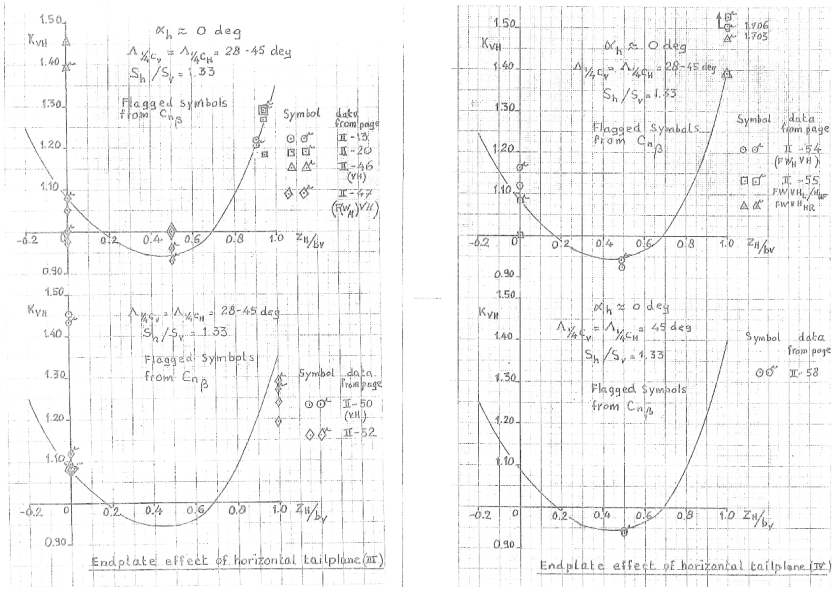

Figure A.13: Positional endplate effect of horizontal tail on vertical tail [1]

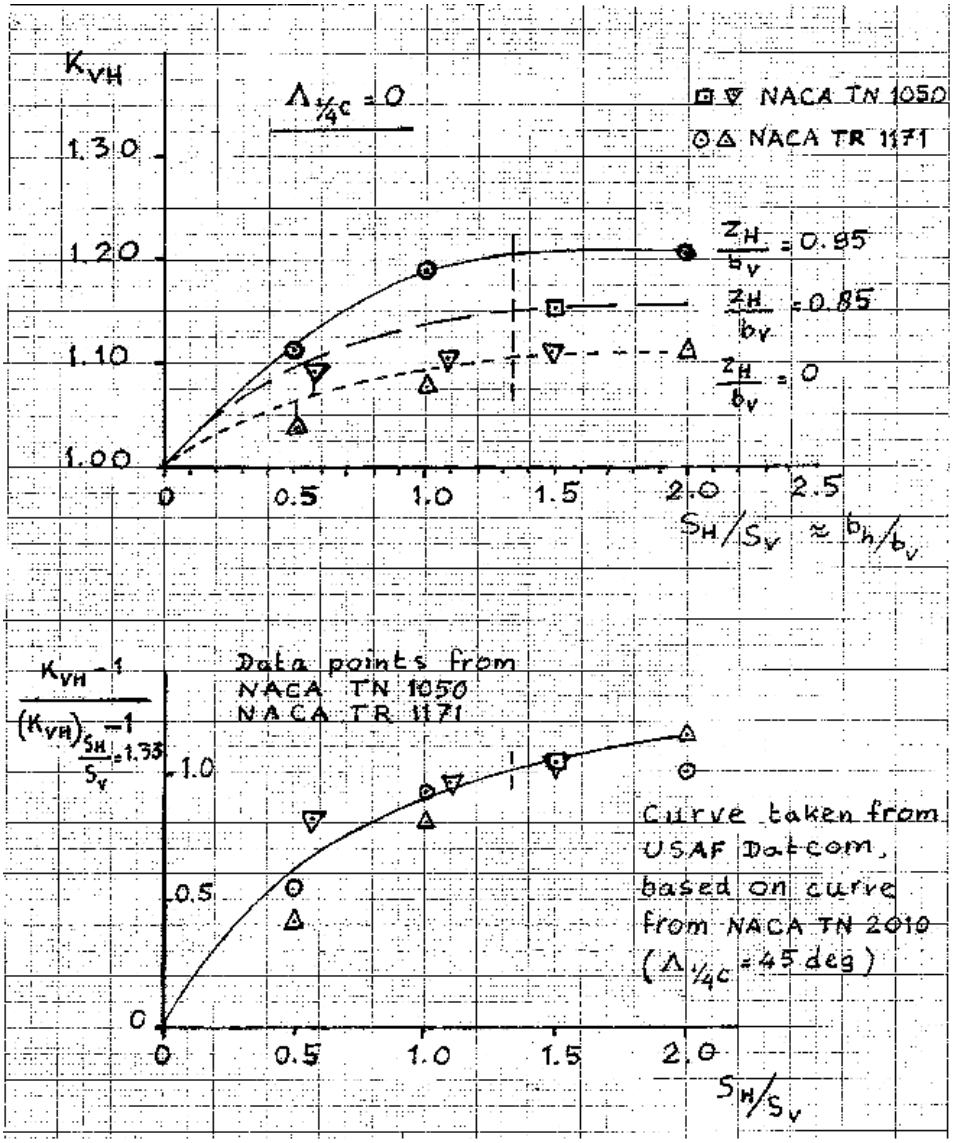

Figure A.14: Area ratio endplate effect of horizontal tail on vertical tail [1]

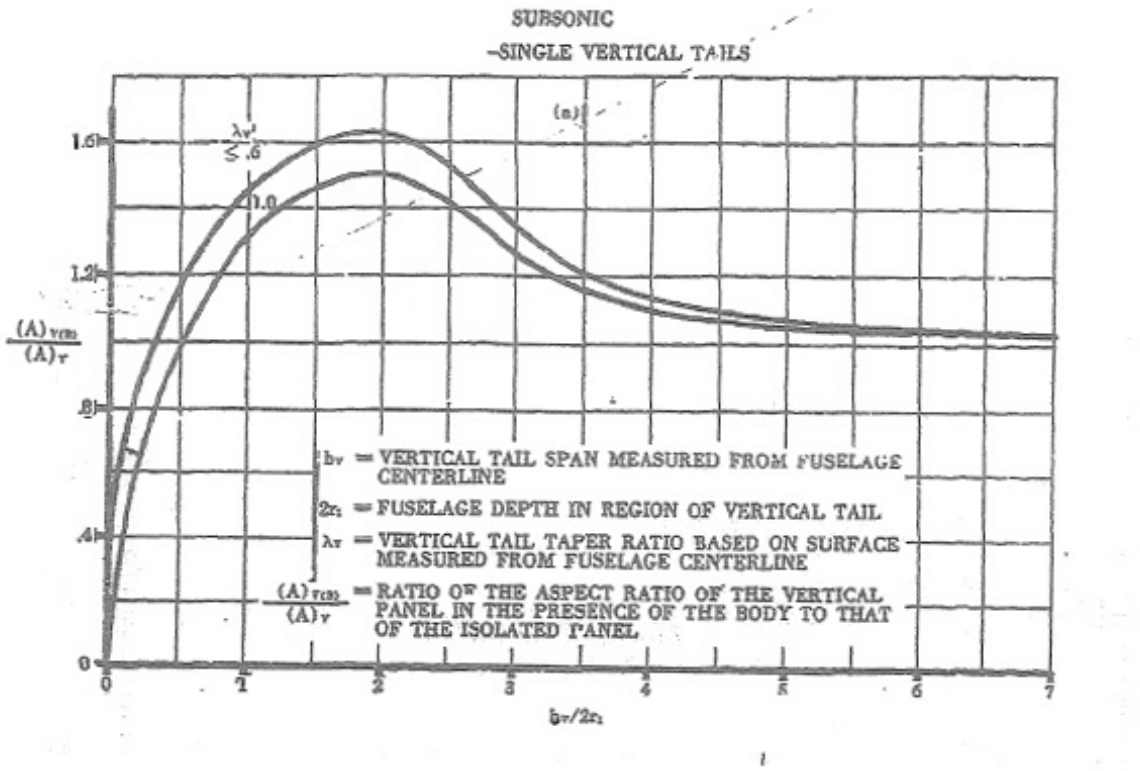

Figure A.15: Endplate effect of fuselage on vertical tail [4]

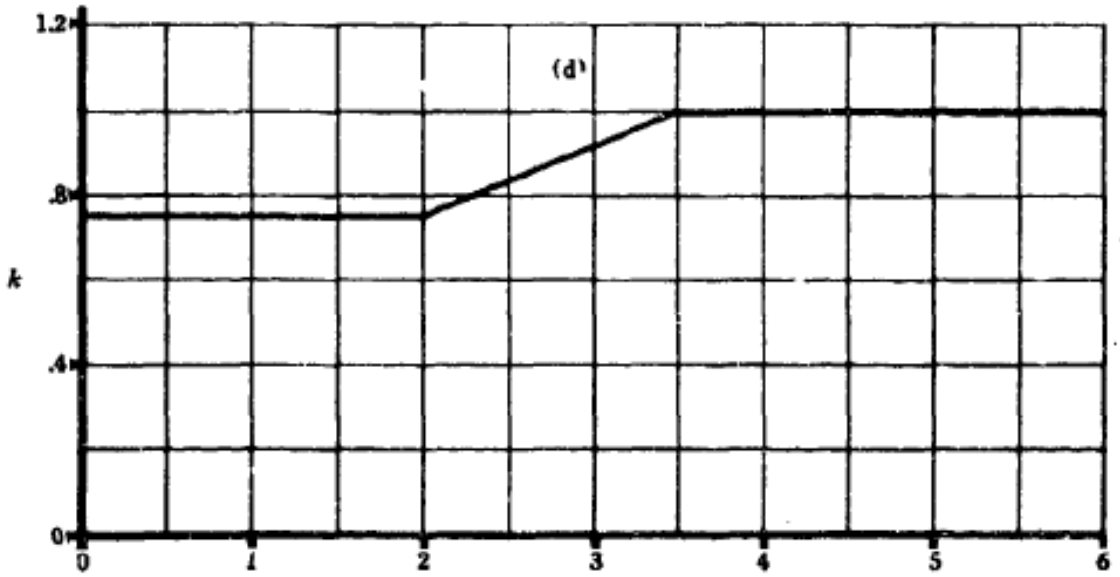

FIGURE 5.3.1.1-22(CONTD) CHARTS FOR ESTIMATING THE SIDESLIP DERIVATIVE $(C_{Y_\beta})_{V(WBH)}$ FOR SINGLE VERTICAL TAILS

Figure A.16: Endplate effect of fuselage on vertical tail [4]

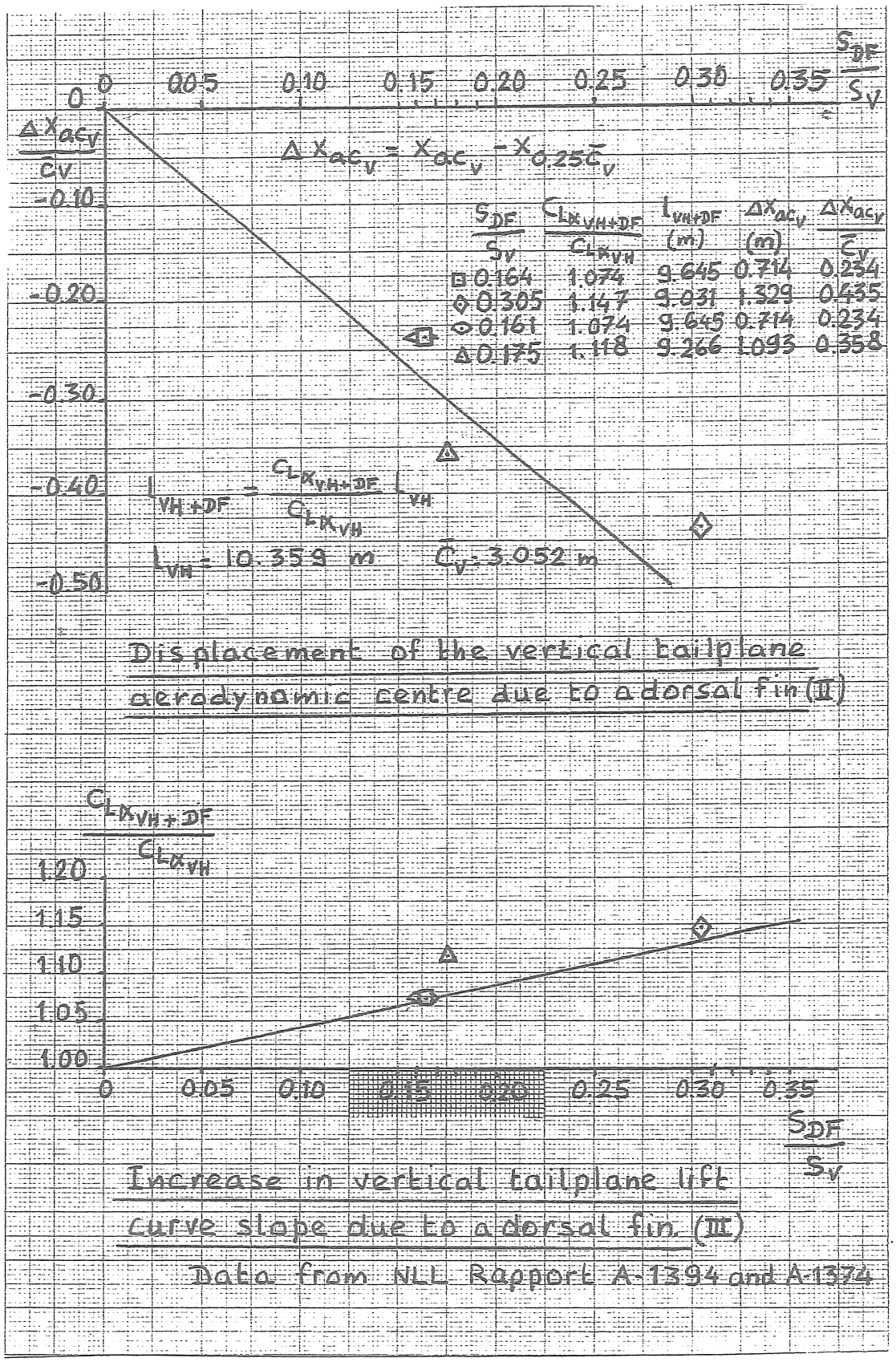

Figure A.17: Effect of dorsal fin on aerodynamic center position and lift curve slope of the vertical tail [1]

A.4. FIGURES FOR THE AILERON STRIP METHOD AND FLAP EFFECTIVENESS

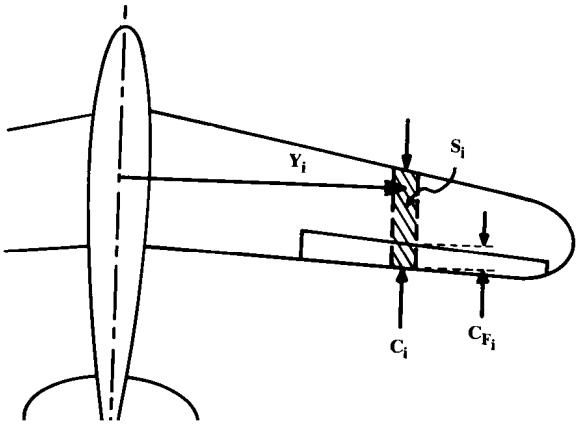

Figure A.18: Strip method for effect of aileron deflection [2]

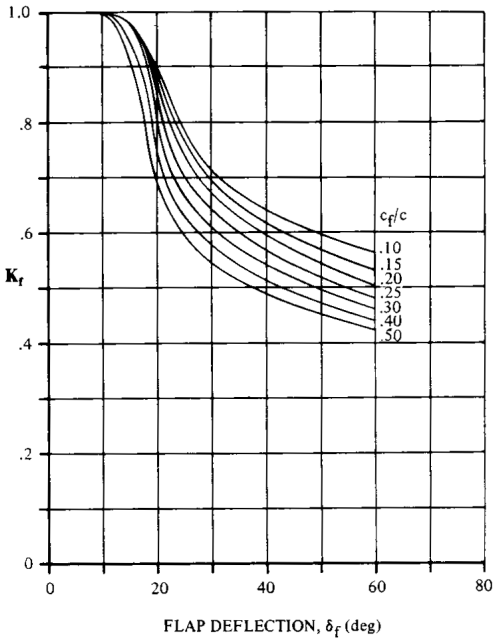

Figure A.19: Empirical correction for plain lift increment [2]

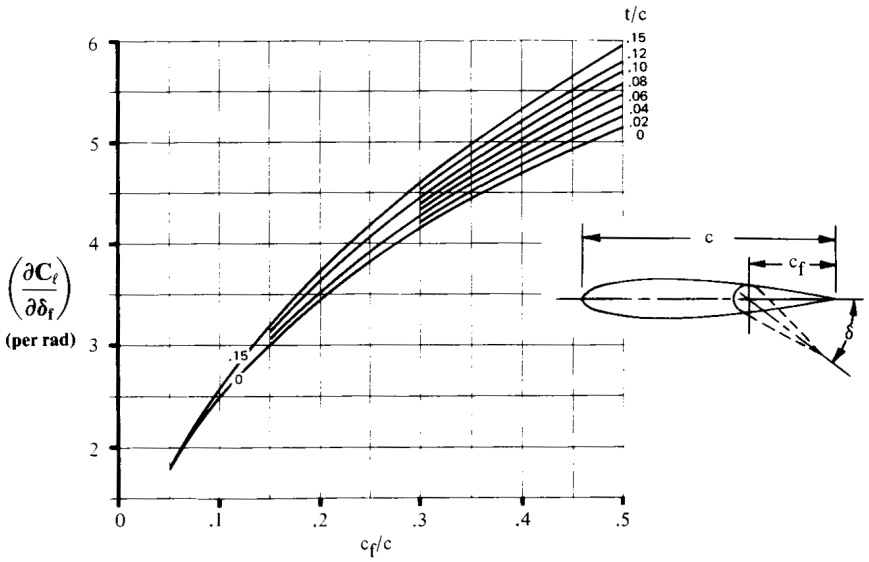

Figure A.20: Theoretical lift increment for plain flaps [2]

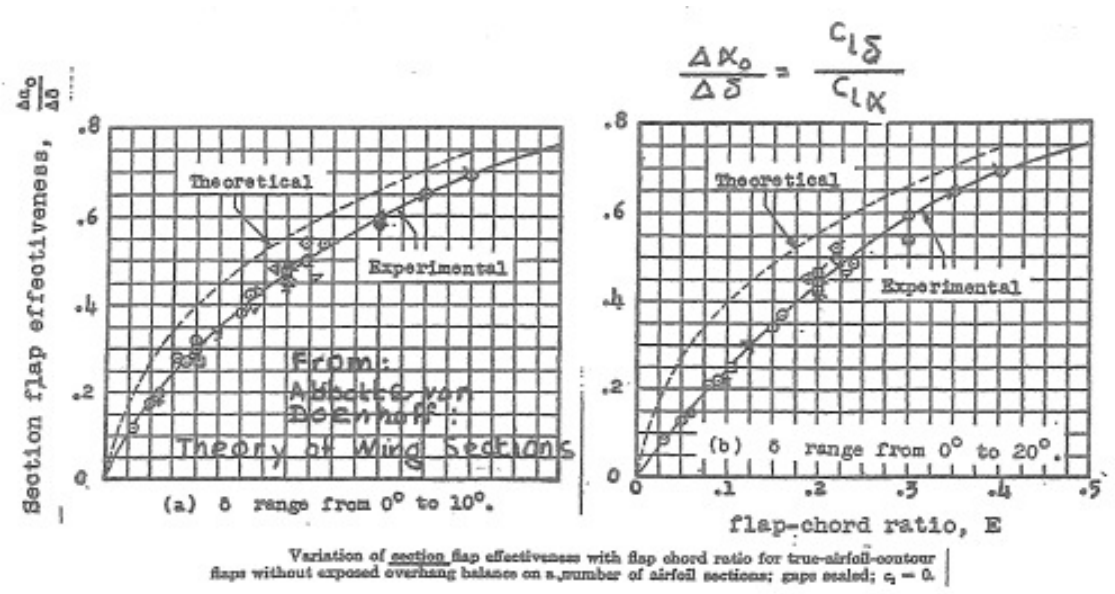

Figure A.21: Flap effectiveness [1]

A.5. FIGURES FOR THE CALCULATION OF MAXIMUM LIFT COEFFICIENT AND THE ANGLE OF ATTACK AT MAXIMUM LIFT

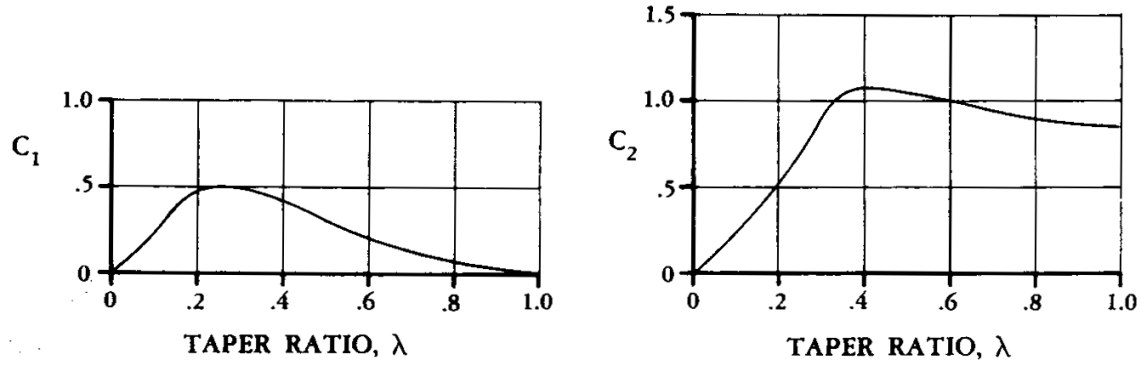

Figure A.22: Taper-ratio correction factors for low-aspect-ratio wings [4]

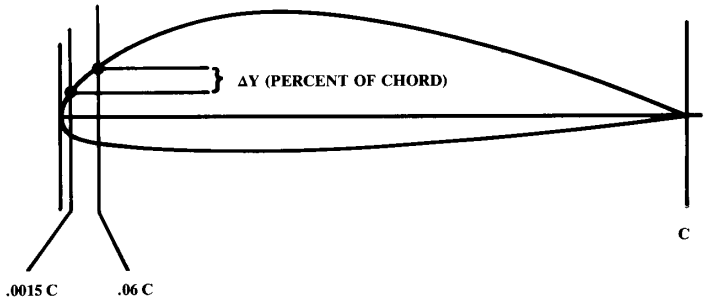

Figure A.23: Airfoil leading edge sharpness parameter [4]

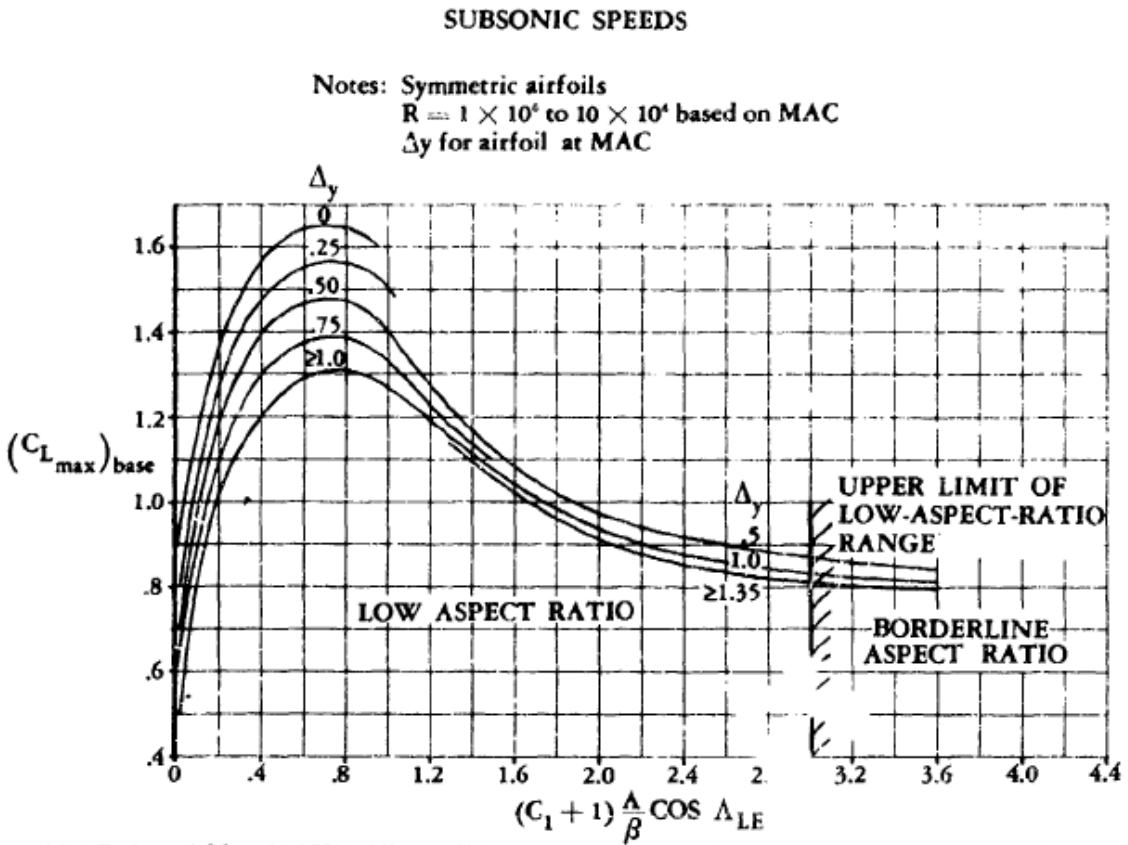

FIGURE 4.1.3.4-23a MAXIMUM LIFT OF WINGS WITH POSITION OF MAXIMUM THICKNESS AT OR FORWARD OF THE 35-PERCENT CHORD

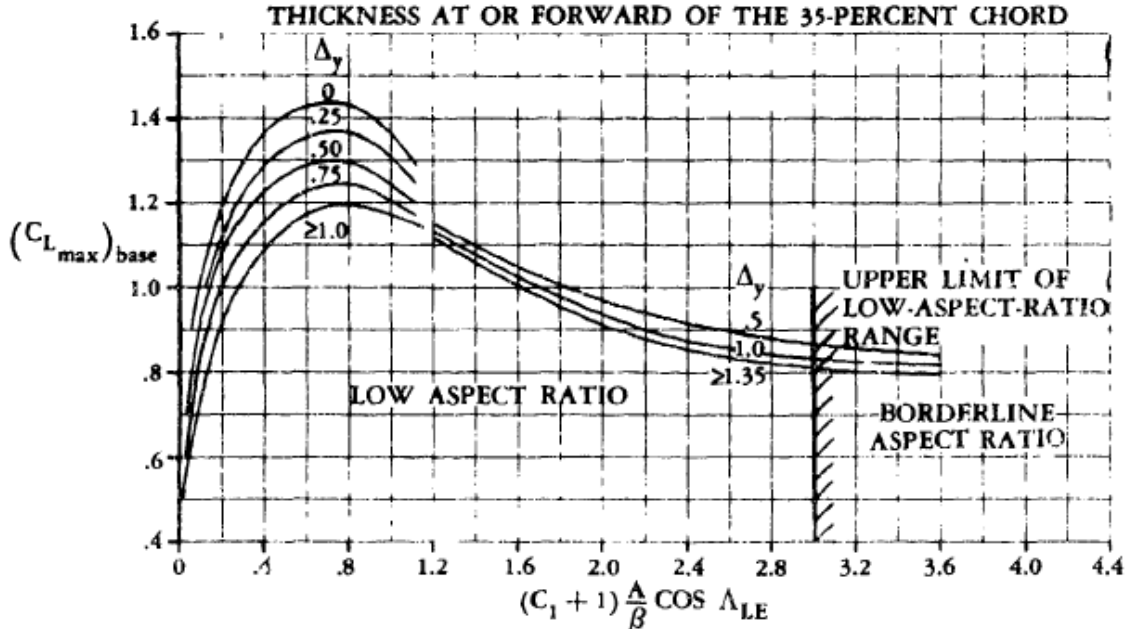

FIGURE 4.1.3.4-23b MAXIMUM LIFT OF WINGS WITH POSITION OF MAXIMUM THICKNESS BETWEEN 35- AND 50-PERCENT CHORD

Figure A.24: $(C_{L_{max}})_{base}$ for low-aspect-ratio wings [4]

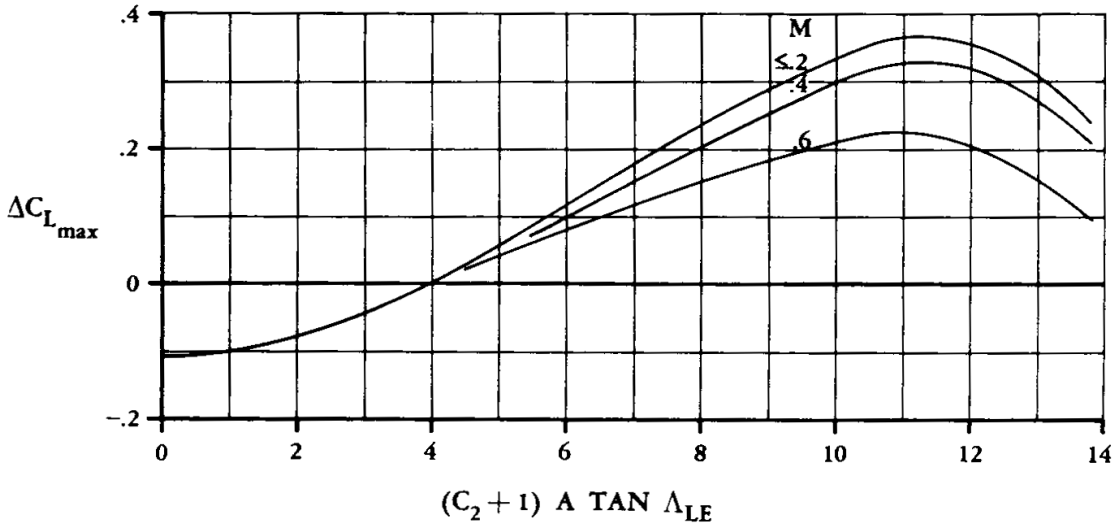

Figure A.25: $\Delta C_{L_{max}}$ for subsonic low-aspect-ratio wings [4]

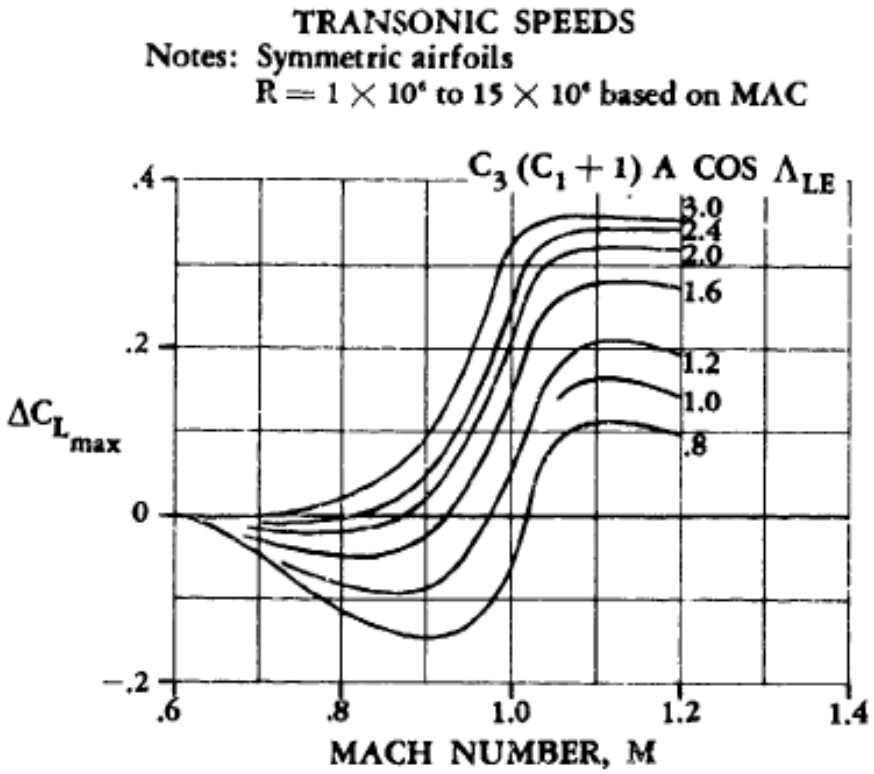

Figure A.26: $\Delta C_{L_{max}}$ for transonic low-aspect-ratio wings [4]

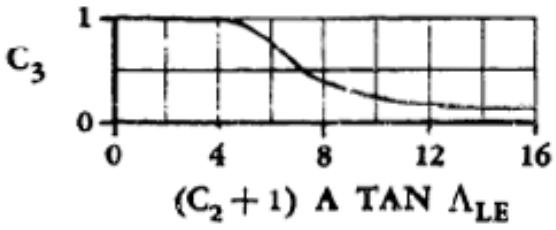

Figure A.27: Coefficient C_3 for determining transonic $\Delta C_{L_{max}}$ [4]

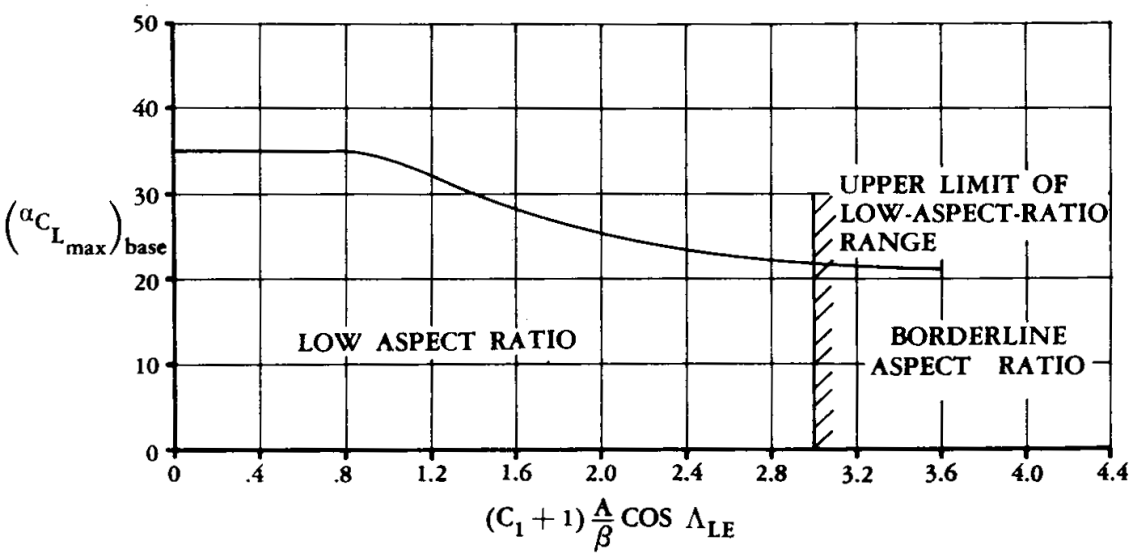

Figure A.28: $\left(\alpha_{C_{L_{max}}}\right)_{base}$ for low-aspect-ratio wings [4]

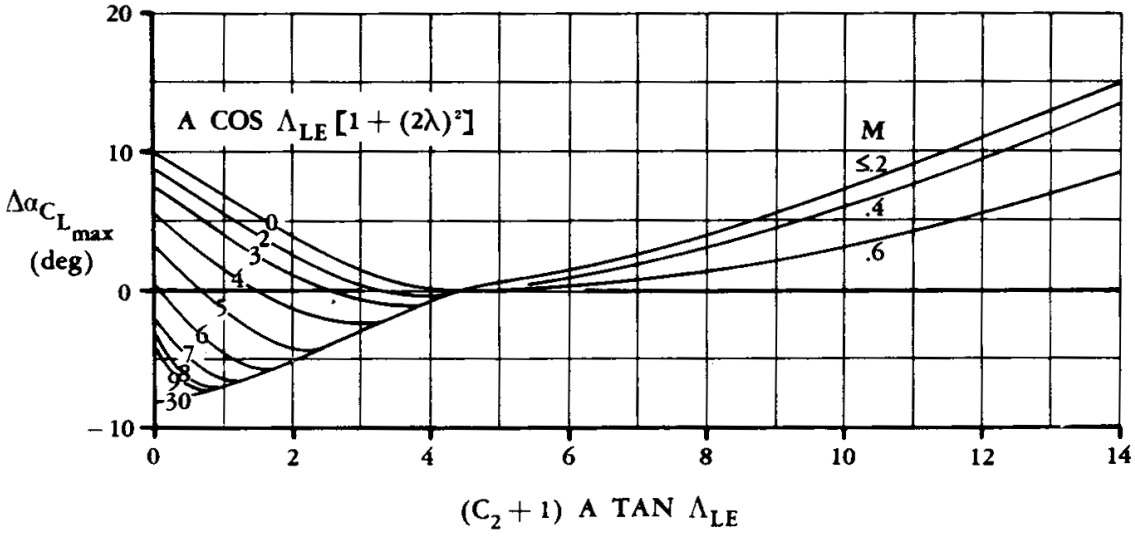

Figure A.29: $\Delta\alpha C_{L_{max}}$ for subsonic low-aspect-ratio wings [4]

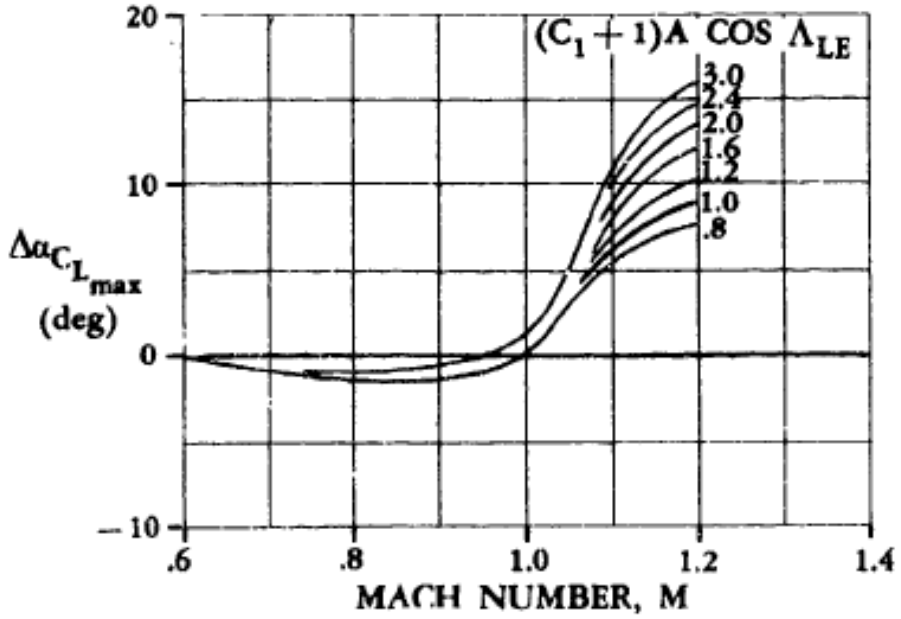

Figure A.30: $\Delta\alpha C_{L_{max}}$ for transonic low-aspect-ratio wings [4]

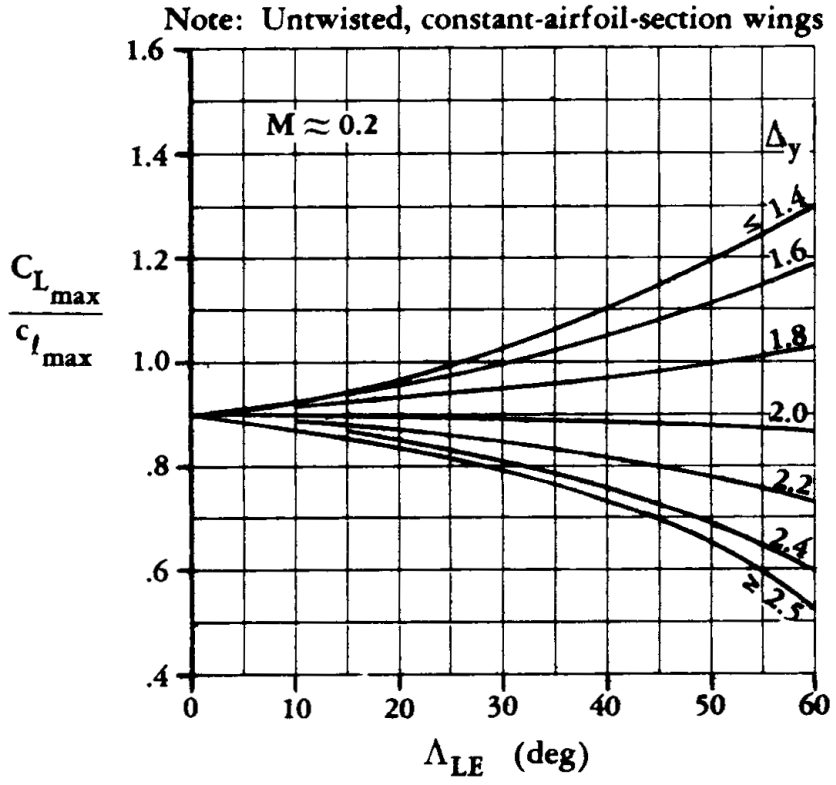

Figure A.31: Subsonic maximum lift of high-aspect-ratio wings [4]

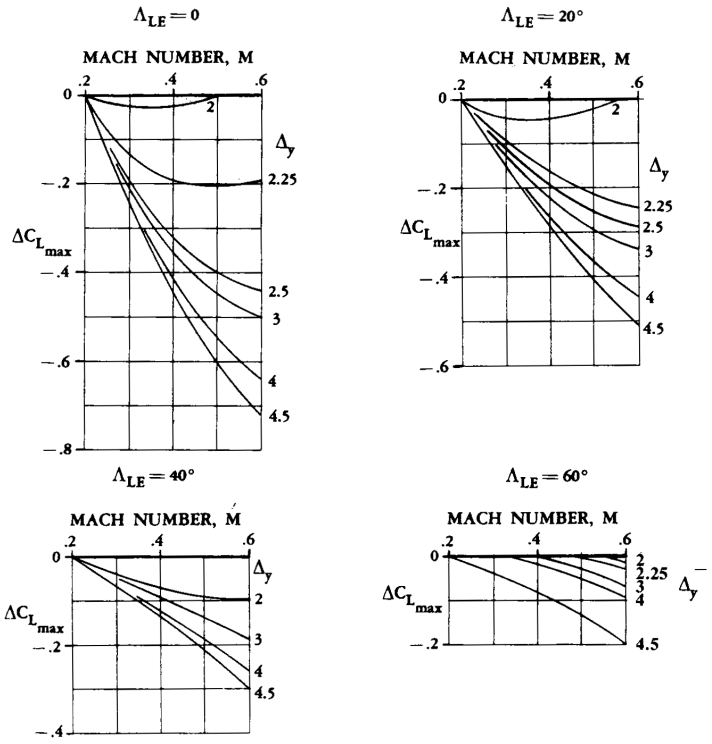

Figure A.32: Mach number correction for subsonic maximum lift of high-aspect-ratio wings [4]

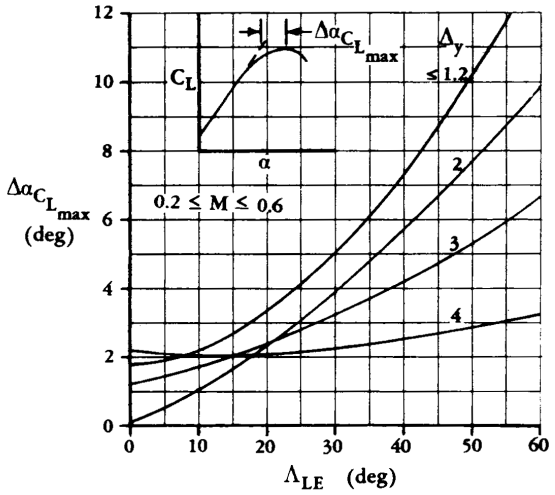

Figure A.33: Angle of attack increment for subsonic maximum lift of high-aspect-ratio wings [4]

B

FLOW CHARTS FOR THE DIRECTIONAL STABILITY ESTIMATION MODULE

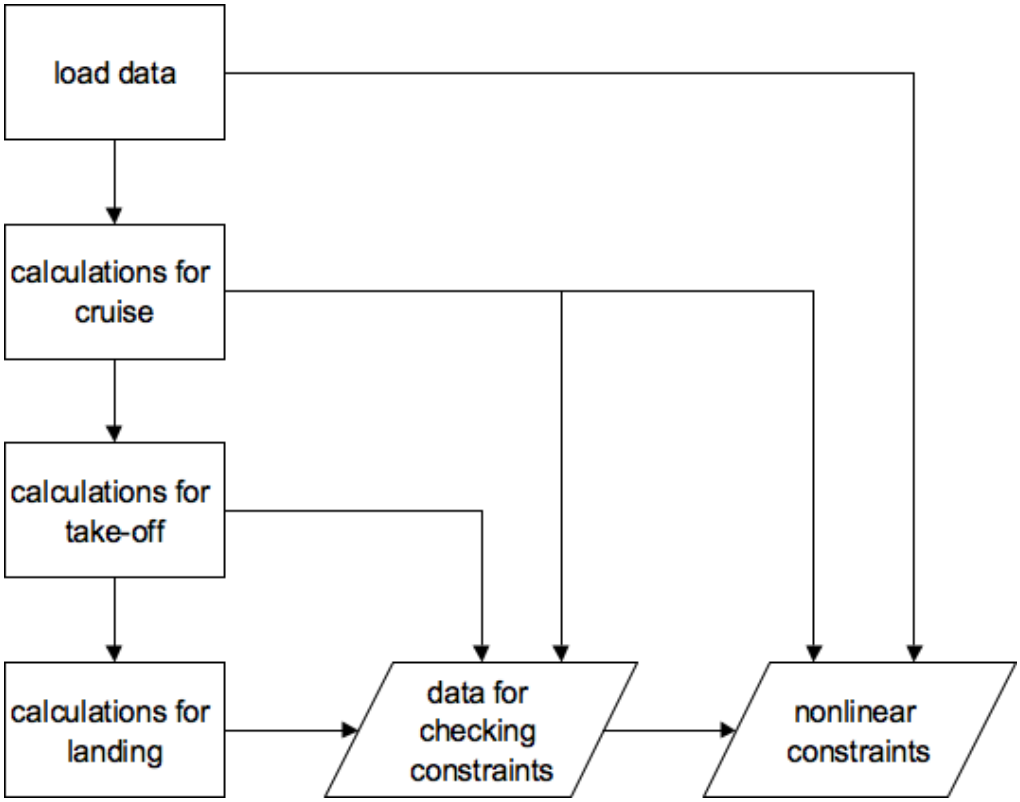

Figure B.1: General flow chart for nonlinear constraints function

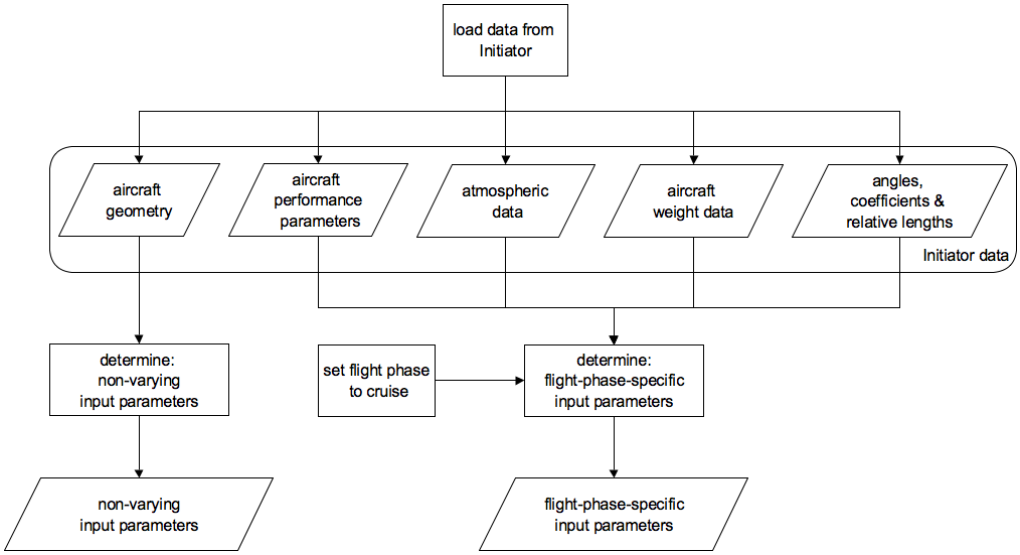

Figure B.2: Detailed flow chart of the 'load data' block in figure B.1

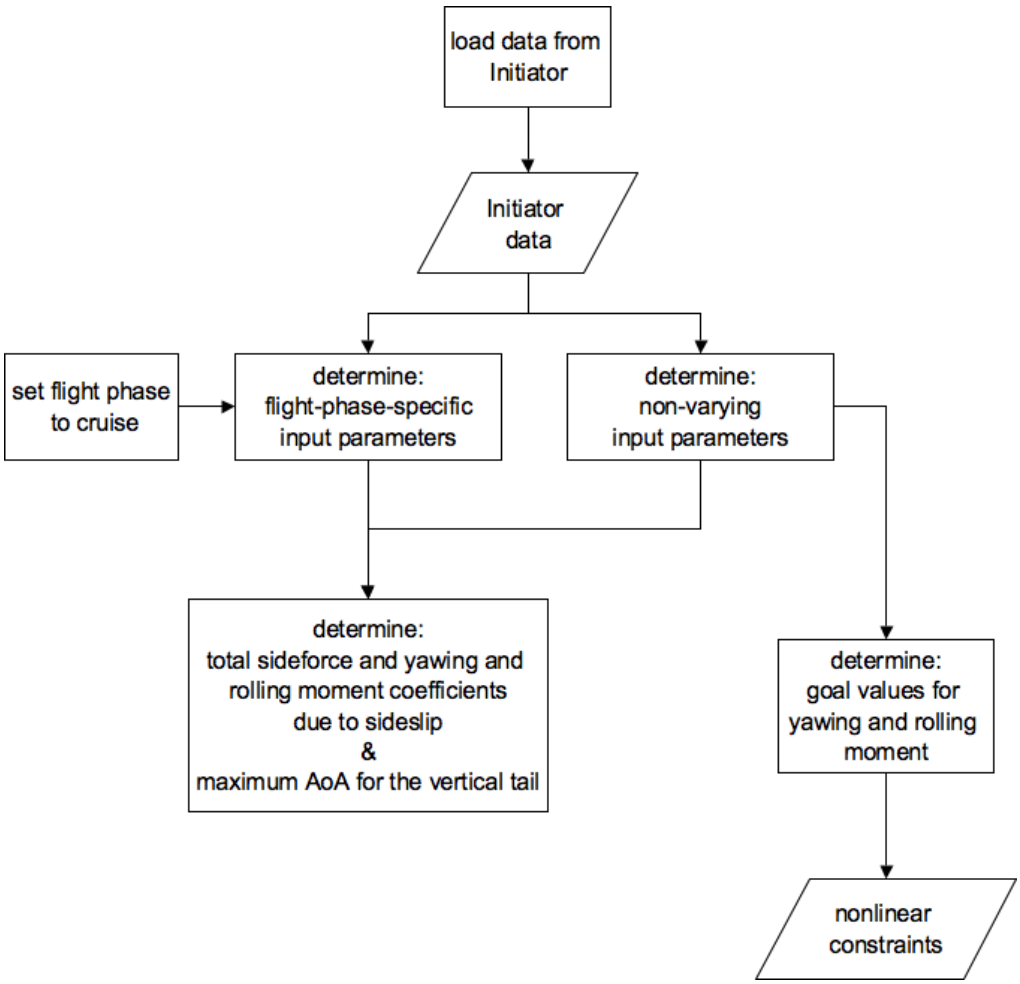

Figure B.3: Detailed flow chart of the 'calculations for cruise' block in figure B.1

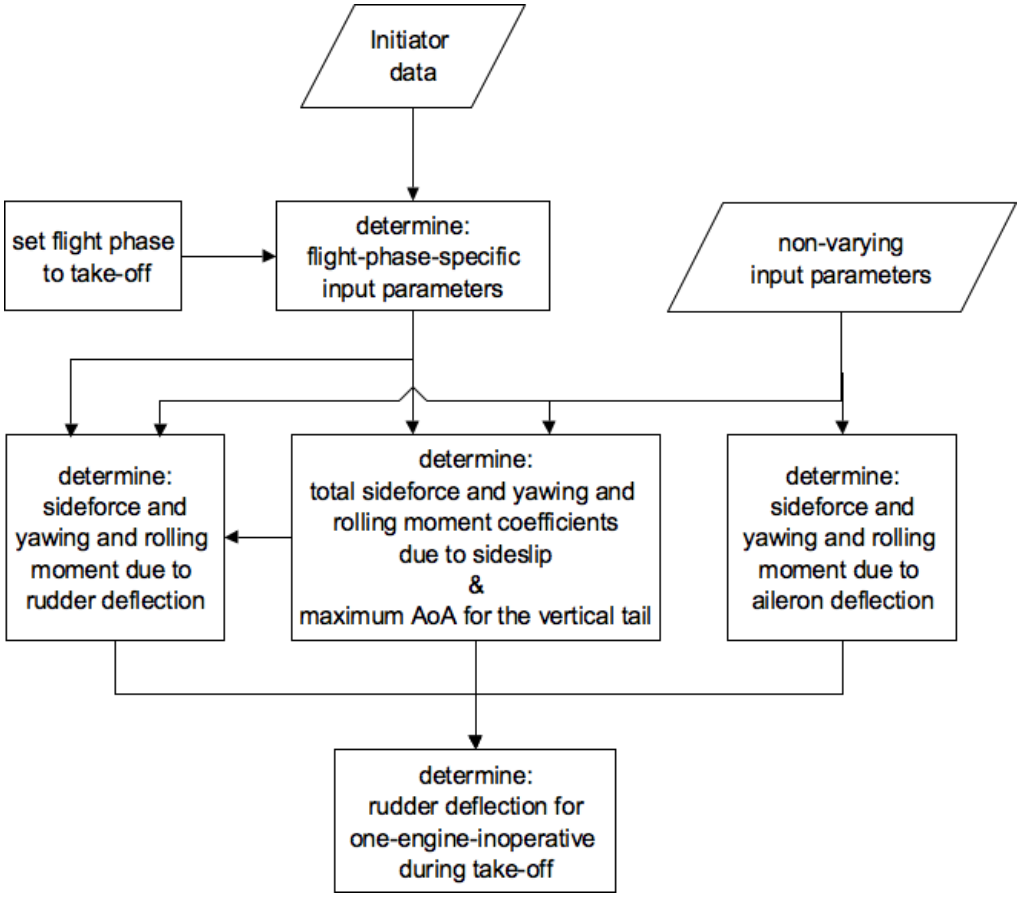

Figure B.4: Detailed flow chart of the 'calculations for take-off' block in figure B.1

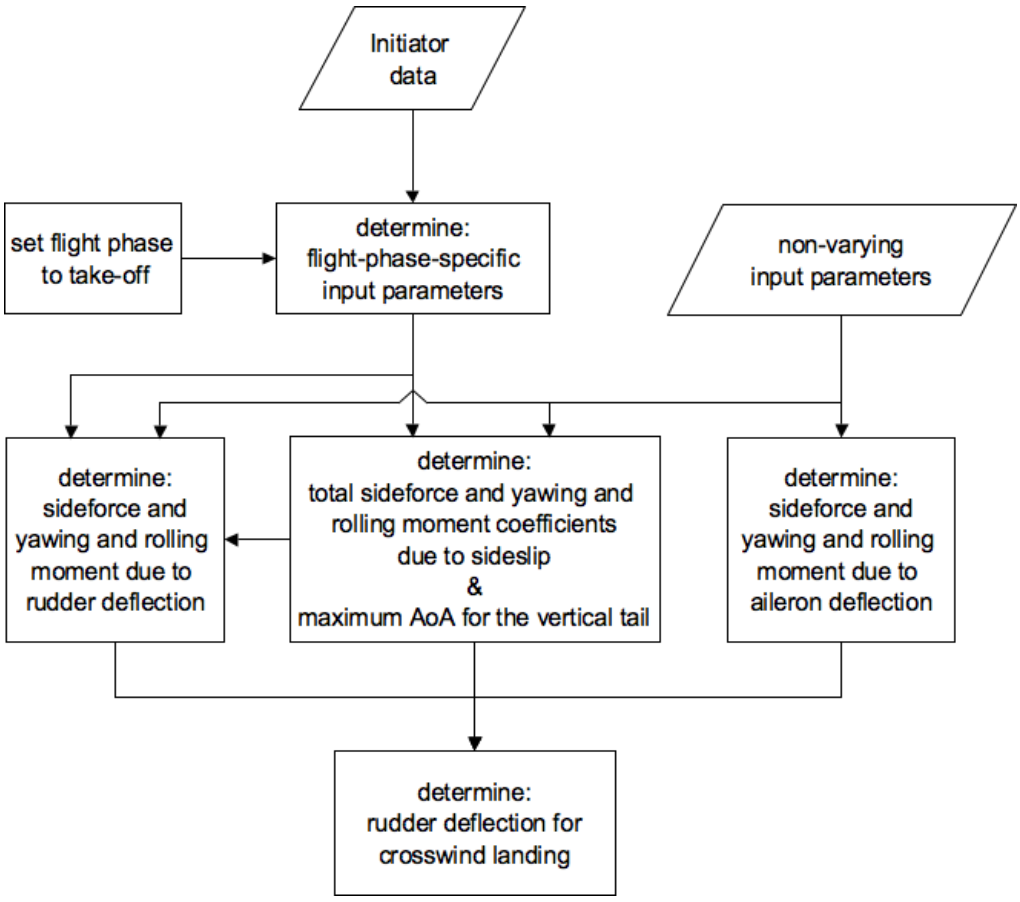

Figure B.5: Detailed flow chart of the 'calculations for landing' block in figure B.1

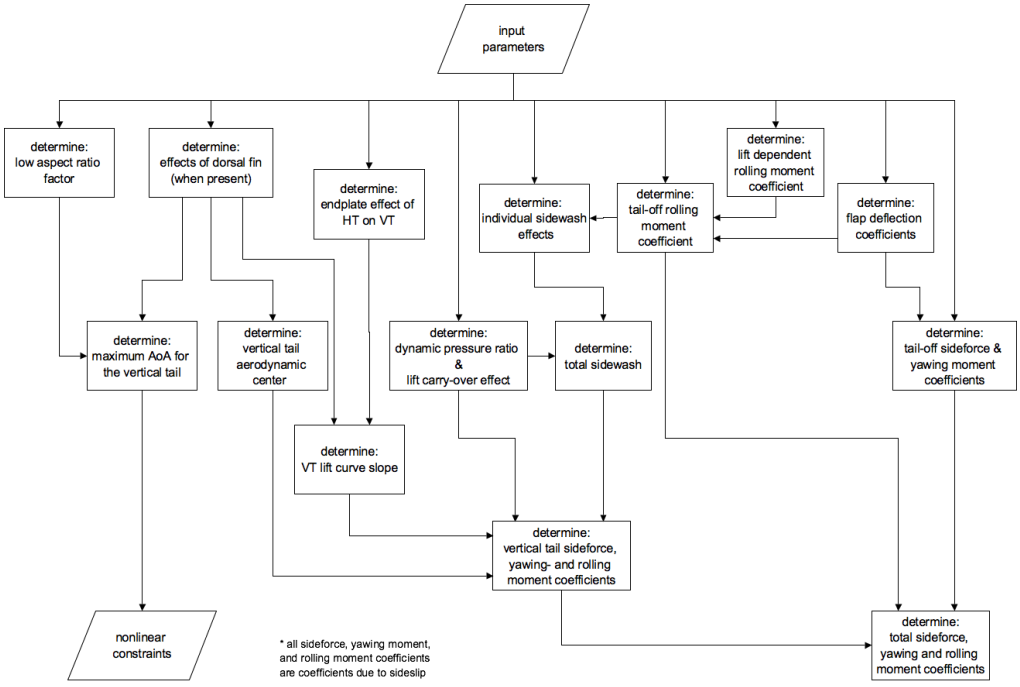

Figure B.6: Detailed flow chart of the coefficients-and-AoA-calculation block in figures B.3, B.4, and B.5

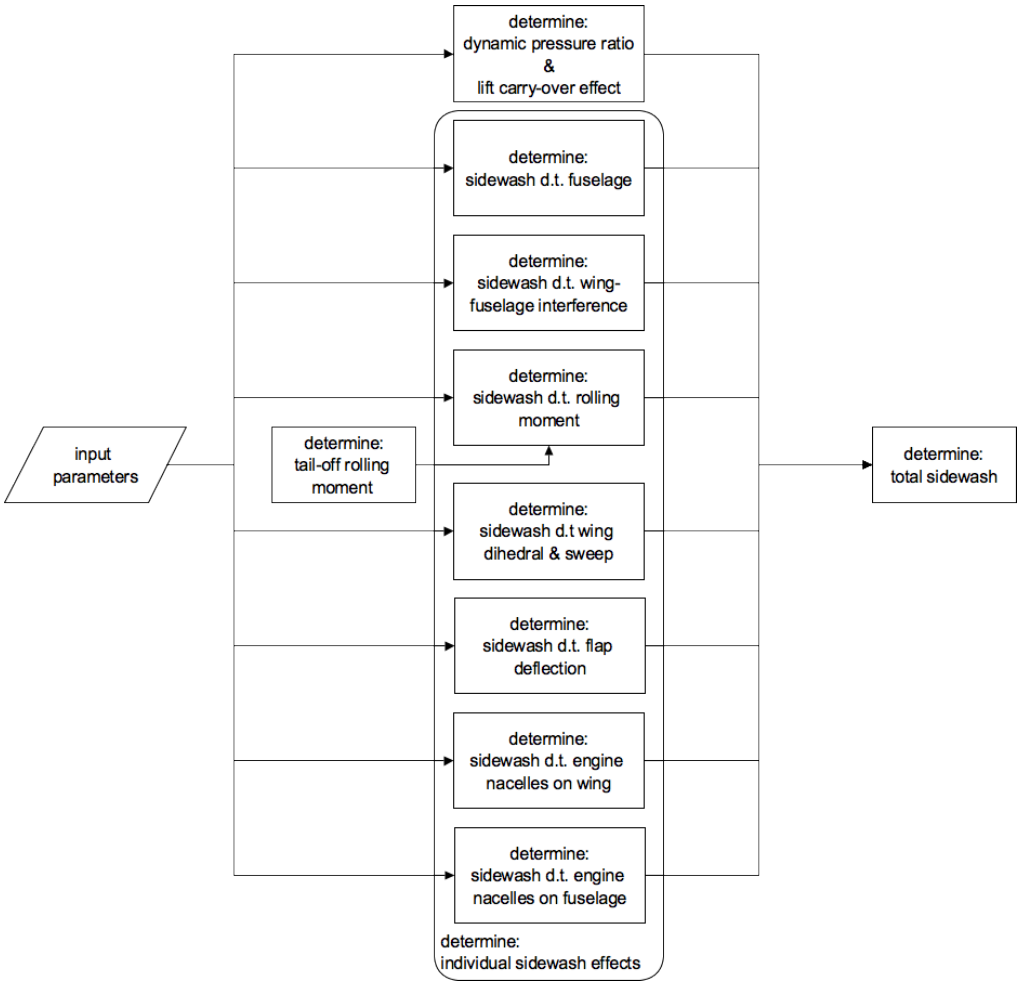

Figure B.7: Detailed flow chart of the sidewash calculations in figure B.6

C

FIGURES FROM THE AVL VALIDATION

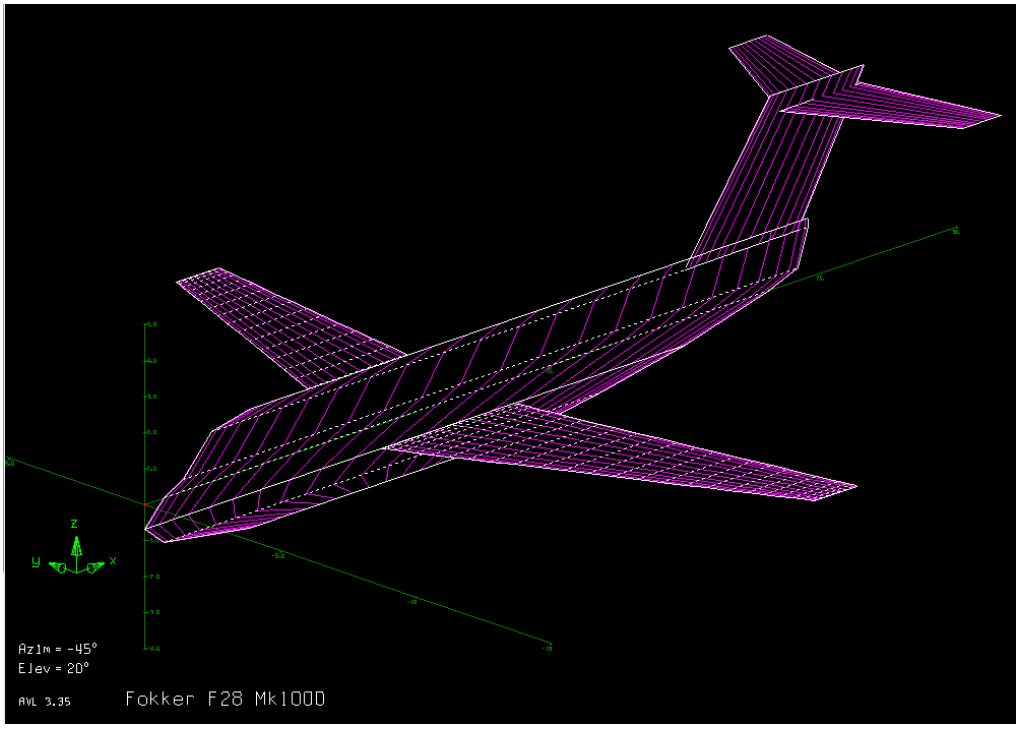

Figure C.1: Fokker F-28 model in AVL

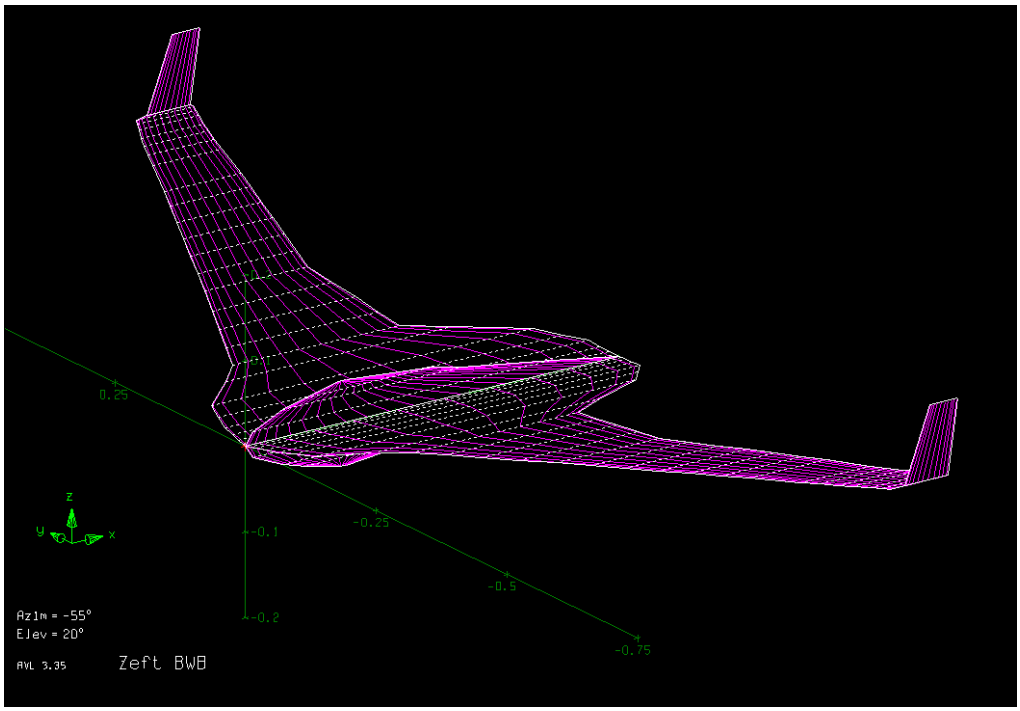

Figure C.2: ZEFT model in AVL

D

WINDTUNNEL DATA SHEETS AND FIGURES

D.1. WINDTUNNEL DATA SHEETS (WITH WINGLETS)

22-8-13 14:33 O:\Windtunnel data Reduced\redsideslipwithwlbmin5 1 of 2

========== ~&v3SLow Speed Laboratory / ~&v3SDelft University of Technology
~&v2S* W 3 D Data output *
========== ~&v3S1.25 x 1.80 m Low Turbulence Tunnel

~&v3SOperator	:TonHettema	Model name	: ZESAR model
~&v3SExperiment nr.	: 1	Scale	: 1 : 1 Processing date : 16-Aug-13
~&v3SSeries	: 10	Configuration	: clean
~&v3STest section	: 9	Input file	: zesar

Moment ref. point -> x_cg =~&v3S .0~&v0S% MAC z_cg =~&v3S .0~&v0S% MAC

Startvalues : Rho [Kg/m3] Temp [degr. C] nu [m2/s] Bar [mBar]

1.190 24.1 .154E-04 1014.9

Settings :	DAL	DAR	DFI	DFO	IH	DELEV	B3/4R	IC	DELEVC	P1	P2	P3	P4	P5
	.00	.00	.00	.00	.00	.00	.0	.00	.00	.000	.000	.000	.000	.000

Dpt	alfa	beta	CN	CT	CL	CD	C-side	Cm-pitch	Cm-roll	Cm-yaw	CL/CD	M	V	Re
1	-6.00	5.00	-.279	.00334	-.277	.03426	-.0214	-.08683	-.00725	.00441	-8.10	.146	50.47	.519E+06
2	-4.00	5.00	-.139	.01766	-.137	.02893	-.0200	-.06123	-.00866	.00355	-4.74	.146	50.54	.520E+06
3	-2.00	5.00	.008	.02426	.009	.02551	-.0189	-.03613	-.00933	.00282	.36	.146	50.56	.520E+06
4	.00	5.00	.157	.02307	.157	.02456	-.0182	-.01023	-.01013	.00215	6.41	.146	50.56	.520E+06
5	2.00	5.00	.309	.01441	.309	.02667	-.0179	.01554	-.01125	.00165	11.58	.146	50.52	.519E+06
6	4.00	5.00	.462	-.00137	.461	.03231	-.0177	.04070	-.01240	.00128	14.28	.146	50.47	.518E+06
7	6.00	5.00	.609	-.02320	.608	.04191	-.0169	.06813	-.01275	.00138	14.51	.146	50.38	.517E+06
8	8.00	5.00	.734	-.04875	.734	.05504	-.0157	.10164	-.00954	.00205	13.33	.145	50.24	.516E+06
9	10.00	5.00	.820	-.06584	.819	.07886	-.0191	.14533	-.00597	.00429	10.38	.145	50.01	.514E+06
10	12.00	5.00	.793	-.03065	.782	.13538	-.0107	.17765	-.01288	-.00383	5.78	.144	49.79	.511E+06
11	14.00	5.00	.773	.00562	.749	.19292	-.0139	.17395	-.00385	.00236	3.88	.143	49.55	.509E+06

22-8-13 14:30 O:\Windtunnel data Reduced\redsideslipwithwlb0 1 of 2

========== ~&v3SLow Speed Laboratory / ~&v3SDelft University of Technology
~&v2S* W 3 D Data output *
========== ~&v3S1.25 x 1.80 m Low Turbulence Tunnel

~&v3SOperator	:onHettema	Model name	: ZESAR model
~&v3SExperiment nr.	: 1	Scale	: 1 : 1 Processing date : 15-Aug-13
~&v3SSeries	: 1	Configuration	: clean
~&v3STest section	: 9	Input file	: zesar

Moment ref. point -> x_cg =~&v3S .0~&v0S% MAC z_cg =~&v3S .0~&v0S% MAC

Startvalues :	Rho [Kg/m3]	Temp [degr. C]	nu [m2/s]	Bar [mBar]
	1.193	24.3	.154E-04	1018.6

Settings :	DAL	DAR	DFI	DFO	IH	DELEV	B3/4R	IC	DELEVC	P1	P2	P3	P4	P5
	.00	.00	.00	.00	.00	.00	.0	.00	.00	.000	.000	.000	.000	.000

Dpt	alfa	beta	CN	CT	CL	CD	C-side	Cm-pitch	Cm-roll	Cm-yaw	CL/CD	M	V	Re
1	-6.00	.00	-.283	.00323	-.281	.03275	.0011	-.08556	-.00221	-.00016	-8.57	.145	50.22	.518E+06
2	-4.00	.00	-.140	.01752	-.138	.02725	.0005	-.05863	-.00207	-.00006	-5.08	.145	50.28	.518E+06
3	-2.00	.00	.009	.02423	.010	.02391	.0006	-.03340	-.00176	-.00015	.40	.145	50.32	.518E+06
4	.00	.00	.158	.02301	.158	.02300	.0005	-.00773	-.00171	-.00022	6.88	.145	50.31	.518E+06
5	2.00	.00	.310	.01425	.310	.02507	.0004	.01824	-.00194	-.00025	12.35	.145	50.27	.517E+06
6	4.00	.00	.465	-.00183	.464	.03060	.0004	.04326	-.00225	-.00033	15.16	.145	50.20	.516E+06
7	6.00	.00	.615	-.02489	.614	.03948	.0003	.06911	-.00258	-.00041	15.55	.145	50.11	.515E+06
8	8.00	.00	.743	-.05125	.743	.05271	.0011	.10209	.00056	.00024	14.10	.144	49.96	.513E+06
9	10.00	.00	.831	-.06813	.831	.07728	-.0016	.14748	.00407	.00303	10.75	.144	49.71	.511E+06
10	12.00	.00	.778	-.02376	.766	.13843	.0056	.17572	-.01189	-.00694	5.53	.143	49.50	.509E+06
11	14.00	.00	.764	.00949	.739	.19396	.0003	.17148	-.00310	-.00048	3.81	.142	49.28	.506E+06

22-8-13 14:30 O:\Windtunnel data Reduced\redsideslipwithwlb2 1 of 2

========== ~&v3SLow Speed Laboratory / ~&v3SDelft University of Technology
~&v2S* W 3 D Data output *
========== ~&v3S1.25 x 1.80 m Low Turbulence Tunnel

~&v3SOperator	:TonHettema	Model name	: ZESAR model
~&v3SExperiment nr.	: 1	Scale	: 1 : 1 Processing date : 15-Aug-13
~&v3SSeries	: 2	Configuration	: clean
~&v3STest section	: 9	Input file	: zesar

Moment ref. point -> x_cg =~&v3S .0~&v0S% MAC z_cg =~&v3S .0~&v0S% MAC

Startvalues :	Rho [Kg/m3]	Temp [degr. C]	nu [m2/s]	Bar [mBar]
	1.191	24.8	.154E-04	1018.4

Settings :	DAL	DAR	DFI	DFO	IH	DELEV	B3/4R	IC	DELEVC	P1	P2	P3	P4	P5
	.00	.00	.00	.00	.00	.00	.0	.00	.00	.000	.000	.000	.000	.000

Dpt	alfa	beta	CN	CT	CL	CD	C-side	Cm-pitch	Cm-roll	Cm-yaw	CL/CD	M	V	Re
1	-6.00	-2.50	-.282	.00344	-.280	.03337	.0120	-.08634	.00050	-.00235	-8.39	.146	50.47	.519E+06
2	-4.00	-2.50	-.140	.01757	-.138	.02775	.0113	-.05950	.00120	-.00199	-4.98	.146	50.54	.519E+06
3	-2.00	-2.50	.008	.02426	.009	.02440	.0106	-.03454	.00192	-.00168	.37	.146	50.58	.519E+06
4	.00	-2.50	.158	.02303	.158	.02345	.0100	-.00840	.00226	-.00141	6.73	.146	50.56	.519E+06
5	2.00	-2.50	.309	.01432	.309	.02550	.0096	.01758	.00263	-.00119	12.10	.146	50.52	.519E+06
6	4.00	-2.50	.464	-.00174	.463	.03097	.0092	.04280	.00279	-.00103	14.94	.146	50.46	.518E+06
7	6.00	-2.50	.613	-.02468	.612	.03990	.0091	.06871	.00289	-.00101	15.35	.145	50.36	.517E+06
8	8.00	-2.50	.741	-.05029	.741	.05378	.0100	.10210	.00573	-.00073	13.78	.145	50.21	.515E+06
9	10.00	-2.50	.832	-.06813	.831	.07763	.0074	.14547	.00913	.00233	10.71	.144	49.99	.513E+06
10	12.00	-2.50	.757	-.00278	.741	.15485	.0081	.17377	-.00532	-.00240	4.78	.144	49.70	.510E+06
11	14.00	-2.50	.763	.01014	.738	.19455	.0076	.16891	-.00278	-.00188	3.79	.143	49.53	.508E+06

22-8-13 14:31 O:\Windtunnel data Reduced\redsideslipwithwlb5 1 of 2

========== ~&v3SLow Speed Laboratory / ~&v3SDelft University of Technology
~&v2S* W 3 D Data output *
========== ~&v3S1.25 x 1.80 m Low Turbulence Tunnel

~&v3SOperator :TonHettema Model name : ZESAR model
~&v3SExperiment nr. : 1 Scale : 1 : 1 Processing date : 15-Aug-13
~&v3SSeries : 3 Configuration : clean
~&v3STest section : 9 Input file : zesar

Moment ref. point -> x_cg =~&v3S .0~&v0S% MAC z_cg =~&v3S .0~&v0S% MAC

Startvalues : Rho [Kg/m3] Temp [degr. C] nu [m2/s] Bar [mBar]

1.189 25.1 .155E-04 1018.3

Settings :	DAL	DAR	DFI	DFO	IH	DELEV	B3/4R	IC	DELEVC	P1	P2	P3	P4	P5
	.00	.00	.00	.00	.00	.00	.0	.00	.00	.000	.000	.000	.000	.000

Dpt	alfa	beta	CN	CT	CL	CD	C-side	Cm-pitch	Cm-roll	Cm-yaw	CL/CD	M	V	Re
1	-6.00	-5.00	-.279	.00561	-.277	.03579	.0135	-.09174	.00615	-.00224	-7.74	.146	50.59	.519E+06
2	-4.00	-5.00	-.139	.01952	-.137	.03019	.0134	-.06524	.00738	-.00171	-4.53	.146	50.66	.519E+06
3	-2.00	-5.00	.009	.02612	.010	.02683	.0130	-.04008	.00814	-.00120	.36	.146	50.69	.519E+06
4	.00	-5.00	.157	.02483	.157	.02585	.0129	-.01429	.00884	-.00075	6.09	.146	50.69	.519E+06
5	2.00	-5.00	.308	.01613	.308	.02790	.0129	.01158	.00948	-.00042	11.02	.146	50.66	.519E+06
6	4.00	-5.00	.461	.00052	.460	.03369	.0128	.03660	.01018	-.00023	13.66	.146	50.59	.518E+06
7	6.00	-5.00	.608	-.02146	.607	.04309	.0121	.06481	.00963	-.00047	14.08	.146	50.48	.517E+06
8	8.00	-5.00	.735	-.04722	.734	.05635	.0120	.09874	.01172	-.00005	13.03	.145	50.34	.516E+06
9	10.00	-5.00	.831	-.06574	.830	.08027	.0120	.13900	.01582	.00271	10.33	.145	50.14	.514E+06
10	12.00	-5.00	.848	-.04624	.839	.13083	.0033	.17628	.02457	.01045	6.41	.144	49.91	.511E+06
11	14.00	-5.00	.765	.01107	.740	.19610	.0115	.16289	-.00056	-.00212	3.77	.143	49.66	.509E+06

22-8-13 14:31 O:\Windtunnel data Reduced\redsideslipwithwlb7 1 of 2

========== ~&v3SLow Speed Laboratory / ~&v3SDelft University of Technology
~&v2S* W 3 D Data output *
========== ~&v3S1.25 x 1.80 m Low Turbulence Tunnel

~&v3SOperator :TonHettema Model name : ZESAR model
~&v3SExperiment nr. : 1 Scale : 1 : 1 Processing date : 16-Aug-13
~&v3SSeries : 4 Configuration : clean
~&v3STest section : 9 Input file : zesar

Moment ref. point -> x_cg =~&v3S .0~&v0S% MAC z_cg =~&v3S .0~&v0S% MAC

Startvalues : Rho [Kg/m3] Temp [degr. C] nu [m2/s] Bar [mBar]

1.194 23.2 .153E-04 1015.3

Settings :	DAL	DAR	DFI	DFO	IH	DELEV	B3/4R	IC	DELEVC	P1	P2	P3	P4	P5
	.00	.00	.00	.00	.00	.00	.0	.00	.00	.000	.000	.000	.000	.000

Dpt	alfa	beta	CN	CT	CL	CD	C-side	Cm-pitch	Cm-roll	Cm-yaw	CL/CD	M	V	Re
1	-6.00	-7.50	-.275	.00590	-.272	.03763	.0258	-.09394	.00909	-.00454	-7.24	.145	50.15	.519E+06
2	-4.00	-7.50	-.135	.01968	-.133	.03198	.0244	-.06742	.01096	-.00357	-4.16	.145	50.21	.519E+06
3	-2.00	-7.50	.011	.02622	.012	.02864	.0233	-.04268	.01229	-.00267	.42	.146	50.24	.519E+06
4	.00	-7.50	.158	.02514	.158	.02784	.0224	-.01676	.01333	-.00196	5.68	.146	50.24	.519E+06
5	2.00	-7.50	.307	.01685	.306	.03015	.0216	.00978	.01444	-.00150	10.16	.145	50.22	.519E+06
6	4.00	-7.50	.456	.00211	.454	.03621	.0201	.03615	.01456	-.00130	12.55	.145	50.15	.518E+06
7	6.00	-7.50	.599	-.01974	.598	.04492	.0176	.06465	.01383	-.00105	13.31	.145	50.06	.517E+06
8	8.00	-7.50	.727	-.04575	.726	.05774	.0178	.09712	.01670	-.00036	12.58	.145	49.94	.516E+06
9	10.00	-7.50	.824	-.06444	.822	.08115	.0174	.13531	.01998	.00230	10.13	.144	49.75	.514E+06
10	12.00	-7.50	.850	-.04725	.841	.13066	.0105	.17174	.02827	.00965	6.43	.143	49.51	.511E+06
11	14.00	-7.50	.770	.01088	.744	.19723	.0167	.15634	.00180	-.00273	3.77	.143	49.24	.508E+06

22-8-13 14:32 O:\Windtunnel data Reduced\redsideslipwithwlb10 1 of 2

========== ~&v3SLow Speed Laboratory / ~&v3SDelft University of Technology
~&v2S* W 3 D Data output *
========== ~&v3S1.25 x 1.80 m Low Turbulence Tunnel

~&v3SOperator	:TonHettema	Model name	: ZESAR model
~&v3SExperiment nr.	: 1	Scale	: 1 : 1 Processing date : 16-Aug-13
~&v3SSeries	: 5	Configuration	: clean
~&v3STest section	: 9	Input file	: zesar

Moment ref. point -> x_cg =~&v3S .0~&v0S% MAC z_cg =~&v3S .0~&v0S% MAC

Startvalues :	Rho [Kg/m3]	Temp [degr. C]	nu [m2/s]	Bar [mBar]
	1.191	23.7	.154E-04	1015.2

Settings :	DAL	DAR	DFI	DFO	IH	DELEV	B3/4R	IC	DELEVC	P1	P2	P3	P4	P5
	.00	.00	.00	.00	.00	.00	.0	.00	.00	.000	.000	.000	.000	.000

Dpt	alfa	beta	CN	CT	CL	CD	C-side	Cm-pitch	Cm-roll	Cm-yaw	CL/CD	M	V	Re
1	-6.00	-10.00	-.270	.00642	-.268	.04146	.0426	-.09411	.01073	-.00755	-6.46	.146	50.33	.519E+06
2	-4.00	-10.00	-.132	.01977	-.131	.03558	.0407	-.06836	.01296	-.00655	-3.67	.146	50.38	.519E+06
3	-2.00	-10.00	.011	.02625	.012	.03212	.0385	-.04374	.01470	-.00558	.38	.146	50.41	.519E+06
4	.00	-10.00	.156	.02533	.156	.03126	.0363	-.01775	.01608	-.00465	5.00	.146	50.41	.519E+06
5	2.00	-10.00	.301	.01780	.300	.03357	.0329	.00928	.01642	-.00393	8.94	.146	50.38	.519E+06
6	4.00	-10.00	.446	.00300	.445	.03870	.0294	.03637	.01672	-.00313	11.50	.146	50.33	.518E+06
7	6.00	-10.00	.589	-.01880	.588	.04699	.0275	.06362	.01719	-.00259	12.50	.145	50.25	.517E+06
8	8.00	-10.00	.716	-.04450	.715	.05953	.0278	.09440	.02036	-.00181	12.01	.145	50.13	.516E+06
9	10.00	-10.00	.813	-.06347	.812	.08220	.0267	.13109	.02326	.00090	9.88	.145	49.96	.514E+06
10	12.00	-10.00	.846	-.04765	.837	.13057	.0192	.16716	.02921	.00734	6.41	.144	49.70	.512E+06
11	14.00	-10.00	.772	.00975	.746	.19781	.0269	.15101	.00279	-.00477	3.77	.143	49.42	.509E+06

22-8-13 14:32 O:\Windtunnel data Reduced\redsideslipwithwlb12 1 of 2

========== ~&v3SLow Speed Laboratory / ~&v3SDelft University of Technology
~&v2S* W 3 D Data output *
========== ~&v3S1.25 x 1.80 m Low Turbulence Tunnel

~&v3SOperator	:TonHettema	Model name	: ZESAR model
~&v3SExperiment nr.	: 1	Scale	: 1 : 1 Processing date : 16-Aug-13
~&v3SSeries	: 6	Configuration	: clean
~&v3STest section	: 9	Input file	: zesar

Moment ref. point -> x_cg =~&v3S .0~&v0S% MAC z_cg =~&v3S .0~&v0S% MAC

Startvalues :	Rho [Kg/m3]	Temp [degr. C]	nu [m2/s]	Bar [mBar]
	1.190	24.0	.154E-04	1015.1

Settings :	DAL	DAR	DFI	DFO	IH	DELEV	B3/4R	IC	DELEVC	P1	P2	P3	P4	P5
	.00	.00	.00	.00	.00	.00	.0	.00	.00	.000	.000	.000	.000	.000

Dpt	alfa	beta	CN	CT	CL	CD	C-side	Cm-pitch	Cm-roll	Cm-yaw	CL/CD	M	V	Re
1	-6.00	-12.50	-.264	.00648	-.262	.04486	.0538	-.09206	.01310	-.00984	-5.83	.146	50.42	.519E+06
2	-4.00	-12.50	-.129	.01991	-.128	.03948	.0521	-.06655	.01551	-.00873	-3.23	.146	50.47	.519E+06
3	-2.00	-12.50	.010	.02634	.011	.03610	.0497	-.04236	.01737	-.00769	.31	.146	50.50	.520E+06
4	.00	-12.50	.151	.02561	.151	.03482	.0454	-.01658	.01817	-.00660	4.34	.146	50.51	.519E+06
5	2.00	-12.50	.293	.01778	.293	.03621	.0410	.01021	.01878	-.00549	8.08	.146	50.49	.519E+06
6	4.00	-12.50	.436	.00310	.435	.04092	.0379	.03602	.01977	-.00454	10.63	.146	50.45	.519E+06
7	6.00	-12.50	.576	-.01821	.575	.04902	.0365	.06263	.02079	-.00390	11.73	.146	50.37	.518E+06
8	8.00	-12.50	.702	-.04358	.701	.06120	.0368	.09260	.02405	-.00309	11.46	.145	50.26	.517E+06
9	10.00	-12.50	.800	-.06257	.799	.08321	.0354	.12616	.02672	-.00040	9.60	.145	50.08	.515E+06
10	12.00	-12.50	.841	-.04979	.833	.12925	.0281	.16341	.02992	.00538	6.44	.144	49.84	.513E+06
11	14.00	-12.50	.770	.00795	.745	.19776	.0385	.14523	.00366	-.00703	3.77	.143	49.54	.509E+06

22-8-13 14:32 O:\Windtunnel data Reduced\redsideslipwithwlb15 1 of 2

========== ~&v3SLow Speed Laboratory / ~&v3SDelft University of Technology
~&v2S* W 3 D Data output *
========== ~&v3S1.25 x 1.80 m Low Turbulence Tunnel

~&v3SOperator :TonHettema Model name : ZESAR model
~&v3SExperiment nr. : 1 Scale : 1 : 1 Processing date : 16-Aug-13
~&v3SSeries : 7 Configuration : clean
~&v3STest section : 9 Input file : zesar

Moment ref. point -> x_cg =~&v3S .0~&v0S% MAC z_cg =~&v3S .0~&v0S% MAC

Startvalues : Rho [Kg/m3] Temp [degr. C] nu [m2/s] Bar [mBar]

1.189 24.2 .154E-04 1015.0

Settings :	DAL	DAR	DFI	DFO	IH	DELEV	B3/4R	IC	DELEVC	P1	P2	P3	P4	P5
	.00	.00	.00	.00	.00	.00	.0	.00	.00	.000	.000	.000	.000	.000

Dpt	alfa	beta	CN	CT	CL	CD	C-side	Cm-pitch	Cm-roll	Cm-yaw	CL/CD	M	V	Re
1	-6.00	-15.00	-.258	.00631	-.256	.04825	.0626	-.08941	.01500	-.01171	-5.30	.146	50.46	.519E+06
2	-4.00	-15.00	-.127	.01961	-.125	.04275	.0591	-.06416	.01734	-.01033	-2.93	.146	50.51	.519E+06
3	-2.00	-15.00	.009	.02602	.010	.03921	.0556	-.03926	.01926	-.00896	.25	.146	50.54	.519E+06
4	.00	-15.00	.146	.02518	.146	.03776	.0520	-.01416	.02064	-.00772	3.87	.146	50.55	.519E+06
5	2.00	-15.00	.285	.01745	.284	.03895	.0483	.01138	.02162	-.00662	7.29	.146	50.53	.519E+06
6	4.00	-15.00	.425	.00295	.424	.04332	.0457	.03640	.02313	-.00561	9.79	.146	50.50	.519E+06
7	6.00	-15.00	.562	-.01779	.561	.05109	.0442	.06163	.02459	-.00490	10.97	.146	50.43	.518E+06
8	8.00	-15.00	.685	-.04269	.684	.06267	.0443	.09080	.02776	-.00402	10.91	.146	50.33	.517E+06
9	10.00	-15.00	.782	-.06050	.781	.08485	.0431	.12097	.02918	-.00175	9.21	.145	50.13	.515E+06
10	12.00	-15.00	.836	-.05368	.829	.12653	.0362	.15910	.03019	.00349	6.55	.144	49.92	.513E+06
11	14.00	-15.00	.769	.00502	.745	.19671	.0477	.13862	.00430	-.00895	3.79	.143	49.60	.510E+06

22-8-13 14:33 O:\Windtunnel data Reduced\redsideslipwithwlb20 1 of 2

========== ~&v3SLow Speed Laboratory / ~&v3SDelft University of Technology
~&v2S* W 3 D Data output *
========== ~&v3S1.25 x 1.80 m Low Turbulence Tunnel

~&v3SOperator :TonHettema Model name : ZESAR model
~&v3SExperiment nr. : 1 Scale : 1 : 1 Processing date : 16-Aug-13
~&v3SSeries : 8 Configuration : clean
~&v3STest section : 9 Input file : zesar

Moment ref. point -> x_cg =~&v3S .0~&v0S% MAC z_cg =~&v3S .0~&v0S% MAC

Startvalues : Rho [Kg/m3] Temp [degr. C] nu [m2/s] Bar [mBar]

1.189 24.2 .154E-04 1014.9

Settings :	DAL	DAR	DFI	DFO	IH	DELEV	B3/4R	IC	DELEVC	P1	P2	P3	P4	P5
	.00	.00	.00	.00	.00	.00	.0	.00	.00	.000	.000	.000	.000	.000

Dpt	alfa	beta	CN	CT	CL	CD	C-side	Cm-pitch	Cm-roll	Cm-yaw	CL/CD	M	V	Re
1	-6.00	-20.00	-.243	.00528	-.242	.05542	.0777	-.07940	.01768	-.01503	-4.36	.146	50.49	.519E+06
2	-4.00	-20.00	-.120	.01777	-.119	.04959	.0732	-.05521	.02036	-.01322	-2.40	.146	50.53	.519E+06
3	-2.00	-20.00	.006	.02414	.006	.04562	.0676	-.03169	.02223	-.01134	.14	.146	50.55	.519E+06
4	.00	-20.00	.136	.02353	.136	.04414	.0644	-.00858	.02459	-.00980	3.07	.146	50.57	.519E+06
5	2.00	-20.00	.267	.01633	.267	.04538	.0622	.01429	.02693	-.00859	5.88	.146	50.55	.519E+06
6	4.00	-20.00	.399	.00258	.398	.04938	.0608	.03815	.02944	-.00758	8.06	.146	50.54	.519E+06
7	6.00	-20.00	.527	-.01698	.526	.05632	.0597	.06093	.03137	-.00683	9.34	.146	50.47	.518E+06
8	8.00	-20.00	.643	-.04064	.642	.06657	.0594	.08616	.03454	-.00587	9.65	.146	50.38	.517E+06
9	10.00	-20.00	.747	-.05721	.745	.08805	.0560	.10866	.03389	-.00234	8.47	.145	50.20	.515E+06
10	12.00	-20.00	.814	-.06377	.809	.11868	.0534	.14002	.03042	-.00091	6.82	.145	50.03	.514E+06
11	14.00	-20.00	.838	-.05353	.826	.15866	.0494	.15339	.02680	-.00029	5.21	.144	49.82	.512E+06

22-8-13 14:33 O:\Windtunnel data Reduced\redsideslipwithwlb25 1 of 2

========== ¯&v3SLow Speed Laboratory / ¯&v3SDelft University of Technology
¯&v2S* W 3 D Data output *
========== ¯&v3S1.25 x 1.80 m Low Turbulence Tunnel

¯&v3SOperator	:TonHettema	Model name	: ZESAR model
¯&v3SExperiment nr.	: 1	Scale	: 1 : 1 Processing date : 16-Aug-13
¯&v3SSeries	: 9	Configuration	: clean
¯&v3STest section	: 9	Input file	: zesar

Moment ref. point -> x_cg =¯&v3S .0¯&v0S% MAC z_cg =¯&v3S .0¯&v0S% MAC

Startvalues :	Rho [Kg/m3]	Temp [degr. C]	nu [m2/s]	Bar [mBar]
	1.188	24.4	.154E-04	1014.9

Settings :	DAL	DAR	DFI	DFO	IH	DELEV	B3/4R	IC	DELEVC	P1	P2	P3	P4	P5
	.00	.00	.00	.00	.00	.00	.0	.00	.00	.000	.000	.000	.000	.000

Dpt	alfa	beta	CN	CT	CL	CD	C-side	Cm-pitch	Cm-roll	Cm-yaw	CL/CD	M	V	Re
1	-6.00	-25.00	-.225	.00400	-.224	.06252	.0889	-.06659	.01829	-.01755	-3.58	.146	50.55	.519E+06
2	-4.00	-25.00	-.113	.01544	-.112	.05804	.0874	-.04380	.02227	-.01605	-1.93	.146	50.57	.519E+06
3	-2.00	-25.00	.005	.02113	.006	.05449	.0840	-.02354	.02548	-.01427	.10	.146	50.59	.519E+06
4	.00	-25.00	.126	.02092	.126	.05277	.0800	-.00308	.02858	-.01244	2.38	.146	50.62	.519E+06
5	2.00	-25.00	.247	.01448	.246	.05353	.0771	.01765	.03136	-.01088	4.60	.146	50.61	.519E+06
6	4.00	-25.00	.369	.00204	.368	.05698	.0753	.03879	.03447	-.00965	6.45	.146	50.60	.519E+06
7	6.00	-25.00	.486	-.01611	.485	.06295	.0744	.05997	.03705	-.00872	7.70	.146	50.55	.519E+06
8	8.00	-25.00	.594	-.03820	.594	.07188	.0739	.08238	.04023	-.00775	8.26	.146	50.46	.518E+06
9	10.00	-25.00	.696	-.05582	.696	.08934	.0699	.09925	.03905	-.00435	7.79	.146	50.33	.516E+06
10	12.00	-25.00	.772	-.06747	.769	.11473	.0690	.11904	.03204	-.00459	6.70	.145	50.18	.515E+06
11	14.00	-25.00	.812	-.07022	.805	.14572	.0695	.13010	.02571	-.00579	5.53	.145	50.00	.513E+06

D.2. WINDTUNNEL DATA SHEETS (WITHOUT WINGLETS)

22-8-13 14:22 O:\Windtunnel data Reduced\redsideslipnowlbmin5 1 of 2

========== ~&v3SLow Speed Laboratory / ~&v3SDelft University of Technology
~&v2S* W 3 D Data output *
========== ~&v3S1.25 x 1.80 m Low Turbulence Tunnel

~&v3SOperator :TonHettema Model name : ZESAR model
~&v3SExperiment nr. : 2 Scale : 1 : 1 Processing date : 16-Aug-13
~&v3SSeries : 10 Configuration : nowinglets
~&v3STest section : 9 Input file : zesar

Moment ref. point -> x_cg =~&v3S .0~&v0S% MAC z_cg =~&v3S .0~&v0S% MAC

Startvalues : Rho [Kg/m3] Temp [degr. C] nu [m2/s] Bar [mBar]

1.190 23.9 .154E-04 1014.6

Settings :	DAL	DAR	DFI	DFO	IH	DELEV	B3/4R	IC	DELEVC	P1	P2	P3	P4	P5
	.00	.00	.00	.00	.00	.00	.0	.00	.00	.000	.000	.000	.000	.000

Dpt	alfa	beta	CN	CT	CL	CD	C-side	Cm-pitch	Cm-roll	Cm-yaw	CL/CD	M	V	Re
1	-6.00	5.00	-.275	.00407	-.273	.03364	-.0107	-.08843	-.00433	.00266	-8.13	.146	50.40	.519E+06
2	-4.00	5.00	-.138	.01790	-.137	.02822	-.0093	-.06042	-.00556	.00211	-4.85	.146	50.47	.519E+06
3	-2.00	5.00	.005	.02430	.005	.02478	-.0086	-.03272	-.00600	.00169	.22	.146	50.50	.520E+06
4	.00	5.00	.150	.02331	.150	.02392	-.0080	-.00442	-.00682	.00130	6.27	.146	50.50	.519E+06
5	2.00	5.00	.298	.01512	.297	.02609	-.0079	.02418	-.00786	.00103	11.38	.146	50.47	.519E+06
6	4.00	5.00	.447	-.00009	.446	.03168	-.0079	.05136	-.00905	.00078	14.08	.146	50.40	.518E+06
7	6.00	5.00	.593	-.02196	.592	.04071	-.0082	.07948	-.01024	.00053	14.54	.146	50.31	.517E+06
8	8.00	5.00	.720	-.04754	.720	.05364	-.0084	.11160	-.00852	.00099	13.41	.145	50.19	.516E+06
9	10.00	5.00	.808	-.06452	.807	.07737	-.0101	.15200	-.00392	.00356	10.43	.145	49.97	.514E+06
10	12.00	5.00	.784	-.02977	.773	.13350	-.0007	.18140	-.01077	-.00447	5.79	.144	49.75	.511E+06
11	14.00	5.00	.764	.00551	.740	.19012	-.0069	.17516	-.00289	.00162	3.89	.143	49.50	.509E+06

22-8-13 14:25 O:\Windtunnel data Reduced\redsideslipnowlb0 1 of 2

========== ~&v3SLow Speed Laboratory / ~&v3SDelft University of Technology
~&v2S* W 3 D Data output *
========== ~&v3S1.25 x 1.80 m Low Turbulence Tunnel

~&v3SOperator :TonHettema Model name : ZESAR model
~&v3SExperiment nr. : 2 Scale : 1 : 1 Processing date : 16-Aug-13
~&v3SSeries : 1 Configuration : nowinglets
~&v3STest section : 9 Input file : zesar

Moment ref. point -> x_cg =~&v3S .0~&v0S% MAC z_cg =~&v3S .0~&v0S% MAC

Startvalues : Rho [Kg/m3] Temp [degr. C] nu [m2/s] Bar [mBar]

1.189 24.2 .154E-04 1014.6

Settings :	DAL	DAR	DFI	DFO	IH	DELEV	B3/4R	IC	DELEVC	P1	P2	P3	P4	P5
	.00	.00	.00	.00	.00	.00	.0	.00	.00	.000	.000	.000	.000	.000

Dpt	alfa	beta	CN	CT	CL	CD	C-side	Cm-pitch	Cm-roll	Cm-yaw	CL/CD	M	V	Re
1	-6.00	.00	-.280	.00331	-.278	.03256	.0014	-.08779	-.00193	-.00019	-8.54	.146	50.49	.519E+06
2	-4.00	.00	-.141	.01715	-.139	.02694	.0007	-.05879	-.00182	-.00009	-5.17	.146	50.55	.519E+06
3	-2.00	.00	.003	.02373	.004	.02360	.0008	-.03118	-.00152	-.00015	.18	.146	50.59	.520E+06
4	.00	.00	.150	.02277	.150	.02277	.0008	-.00225	-.00157	-.00021	6.57	.146	50.59	.520E+06
5	2.00	.00	.297	.01461	.297	.02498	.0008	.02651	-.00176	-.00024	11.88	.146	50.55	.519E+06
6	4.00	.00	.449	-.00059	.448	.03071	.0007	.05405	-.00198	-.00030	14.57	.146	50.48	.518E+06
7	6.00	.00	.596	-.02251	.595	.03989	.0006	.08196	-.00238	-.00036	14.91	.146	50.39	.517E+06
8	8.00	.00	.725	-.04839	.725	.05300	.0003	.11441	-.00012	.00020	13.68	.145	50.27	.516E+06
9	10.00	.00	.818	-.06644	.818	.07669	-.0021	.15506	.00362	.00286	10.66	.145	50.02	.514E+06
10	12.00	.00	.768	-.02376	.756	.13643	.0074	.17976	-.01119	-.00675	5.54	.144	49.82	.512E+06
11	14.00	.00	.755	.00861	.730	.19098	.0002	.17403	-.00313	-.00047	3.82	.143	49.58	.509E+06

22-8-13 14:25 O:\Windtunnel data Reduced\redsideslipnowlb2 1 of 2

========== ¯&v3SLow Speed Laboratory / ¯&v3SDelft University of Technology
¯&v2S* W 3 D Data output *
========== ¯&v3S1.25 x 1.80 m Low Turbulence Tunnel

¯&v3SOperator	:TonHettema	Model name	: ZESAR model
¯&v3SExperiment nr.	: 2	Scale	: 1 : 1 Processing date : 16-Aug-13
¯&v3SSeries	: 2	Configuration	: nowinglets
¯&v3STest section	: 9	Input file	: zesar

Moment ref. point -> x_cg =¯&v3S .0¯&v0S% MAC z_cg =¯&v3S .0¯&v0S% MAC

Startvalues :	Rho [Kg/m3]	Temp [degr. C]	nu [m2/s]	Bar [mBar]
	1.187	24.5	.155E-04	1014.5

Settings :	DAL	DAR	DFI	DFO	IH	DELEV	B3/4R	IC	DELEVC	P1	P2	P3	P4	P5
	.00	.00	.00	.00	.00	.00	.0	.00	.00	.000	.000	.000	.000	.000

Dpt	alfa	beta	CN	CT	CL	CD	C-side	Cm-pitch	Cm-roll	Cm-yaw	CL/CD	M	V	Re
1	-6.00	-2.50	-.280	.00370	-.278	.03318	.0070	-.08869	-.00074	-.00152	-8.37	.146	50.61	.519E+06
2	-4.00	-2.50	-.141	.01730	-.139	.02733	.0063	-.05915	-.00008	-.00130	-5.09	.146	50.67	.520E+06
3	-2.00	-2.50	.003	.02387	.004	.02396	.0057	-.03168	.00060	-.00115	.18	.147	50.70	.520E+06
4	.00	-2.50	.149	.02290	.149	.02310	.0053	-.00303	.00098	-.00100	6.45	.147	50.70	.520E+06
5	2.00	-2.50	.297	.01471	.296	.02525	.0048	.02592	.00128	-.00090	11.73	.146	50.67	.519E+06
6	4.00	-2.50	.448	-.00042	.446	.03097	.0047	.05325	.00143	-.00081	14.41	.146	50.60	.519E+06
7	6.00	-2.50	.594	-.02231	.593	.04006	.0047	.08175	.00158	-.00081	14.80	.146	50.50	.518E+06
8	8.00	-2.50	.724	-.04821	.723	.05312	.0045	.11392	.00399	-.00025	13.62	.146	50.38	.516E+06
9	10.00	-2.50	.819	-.06665	.818	.07657	.0020	.15383	.00737	.00248	10.68	.145	50.15	.514E+06
10	12.00	-2.50	.749	-.00344	.733	.15244	.0046	.17686	-.00603	-.00202	4.81	.144	49.87	.511E+06
11	14.00	-2.50	.755	.00957	.730	.19187	.0040	.17104	-.00328	-.00154	3.80	.144	49.68	.509E+06

22-8-13 14:25 O:\Windtunnel data Reduced\redsideslipnowlb5 1 of 2

========== ¯&v3SLow Speed Laboratory / ¯&v3SDelft University of Technology
¯&v2S* W 3 D Data output *
========== ¯&v3S1.25 x 1.80 m Low Turbulence Tunnel

¯&v3SOperator	:TonHettema	Model name	: ZESAR model
¯&v3SExperiment nr.	: 2	Scale	: 1 : 1 Processing date : 16-Aug-13
¯&v3SSeries	: 3	Configuration	: nowinglets
¯&v3STest section	: 9	Input file	: zesar

Moment ref. point -> x_cg =¯&v3S .0¯&v0S% MAC z_cg =¯&v3S .0¯&v0S% MAC

Startvalues :	Rho [Kg/m3]	Temp [degr. C]	nu [m2/s]	Bar [mBar]
	1.187	24.4	.154E-04	1014.4

Settings :	DAL	DAR	DFI	DFO	IH	DELEV	B3/4R	IC	DELEVC	P1	P2	P3	P4	P5
	.00	.00	.00	.00	.00	.00	.0	.00	.00	.000	.000	.000	.000	.000

Dpt	alfa	beta	CN	CT	CL	CD	C-side	Cm-pitch	Cm-roll	Cm-yaw	CL/CD	M	V	Re
1	-6.00	-5.01	-.277	.00613	-.275	.03525	.0033	-.09344	.00362	-.00061	-7.81	.146	50.60	.519E+06
2	-4.00	-5.01	-.140	.01957	-.138	.02945	.0033	-.06409	.00466	-.00034	-4.69	.146	50.66	.519E+06
3	-2.00	-5.01	.004	.02610	.005	.02613	.0031	-.03710	.00534	-.00009	.18	.147	50.70	.520E+06
4	.00	-5.01	.149	.02500	.149	.02519	.0032	-.00848	.00596	.00007	5.90	.147	50.71	.520E+06
5	2.00	-5.01	.296	.01675	.295	.02726	.0034	.02042	.00656	.00023	10.83	.146	50.66	.519E+06
6	4.00	-5.01	.445	.00160	.444	.03285	.0036	.04769	.00710	.00037	13.52	.146	50.60	.518E+06
7	6.00	-5.01	.591	-.02030	.590	.04179	.0040	.07569	.00761	.00042	14.12	.146	50.51	.517E+06
8	8.00	-5.01	.721	-.04633	.720	.05456	.0042	.10781	.01011	.00097	13.20	.146	50.39	.516E+06
9	10.00	-5.01	.817	-.06505	.816	.07770	.0017	.14669	.01271	.00362	10.50	.145	50.18	.514E+06
10	12.00	-5.01	.838	-.04554	.829	.12855	-.0074	.18035	.02218	.01111	6.45	.144	49.94	.512E+06
11	14.00	-5.01	.758	.01066	.733	.19343	.0042	.16461	-.00204	-.00139	3.79	.144	49.69	.509E+06

22-8-13 14:27 O:\Windtunnel data Reduced\redsideslipnowlb7 1 of 2

========== ~&v3SLow Speed Laboratory / ~&v3SDelft University of Technology
~&v2S* W 3 D Data output *
========== ~&v3S1.25 x 1.80 m Low Turbulence Tunnel

~&v3SOperator :TonHettema Model name : ZESAR model
~&v3SExperiment nr. : 2 Scale : 1 : 1 Processing date : 16-Aug-13
~&v3SSeries : 4 Configuration : nowinglets
~&v3STest section : 9 Input file : zesar

Moment ref. point -> x_cg =~&v3S .0~&v0S% MAC z_cg =~&v3S .0~&v0S% MAC

Startvalues : Rho [Kg/m3] Temp [degr. C] nu [m2/s] Bar [mBar]

1.187 24.6 .155E-04 1014.3

Settings :	DAL	DAR	DFI	DFO	IH	DELEV	B3/4R	IC	DELEVC	P1	P2	P3	P4	P5
	.00	.00	.00	.00	.00	.00	.0	.00	.00	.000	.000	.000	.000	.000

Dpt	alfa	beta	CN	CT	CL	CD	C-side	Cm-pitch	Cm-roll	Cm-yaw	CL/CD	M	V	Re
1	-6.00	-7.50	-.274	.00683	-.272	.03648	.0102	-.09513	.00501	-.00214	-7.46	.146	50.62	.519E+06
2	-4.00	-7.50	-.138	.02026	-.136	.03077	.0090	-.06628	.00664	-.00145	-4.43	.146	50.68	.519E+06
3	-2.00	-7.50	.004	.02670	.005	.02737	.0081	-.03930	.00777	-.00092	.19	.147	50.71	.519E+06
4	.00	-7.50	.148	.02561	.148	.02637	.0075	-.01100	.00886	-.00049	5.62	.147	50.71	.519E+06
5	2.00	-7.50	.294	.01744	.293	.02840	.0073	.01744	.00994	-.00015	10.32	.146	50.67	.519E+06
6	4.00	-7.50	.441	.00241	.440	.03385	.0074	.04422	.01106	.00014	12.99	.146	50.62	.518E+06
7	6.00	-7.50	.586	-.01929	.584	.04269	.0077	.07218	.01190	.00031	13.69	.146	50.54	.517E+06
8	8.00	-7.50	.715	-.04520	.714	.05522	.0077	.10403	.01474	.00096	12.93	.146	50.42	.516E+06
9	10.00	-7.50	.812	-.06413	.811	.07791	.0050	.14109	.01713	.00369	10.41	.145	50.23	.514E+06
10	12.00	-7.50	.839	-.04630	.831	.12762	-.0039	.17599	.02464	.01073	6.51	.144	49.98	.512E+06
11	14.00	-7.50	.762	.01051	.737	.19364	.0058	.15837	-.00023	-.00157	3.81	.144	49.71	.509E+06

22-8-13 14:28 O:\Windtunnel data Reduced\redsideslipnowlb10 1 of 2

========== ~&v3SLow Speed Laboratory / ~&v3SDelft University of Technology
~&v2S* W 3 D Data output *
========== ~&v3S1.25 x 1.80 m Low Turbulence Tunnel

~&v3SOperator :TonHettema Model name : ZESAR model
~&v3SExperiment nr. : 2 Scale : 1 : 1 Processing date : 16-Aug-13
~&v3SSeries : 5 Configuration : nowinglets
~&v3STest section : 9 Input file : zesar

Moment ref. point -> x_cg =~&v3S .0~&v0S% MAC z_cg =~&v3S .0~&v0S% MAC

Startvalues : Rho [Kg/m3] Temp [degr. C] nu [m2/s] Bar [mBar]

1.187 24.6 .155E-04 1014.4

Settings :	DAL	DAR	DFI	DFO	IH	DELEV	B3/4R	IC	DELEVC	P1	P2	P3	P4	P5
	.00	.00	.00	.00	.00	.00	.0	.00	.00	.000	.000	.000	.000	.000

Dpt	alfa	beta	CN	CT	CL	CD	C-side	Cm-pitch	Cm-roll	Cm-yaw	CL/CD	M	V	Re
1	-6.00	-10.00	-.269	.00719	-.267	.03849	.0215	-.09483	.00499	-.00465	-6.94	.146	50.63	.519E+06
2	-4.00	-10.00	-.135	.02047	-.134	.03275	.0193	-.06688	.00719	-.00369	-4.08	.146	50.68	.519E+06
3	-2.00	-10.00	.005	.02684	.006	.02933	.0178	-.04029	.00889	-.00296	.20	.147	50.71	.519E+06
4	.00	-10.00	.147	.02571	.147	.02822	.0167	-.01236	.01039	-.00228	5.20	.147	50.72	.519E+06
5	2.00	-10.00	.291	.01764	.290	.03011	.0159	.01537	.01202	-.00175	9.63	.146	50.68	.519E+06
6	4.00	-10.00	.436	.00285	.435	.03548	.0157	.04152	.01370	-.00127	12.25	.146	50.64	.518E+06
7	6.00	-10.00	.578	-.01862	.576	.04395	.0158	.06928	.01505	-.00097	13.11	.146	50.56	.517E+06
8	8.00	-10.00	.705	-.04432	.705	.05617	.0156	.10046	.01808	-.00019	12.55	.146	50.45	.516E+06
9	10.00	-10.00	.804	-.06325	.803	.07840	.0126	.13495	.02032	.00260	10.24	.145	50.27	.515E+06
10	12.00	-10.00	.837	-.04741	.828	.12617	.0032	.17114	.02524	.00911	6.56	.145	50.02	.512E+06
11	14.00	-10.00	.765	.00967	.740	.19352	.0117	.15261	-.00002	-.00303	3.82	.144	49.73	.509E+06

22-8-13 14:28 O:\Windtunnel data Reduced\redsideslipnowlb12 1 of 2

========== ~&v3SLow Speed Laboratory / ~&v3SDelft University of Technology
~&v2S* W 3 D Data output *
========== ~&v3S1.25 x 1.80 m Low Turbulence Tunnel

~&v3SOperator	:TonHettema	Model name	: ZESAR model
~&v3SExperiment nr.	: 2	Scale	: 1 : 1 Processing date : 16-Aug-13
~&v3SSeries	: 6	Configuration	: nowinglets
~&v3STest section	: 9	Input file	: zesar

Moment ref. point -> x_cg =~&v3S .0~&v0S% MAC z_cg =~&v3S .0~&v0S% MAC

Startvalues :	Rho [Kg/m3]	Temp [degr. C]	nu [m2/s]	Bar [mBar]
	1.187	24.6	.155E-04	1014.4

Settings :	DAL	DAR	DFI	DFO	IH	DELEV	B3/4R	IC	DELEVC	P1	P2	P3	P4	P5
	.00	.00	.00	.00	.00	.00	.0	.00	.00	.000	.000	.000	.000	.000

Dpt	alfa	beta	CN	CT	CL	CD	C-side	Cm-pitch	Cm-roll	Cm-yaw	CL/CD	M	V	Re
1	-6.00	-12.50	-.264	.00700	-.262	.04001	.0291	-.09375	.00597	-.00633	-6.54	.146	50.62	.519E+06
2	-4.00	-12.50	-.132	.02016	-.130	.03442	.0269	-.06568	.00838	-.00532	-3.77	.146	50.67	.519E+06
3	-2.00	-12.50	.006	.02646	.007	.03105	.0251	-.03992	.01046	-.00442	.22	.147	50.70	.519E+06
4	.00	-12.50	.145	.02541	.145	.02996	.0238	-.01281	.01242	-.00361	4.85	.147	50.70	.519E+06
5	2.00	-12.50	.287	.01743	.286	.03174	.0229	.01400	.01445	-.00295	9.01	.146	50.66	.519E+06
6	4.00	-12.50	.429	.00290	.428	.03692	.0225	.03959	.01653	-.00239	11.59	.146	50.62	.518E+06
7	6.00	-12.50	.568	-.01818	.566	.04517	.0227	.06684	.01823	-.00200	12.54	.146	50.55	.518E+06
8	8.00	-12.50	.693	-.04348	.693	.05705	.0225	.09682	.02134	-.00118	12.14	.146	50.45	.517E+06
9	10.00	-12.50	.793	-.06224	.792	.07879	.0194	.12913	.02338	.00150	10.05	.145	50.26	.515E+06
10	12.00	-12.50	.836	-.04994	.829	.12431	.0102	.16652	.02568	.00745	6.67	.145	50.03	.512E+06
11	14.00	-12.50	.765	.00837	.740	.19279	.0195	.14482	.00015	-.00490	3.84	.144	49.73	.509E+06

22-8-13 14:29 O:\Windtunnel data Reduced\redsideslipnowlb15 1 of 2

========== ~&v3SLow Speed Laboratory / ~&v3SDelft University of Technology
~&v2S* W 3 D Data output *
========== ~&v3S1.25 x 1.80 m Low Turbulence Tunnel

~&v3SOperator	:TonHettema	Model name	: ZESAR model
~&v3SExperiment nr.	: 2	Scale	: 1 : 1 Processing date : 16-Aug-13
~&v3SSeries	: 7	Configuration	: nowinglets
~&v3STest section	: 9	Input file	: zesar

Moment ref. point -> x_cg =~&v3S .0~&v0S% MAC z_cg =~&v3S .0~&v0S% MAC

Startvalues :	Rho [Kg/m3]	Temp [degr. C]	nu [m2/s]	Bar [mBar]
	1.186	24.7	.155E-04	1014.4

Settings :	DAL	DAR	DFI	DFO	IH	DELEV	B3/4R	IC	DELEVC	P1	P2	P3	P4	P5
	.00	.00	.00	.00	.00	.00	.0	.00	.00	.000	.000	.000	.000	.000

Dpt	alfa	beta	CN	CT	CL	CD	C-side	Cm-pitch	Cm-roll	Cm-yaw	CL/CD	M	V	Re
1	-6.00	-15.00	-.255	.00653	-.253	.04128	.0357	-.09084	.00700	-.00775	-6.13	.146	50.65	.519E+06
2	-4.00	-15.00	-.127	.01946	-.126	.03590	.0332	-.06397	.00982	-.00660	-3.50	.147	50.71	.519E+06
3	-2.00	-15.00	.007	.02562	.008	.03256	.0312	-.03838	.01236	-.00554	.23	.147	50.73	.519E+06
4	.00	-15.00	.143	.02475	.143	.03156	.0296	-.01289	.01464	-.00459	4.54	.147	50.72	.519E+06
5	2.00	-15.00	.281	.01693	.281	.03321	.0285	.01325	.01697	-.00381	8.45	.146	50.70	.519E+06
6	4.00	-15.00	.421	.00273	.419	.03823	.0281	.03811	.01950	-.00316	10.97	.146	50.66	.518E+06
7	6.00	-15.00	.555	-.01789	.554	.04614	.0280	.06463	.02153	-.00265	12.01	.146	50.60	.518E+06
8	8.00	-15.00	.679	-.04271	.678	.05761	.0278	.09332	.02469	-.00179	11.77	.146	50.48	.516E+06
9	10.00	-15.00	.777	-.06028	.776	.07949	.0251	.12309	.02558	.00049	9.76	.145	50.30	.515E+06
10	12.00	-15.00	.832	-.05321	.825	.12117	.0168	.16032	.02539	.00563	6.81	.145	50.08	.512E+06
11	14.00	-15.00	.764	.00538	.740	.19026	.0257	.13754	-.00004	-.00657	3.89	.144	49.77	.509E+06

22-8-13 14:29 O:\Windtunnel data Reduced\redsideslipnowlb20 1 of 2

========== ~&v3SLow Speed Laboratory / ~&v3SDelft University of Technology
~&v2S* W 3 D Data output *
========== ~&v3S1.25 x 1.80 m Low Turbulence Tunnel

~&v3SOperator :TonHettema Model name : ZESAR model
~&v3SExperiment nr. : 2 Scale : 1 : 1 Processing date : 16-Aug-13
~&v3SSeries : 8 Configuration : nowinglets
~&v3STest section : 9 Input file : zesar

Moment ref. point -> x_cg =~&v3S .0~&v0S% MAC z_cg =~&v3S .0~&v0S% MAC

Startvalues : Rho [Kg/m3] Temp [degr. C] nu [m2/s] Bar [mBar]

1.186 24.7 .155E-04 1014.4

Settings :	DAL	DAR	DFI	DFO	IH	DELEV	B3/4R	IC	DELEVC	P1	P2	P3	P4	P5
	.00	.00	.00	.00	.00	.00	.0	.00	.00	.000	.000	.000	.000	.000

Dpt	alfa	beta	CN	CT	CL	CD	C-side	Cm-pitch	Cm-roll	Cm-yaw	CL/CD	M	V	Re
1	-6.00	-20.00	-.239	.00546	-.237	.04518	.0487	-.08419	.00892	-.01056	-5.24	.146	50.68	.519E+06
2	-4.00	-20.00	-.118	.01773	-.116	.03986	.0454	-.05902	.01235	-.00905	-2.91	.147	50.73	.519E+06
3	-2.00	-20.00	.009	.02370	.010	.03663	.0429	-.03512	.01563	-.00769	.27	.147	50.74	.519E+06
4	.00	-20.00	.138	.02289	.138	.03545	.0407	-.01125	.01867	-.00647	3.90	.147	50.75	.519E+06
5	2.00	-20.00	.269	.01558	.268	.03691	.0394	.01250	.02164	-.00545	7.27	.147	50.71	.519E+06
6	4.00	-20.00	.398	.00212	.397	.04133	.0387	.03577	.02465	-.00460	9.61	.146	50.69	.518E+06
7	6.00	-20.00	.525	-.01739	.524	.04845	.0384	.06007	.02740	-.00395	10.81	.146	50.64	.518E+06
8	8.00	-20.00	.641	-.04084	.640	.05877	.0379	.08560	.03061	-.00299	10.89	.146	50.54	.517E+06
9	10.00	-20.00	.748	-.05668	.747	.08102	.0331	.10584	.02887	.00090	9.22	.145	50.35	.515E+06
10	12.00	-20.00	.813	-.06309	.809	.11143	.0308	.13925	.02441	.00156	7.26	.145	50.18	.513E+06
11	14.00	-20.00	.838	-.05356	.826	.15073	.0266	.15247	.02165	.00235	5.48	.144	49.98	.511E+06

22-8-13 14:29 O:\Windtunnel data Reduced\redsideslipnowlb25 1 of 2

========== ~&v3SLow Speed Laboratory / ~&v3SDelft University of Technology
~&v2S* W 3 D Data output *
========== ~&v3S1.25 x 1.80 m Low Turbulence Tunnel

~&v3SOperator :TonHettema Model name : ZESAR model
~&v3SExperiment nr. : 2 Scale : 1 : 1 Processing date : 16-Aug-13
~&v3SSeries : 9 Configuration : nowinglets
~&v3STest section : 9 Input file : zesar

Moment ref. point -> x_cg =~&v3S .0~&v0S% MAC z_cg =~&v3S .0~&v0S% MAC

Startvalues : Rho [Kg/m3] Temp [degr. C] nu [m2/s] Bar [mBar]

1.187 24.7 .155E-04 1014.4

Settings :	DAL	DAR	DFI	DFO	IH	DELEV	B3/4R	IC	DELEVC	P1	P2	P3	P4	P5
	.00	.00	.00	.00	.00	.00	.0	.00	.00	.000	.000	.000	.000	.000

Dpt	alfa	beta	CN	CT	CL	CD	C-side	Cm-pitch	Cm-roll	Cm-yaw	CL/CD	M	V	Re
1	-6.00	-25.01	-.216	.00396	-.214	.05005	.0615	-.07488	.00997	-.01326	-4.29	.147	50.71	.520E+06
2	-4.00	-25.01	-.105	.01538	-.103	.04492	.0577	-.05174	.01421	-.01157	-2.30	.147	50.77	.520E+06
3	-2.00	-25.01	.012	.02098	.013	.04170	.0546	-.03026	.01815	-.00993	.31	.147	50.78	.520E+06
4	.00	-25.01	.132	.02040	.132	.04051	.0521	-.00876	.02177	-.00845	3.25	.147	50.79	.520E+06
5	2.00	-25.01	.253	.01369	.252	.04169	.0504	.01220	.02527	-.00722	6.04	.147	50.77	.519E+06
6	4.00	-25.01	.373	.00121	.372	.04552	.0494	.03373	.02898	-.00617	8.16	.147	50.75	.519E+06
7	6.00	-25.01	.488	-.01678	.487	.05174	.0488	.05555	.03220	-.00534	9.42	.147	50.71	.519E+06
8	8.00	-25.01	.596	-.03863	.596	.06090	.0482	.07791	.03547	-.00433	9.78	.146	50.61	.518E+06
9	10.00	-25.01	.703	-.05607	.702	.07919	.0441	.09135	.03209	-.00108	8.86	.146	50.48	.516E+06
10	12.00	-25.01	.776	-.06693	.773	.10493	.0428	.11051	.02498	-.00123	7.36	.145	50.33	.515E+06
11	14.00	-25.01	.819	-.06946	.811	.13652	.0427	.12320	.01791	-.00272	5.94	.145	50.13	.513E+06

D.3. GRAPHS OF WIND TUNNEL TEST RESULTS

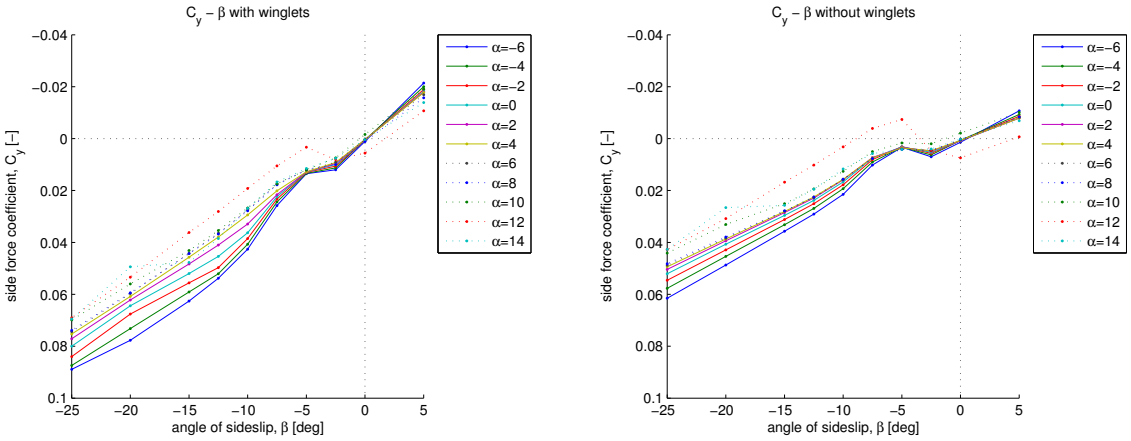

(a) With winglets (b) Without winglets

Figure D.1: Side force coefficient versus angle of sideslip

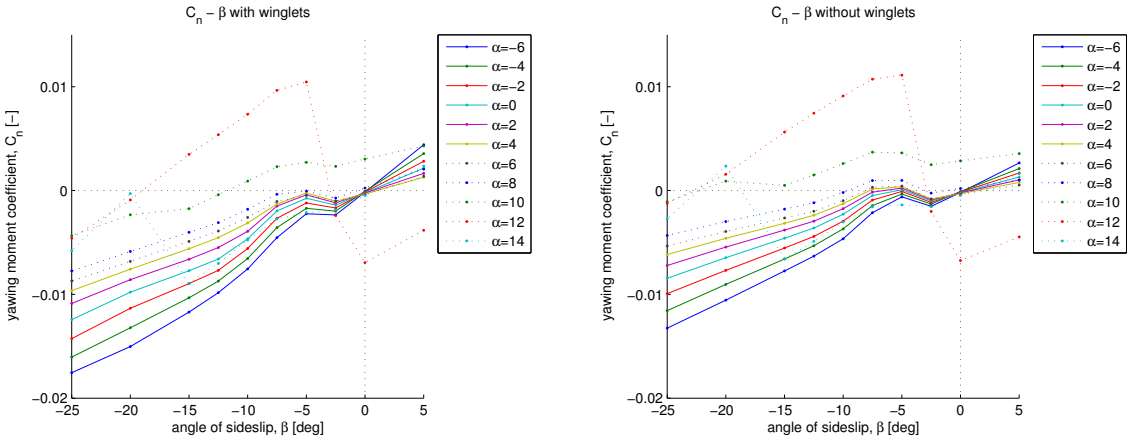

(a) With winglets (b) Without winglets

Figure D.2: Yawing moment coefficient versus angle of sideslip

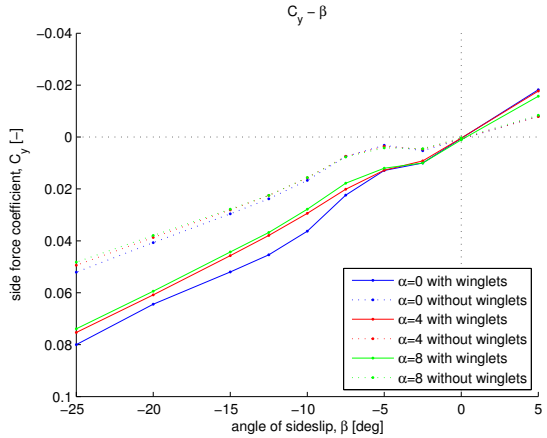

(a) Side force coefficient versus angle of sideslip

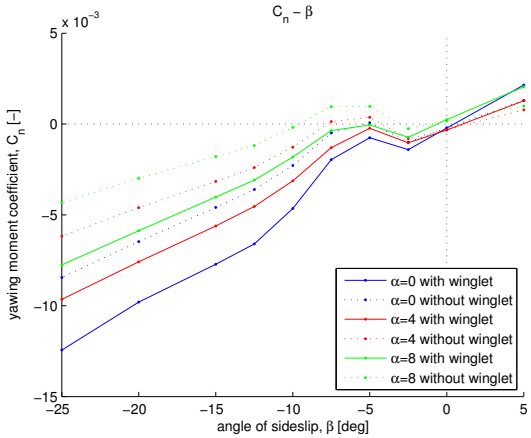

(b) Yawing moment coefficient versus angle of sideslip

Figure D.3: Side force and yawing moment coefficient versus angle of sideslip at three angles of attack

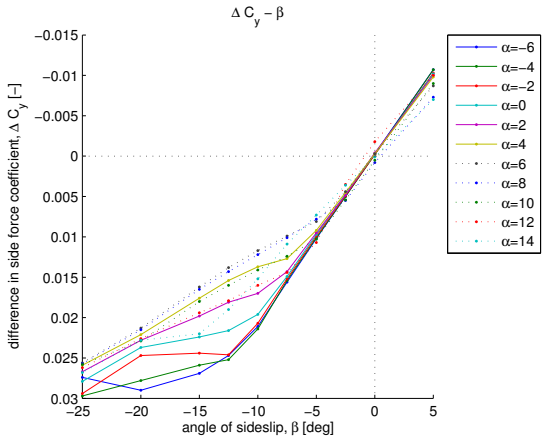

(a) For all angles of attack

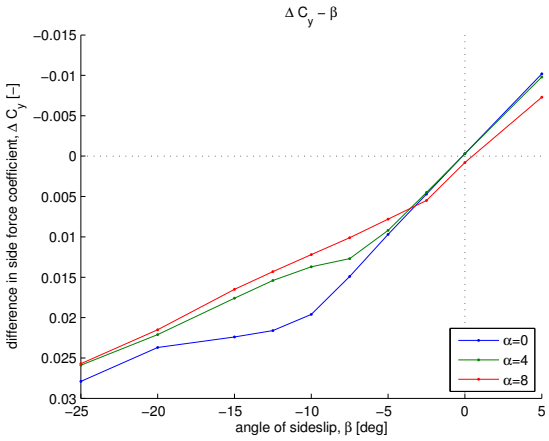

(b) For three selected angles of attack

Figure D.4: Difference in side force coefficient (with minus without winglets) versus angle of sideslip

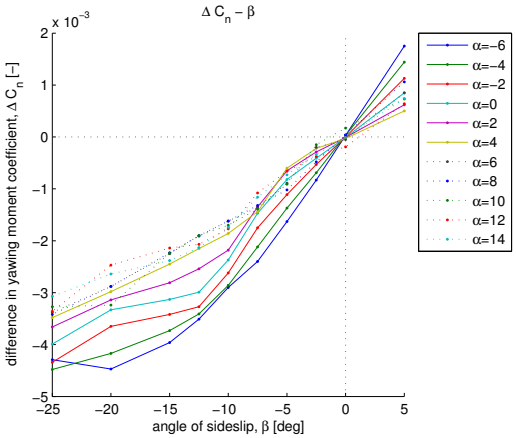

(a) For all angles of attack

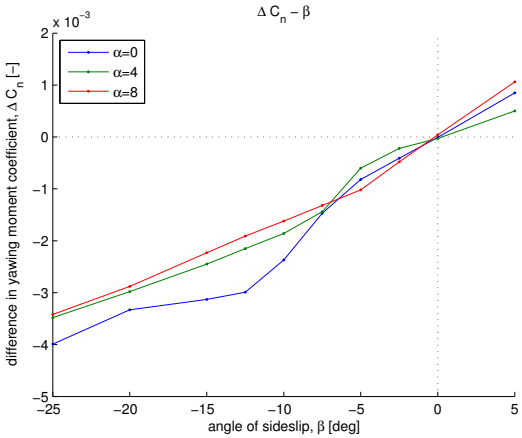

(b) For three selected angles of attack

Figure D.5: Difference in yawing moment coefficient (with minus without winglets) versus angle of sideslip

E

INPUT FILES FOR THE AVL VALIDATION

```
Fokker F28 Mk1000
0.75
0 0 0
76.4 3.506 23.58
12.00 0.000 0.000
###################
SURFACE
Wing
12 1.0 26 -1.1
COMPONENT
1
YDUPLICATE
0
SECTION
#Xle    Yle     Zle      Chord    Ainc  Nspanwise  Sspace

8.750   0.000    -0.70     4.90   0.    1          0


SECTION

10.50   4.950    -0.48     3.48   0.    1          0
SECTION

12.95   11.79    -0.19     1.57   0.    1          0
###################
SURFACE
HorizontalTail
12 1
COMPONENT
3
YDUPLICATE
0
SECTION
23.45   0.00    4.9     3.00   0.    1          0
SECTION
25.90   4.32    4.9     1.44   0.    1          0
###################
SURFACE
VerticalTail
12 1
COMPONENT
4
SECTION
19.95   0    1.4     4.20   0.    1          0
SECTION
23.10   0    5.4     3.49   0.    1          0
###################
SURFACE
BodyV1
24 1
COMPONENT
2
SECTION
```

```
Zeft BWB
0.146
0 0 0
0.2869 0.1585 1.45
0.240 0.000 0.024
##################
SURFACE
Wingbody
12 1.0 26 -1.1
COMPONENT
1
YDUPLICATE
0
SECTION
#Xle    Yle     Zle      Chord    Ainc  Nspanwise  Sspace

0.000   0.000    0.000     0.500   0.    1          0


SECTION

0.007   0.049    0.006     0.487   0.    1          0


SECTION

0.023   0.099    0.013     0.431   0.    1          0
SECTION

0.072   0.141    0.019     0.303   0.    1          0
SECTION

0.102   0.171    0.022     0.224   0.    1          0
SECTION

0.181   0.336    0.043     0.138   0.    1          0
SECTION

0.283   0.560    0.071     0.103   0.    1          0
SECTION

0.309   0.620    0.078     0.093   0.    1          0
SECTION

0.336   0.680    0.086     0.084   0.    1          0
SECTION

0.359   0.721    0.090     0.077   0.    1          0
SECTION

0.375   0.725    0.092     0.059   0.    1          0
##################
SURFACE
Winglet1
```

F

Erratum for 'Static Directional Stability and Control of Transport Aircraft' [1]

On page 4,
The equation should be:

$$(C_{Y_\beta})_{\text{WFN}} = -\frac{S_{\text{F.cross}}}{S_{\text{W}}} K_i \frac{2\pi}{180} - 0.0001\Gamma + (\Delta C_{Y_\beta})_{\text{f}} - 0.00175 n_{\text{N}_\text{W}} - 0.00025 n_{\text{N}_\text{F}} \tag{F.1}$$

Instead of:

$$(C_{Y_\beta})_{\text{WFN}} = \frac{S_{\text{F.cross}}}{S_{\text{W}}} K_i \frac{2\pi}{180} - 0.0001\Gamma + (\Delta C_{Y_\beta})_{\text{f}} - 0.00175 n_{\text{N}_\text{W}} - 0.00025 n_{\text{N}_\text{F}} \tag{F.2}$$

On page 11,
The equation should be:

$$\left(\Delta \frac{\partial \sigma}{\partial \beta}\right)_{C_{l_\beta}} = 50 \left[(C_{l_\beta})_{\text{WFN}} - (C_{l_\beta})_{\text{WFN},C_L=0}\right] \tag{F.3}$$

Instead of:

$$\left(\Delta \frac{\partial \sigma}{\partial \beta}\right)_{C_{l_\beta}} = -0.50 \left[(C_{l_\beta})_{\text{WFN}} - (C_{l_\beta})_{\text{WFN},C_L=0}\right] \tag{F.4}$$

On page 11,
The equation should be:

$$\left(\Delta \frac{\partial \sigma}{\partial \beta}\right)_{\text{f}} = -0.80 \left(\frac{b_{\text{f}}}{b_{\text{W}}} - 0.67\right) \frac{\delta_{\text{f}}}{\delta_{\text{f}_{\text{max}}}} \tag{F.5}$$

Instead of:

$$\left(\Delta \frac{\partial \sigma}{\partial \beta}\right)_{\text{f.landing}} = -0.80 \left(\frac{b_{\text{f}}}{b_{\text{W}}} - 0.67\right) \tag{F.6}$$

On page 14,
The equation should be:

$$(C_n)_{\delta_{\text{r}}} = C_{n_{\delta_{\text{r}}}} \delta_{\text{r}} = C_{L_{\alpha_{\text{V}}}} \frac{q_{\text{V}}}{q} K_{\text{FV}} K_{\text{VH}} \frac{c_{l_\delta}}{c_{l_\alpha}} \frac{S_{\text{V}_\text{r}}}{S_{\text{W}}} \frac{l_{\text{V+DF}} + 0.30\bar{c}_{\text{V}}}{b_{\text{W}}} \delta_{\text{r}} \tag{F.7}$$

Instead of:

$$(C_n)_{\delta_{\text{r}}} = C_{n_{\delta_{\text{r}}}} \delta_{\text{r}} = C_{L_{\alpha_{\text{V}}}} \frac{q_{\text{V}}}{q} K_{\text{FV}} K_{\text{VH}} \frac{c_{l_\delta}}{c_{l_\alpha}} \frac{S_{\text{V}_\text{r}}}{S_{\text{W}}} \frac{l_{\text{V+DF}} + 0.30\bar{c}_{\text{V}}}{b_{\text{V}}} \delta_{\text{r}} \tag{F.8}$$

G

Aircraft used in 'Static Directional Stability and Control of Transport Aircraft' [1]

Table G.1: Aircraft used in 'Static Directional Stability and Control of Transport Aircraft' [1]

Aircraft manufacturer	Fokker								Piaggio-Douglas
Aircraft type number	F-27	F-28	F-28 SKV	F-29	50	70	100	VFW 614	PD-808
Aircraft year of introduction	1955	1967		1983	1987	1993	1986	1971	1964
Tail-off sideforce and yawing moment	X	X	X	X			X	X	X
Effect of flap deflection		X	X	X			X		
Effect of Dorsal fin	X	X							
Endplate effect		X	X	X					
Sidewash		X		X		X	X		
Sidewash (engine position)		X	X	X					
Sidewash (dynamic pressure)			X						
Yawing moment		X							
Rolling moment	X	X	X	X	X		X		
Tail-off rolling moment		X	X	X		X	X		
Sidewash ($C_{l_{T-O}}$)			X						
Sidewash versus rolling moment		X	X	X		X	X		
Sidewash (flap deflection)		X	X	X					
Tail moment arm	X	X	X	X			X		
Rudder deflection	X	X	X	X					
App. II: Aircraft geometry and aerodynamic data	X	X	X	X				X	
App. III: Determination of the horizontal endplate factor	X	X	X	X					
App. IV: Tail moment arm ratio	X	X	X	X	X		X		
App. V: Wind tunnel test data	X	X							

Table G.2: Aircraft used in 'Static Directional Stability and Control of Transport Aircraft' [1]

Aircraft manufacturer	McDonnell-Douglas				Lockheed	Grumman	Boeing		Airbus		
Aircraft type number	DC-8-62	DC-9-10	DC-9-30	DC-10-30	F-104A	F6F	737-300	XB-47	A-300	A-320	A-340-300
Aircraft year of introduction	1967	1965	1966	1972	1954	1942	1981	1947	1972	1987	1991
Tail-off sideforce and yawing moment	X	X	X	X							
Effect of flap deflection											
Effect of Dorsal fin											
Endplate effect					X	X		X			
Sidewash			X				X		X	X	X
Sidewash (engine position)											
Sidewash (dynamic pressure)											
Yawing moment											
Rolling moment							X			X	X
Tail-off rolling moment										X	X
Sidewash ($C_{l_{T-O}}$)											
Sidewash versus rolling moment										X	X
Sidewash (flap deflection)										X	X
Tail moment arm			X		X		X	X	X	X	X
Rudder deflection							X			X	X
App. II: Aircraft geometry and aerodynamic data			X		X	X	X	X	X	X	X
App. III: Determination of the horizontal endplate factor					X	X		X		X	
App. IV: Tail moment arm ratio			X		X		X	X	X	X	X
App. V: Wind tunnel test data											

BIBLIOGRAPHY

[1] E. Obert, *Static directional stability and control of transport aircraft*, Tech. Rep. A-128 (Fokker-VFW B.V., 1979-2013) department CB-AP.

[2] D. Raymer, *Aircraft Design: A Conceptual Approach*, 2nd ed. (American Institute of Aeronautics and Astronautics, Inc., 1992).

[3] S. Waters, *Control allocation performance for a blended wing body Wind-tunnel and numerical investigation into non-linear aerodynamic control surface effects and their impact on design*, Master's thesis, Delft University of Technology (2012).

[4] R. Fink, *USAF Stability and Control DATCOM*, Tech. Rep. AFWAL-TR-83-3048 (McDonnell Douglas Corporation, 1978).

[5] D. Raymer, *Aircraft design: A conceptual approach*, 5th ed. (American Institute of Aeronautics and Astronautics, Inc., 2012).

[6] J. Roskam, *Airplane design, Part II: Preliminary configuration design and integration of the propulsion system*, 1st ed. (Roskam Aviation and Engineering Corporation, 1985).

[7] J. Roskam, *Airplane flight dynamics and automatic flight controls, Part I* (Design, Analysis and Research Corporation Corporation, 1995).

[8] E. Torenbeek, *Synthesis of subsonic airplane design* (Delft University Press, 1976).

[9] J. Roskam, *Airplane design, Part III: Layout design of cockpit, fuselage, wing and empennage: Cutaways and inboard profiles*, 1st ed. (Roskam Aviation and Engineering Corporation, 1986).

[10] J. Campbell and M. McKinney, *Summary of methods for calculating dynamic lateral stability and response and for estimating lateral stability derivatives*, Tech. Rep. 1098 (National Advisory Committee for Aeronautics, 1950).

[11] P. Goudou, *Certification Specifications for Large Aeroplanes*, Tech. Rep. CS-25 (European Aviation Safety Agency, 2003).

[12] J. Mulder, W. van Staveren, J. van der Vaart, and E. de Weerdt, *Flight Dynamics (Lecture Notes) AE3-302* (Delft University of Technology, 2007).

[13] C. Hollis and R. Williams, *Aerofoil maximum lift coefficient for Mach numbers up to 0.4*, Tech. Rep. ESDU 84026 (ESDU, 1999).

[14] R. Elmendorp, *Synthesis of Novel Aircraft Concepts for Future Air Travel*, Master's thesis, Delft University of Technology (2014).

[15] C. Huijts, *Literature report*, Master's thesis, Delft University of Technology (2013).

[16] T. Toll and M. Queijo, *Approximate relations and charts for low-speed stability derivatives of swept wings*, Tech. Rep. (National Advisory Committee for Aeronautics, 1948).